Journal of Iberian Geology
https://doi.org/10.1007/s41513-024-00248-8

RESEARCH PAPER

Plio-Pleistocene hydrothermal events of the Baza Basin (Betic Cordillera, SE Spain) and their paleoecological implications

José Manuel García-Aguilar[1] · Isidoro Campaña[1] · Bienvenido Martínez-Navarro[2,3,4] · Antonio Guerra-Merchán[1] · M. Dolores Rodríguez-Ruiz[1] · Guillermo Rodríguez-Gómez[1,6,7] · Alejandro Granados[1] · Laura León-Reina[5] · M. Patrocinio Espigares[1] · Sergio Ros-Montoya[1] · Paul Palmqvist[1]

Received: 23 March 2024 / Accepted: 8 July 2024

Abstract

The Lower Pliocene to upper Middle Pleistocene continental sedimentary infillings of the Baza Basin (Guadix-Baza Depression, SE Spain) are worldwide unique by their high stratigraphic completeness and exceptional preservation of their fossil record of terrestrial vertebrates. These sediments were deposited in fluvio-lacustrine environments and preserve huge assemblages of large mammals, including the oldest evidence of hominin presence in Western Europe at the late Lower Pleistocene sites of Barranco León and Fuente Nueva-3, dated to ~1.4 Ma. Since latest Miocene times, the basin was subject to intense tectonic activity, showing sedimentary deposits originated from ancient hot springs. These hot springs were developed in a spatio-temporal network related to tectonic fractures, showing a higher concentration in the Orce sub-basin during Late Pliocene to Holocene times. Compositional analyses of cherts and other facies associated with these hot springs show geochemical and mineralogical markers linked to hydrothermal scenarios. The contribution of hot springs in the Baza Basin resulted in rich and productive biotopes, which supported a high diversity and biomass of terrestrial mammals. Similar geological, hydrochemical and ecological environments are found along hotspot lines in East Africa, the Levantine Corridor and the circum-Mediterranean realm. We hypothesize here that the presence of these hot springs corridors favored the dispersal of hominins and other large mammals during the Plio-Pleistocene, which led to the first hominin arrival in Europe.

Keywords Hot springs · Biomass of large mammals · Orce sites · Hominin dispersal in Europe · African Rift

✉ Paul Palmqvist
ppb@uma.es

Bienvenido Martínez-Navarro
bienvenido.martinez@icrea.cat

[1] Departamento de Ecología y Geología, Universidad de Málaga, Campus de Teatinos, 29071 Málaga, Spain

[2] IPHES-CERCA, Institut Català de Paleoecologia Humana i Evolució Social, C/ Marcel.lí Domingo s/n, Campus Sescelades, Edifici W3, 43007 Tarragona, Spain

[3] Área de Prehistoria, Universitat Rovira i Virgili (URV), Avda. Catalunya 35, 43002 Tarragona, Spain

[4] ICREA, Pg. Lluís Companys 23, 08010 Barcelona, Spain

[5] Servicio Central de Apoyo a la Investigación, Universidad de Málaga, Campus de Teatinos, 29071 Málaga, Spain

[6] Departamento de Geodinámica, Estratigrafía y Paleontología, Universidad Complutense de Madrid, C/ José Antonio Novais 12, 28040 Madrid, Spain

[7] Centro UCM-ISCIII de Evolución y Comportamiento Humanos, Avd/ Monforte de Lemos, 5, Pabellón 14, 28029 Madrid, Spain

Published online: 03 September 2024

Eventos hidrotermales en el Plio-Pleistoceno de la cuenca de Baza (cordillera Bética, sureste de España) y sus implicaciones paleoecológicas

Resumen
Los rellenos continentales sedimentarios de edad Plioceno inferior a finales del Pleistoceno medio en la cuenca de Baza (depresión de Guadix-Baza, SE de España) son mundialmente conocidos por su elevado grado de completitud estratigráfica y la excepcional conservación de su registro fósil de vertebrados terrestres. Estos sedimentos se depositaron en ambientes fluvio-lacustres y conservan abundantes asociaciones de restos de grandes mamíferos, incluyendo las evidencias más arcaicas de presencia humana en Europa occidental, ubicadas en los yacimientos de finales del Pleistoceno inferior de Barranco León y Fuente Nueva-3, datados ambos en ~1,4 Ma. Desde finales del Mioceno, la cuenca se vio sometida a intensa actividad tectónica, mostrando depósitos originados en antiguas surgencias de aguas termales. Estas surgencias se desarrollaron a lo largo de una amplia malla espacio-temporal, ligada a fracturas tectónicas, mostrando mayor concentración en la subcuenca de Orce desde el Plioceno superior al Holoceno. El análisis de la composición de las silexitas y otras facies asociadas a estas fuentes termales muestra la presencia de marcadores geoquímicos y mineralógicos ligados a escenarios hidrotermales. El aporte continuado de las fuentes termales en la cuenca de Baza dio como resultado biotopos muy ricos y productivos, capaces de soportar una elevada diversidad y biomasa de mamíferos terrestres. Ambientes geológicos, hidroquímicos y ecológicos similares se encuentran alineados con surgencias termales en África oriental, el Corredor Levantino y el área circum-mediterránea. Proponemos como hipótesis que la presencia de tales corredores hidrotermales favoreció la dispersión de los homininos y otros grandes mamíferos durante el Plio-Pleistoceno, dando lugar a la primera colonización humana de Europa.

Palabras clave Fuentes termales · Biomasa de grandes mamíferos · Yacimientos de Orce · Primera dispersión humana en Europa · Rift africano.

1 Introduction and background

The Baza Basin lies in the northeastern sector of the Guadix-Baza Depression (Granada, SE Spain; Fig. 1A), which extends over an area of ~ 4000 km^2 (Palmqvist et al., 2022a) and is surrounded by the highest reliefs of the Alpine Betic cordillera. This inland basin preserves a unique Plio-Pleistocene sedimentary record of high preservational completeness, which is composed of fluvio-lacustrine deposits that preserve many paleontological and archaeological localities distributed throughout the whole sedimentary depression, and especially in the Baza Basin (Martínez-Navarro, 1991; Palmqvist et al., 1996, 2011, 2022a, 2022b, 2023; Arribas & Palmqvist, 1998; Palmqvist & Arribas, 2001; Espigares et al., 2013, 2019; Toro-Moyano et al., 2013; Rodríguez-Gómez et al., 2016, 2017; Ros-Montoya et al., 2017, 2018; Martínez-Navarro et al., 2018; Table 1). The presence of Plio-Pleistocene hydrothermal events in the Baza Basin and their paleoecological consequences has been documented since the end of the twentieth century by means of sedimentological, tectonic, and mineralogical data (e.g., García-Aguilar, 1997; García-Aguilar et al., 2014, 2015; Sánchez-Roa et al., 2016; Sebastián Pardo, 1979).

1.1 Geological and paleontological setting

According to the classification of Miall (1984), the Baza Basin is an intramountainous basin with tectonic subsidence and continental sedimentation, features inherited from an ancient marine basin formed during the Late Miocene in the interior of the Betic mountain range (Platt et al., 2013; Sanz de Galdeano & Vera, 1992). The transition from a marine to a continental sedimentary regime took place 7.5–7.0 Ma ago, being the result of major regional tectonic movements that caused the isostatic uplifting of the basin (average uplift rate of ~ 200 m/Ma, as estimated from Upper Neogene coastal marine conglomerates and coral reefs; Braga et al., 2003), which resulted in its disconnection from the Mediterranean Sea (Soria, 1993; García-Aguilar, 1997; Playá et al., 2000; Guerra-Merchán et al., 2014). The Baza Basin is bounded to the north by reliefs of Mesozoic age, mostly carbonates (Thetys type), which belong to the External Zones of the Betic Cordillera. To the south, it is surrounded by reliefs composed of sedimentary and metamorphic rocks of Paleozoic-Triassic age, which belong to the Internal Zones. To the west, it is connected with the Neogene Guadix Basin and to the southeast with the Neogene Almanzora Corridor Basin (Fig. 1B).

The Plio-Pleistocene stratigraphic model of the Baza Basin shows three major stages (Fig. 1C), which are represented by tectono-sedimentary units (TSU) according to Megías (1982) (see also Guerra-Merchán, 1992; Soria, 1993; García-Aguilar, 1997; García-Aguilar & Martín, 2000; García-Aguilar & Palmqvist, 2011). The three TSUs are bounded by sedimentary hiatuses and/or unconformities that represent stages in which the basin was subject to intense tectonic activity, showing little or no sedimentation. These units have been dated using biochronological (e.g., Alberdi

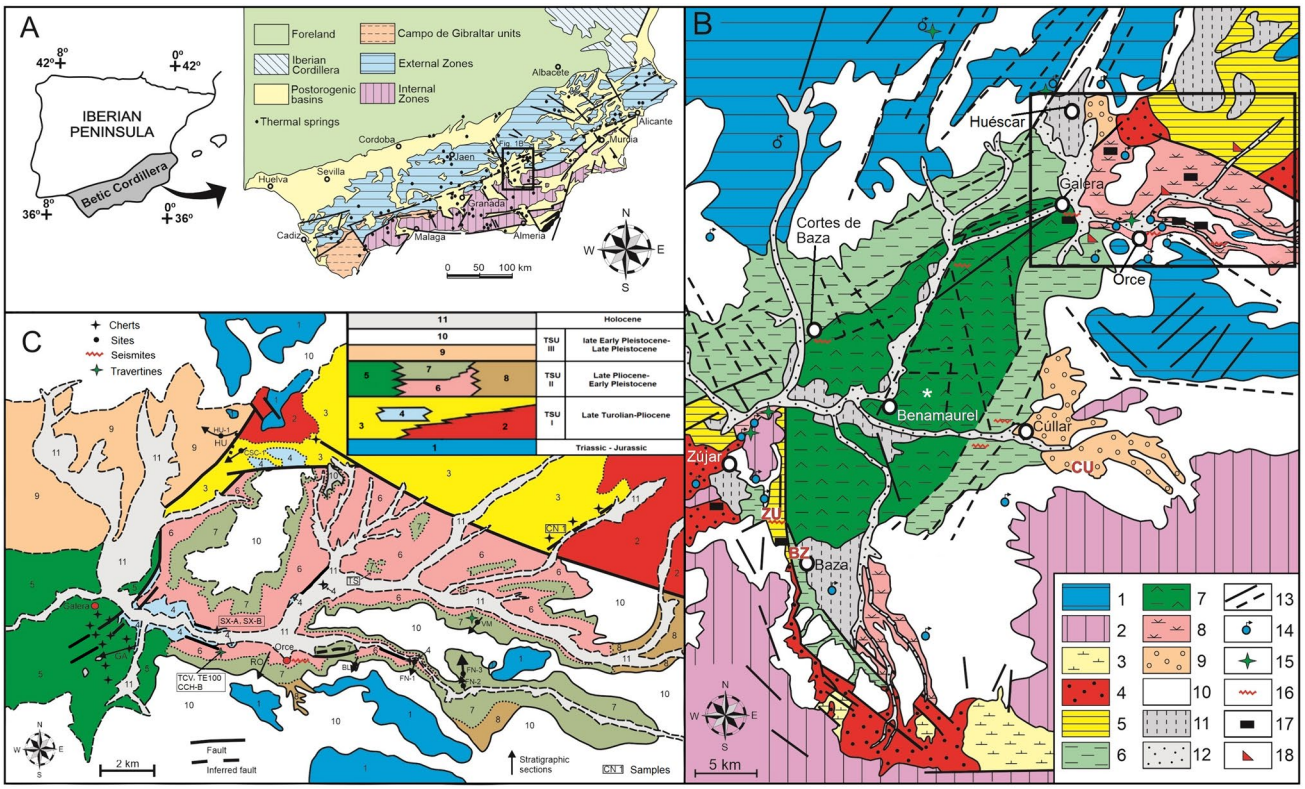

Fig. 1 **A** High-scale geological context of the Baza Basin; the points mark the hot springs that are currently active. **B** Geologic map of the Baza Basin. 1-substrate of the external zones; 2-substrate of the internal zones; 3-tortonian, marine facies; 4-late turolian-pliocene, alluvial facies s.l.; 5-pliocene-lower villafranchian, mainly lacustrine facies; 6-early and middle villafranchian, distal fluvial facies (sandstones and lutites); 7-early and middle villafranchian, marly-evaporitic lacustrine facies; 8-late villafranchian-epivillafranchian, lacustrine and distal fluvial facies; 9-middle and late pleistocene, proximal alluvial and locally lacustrine facies; 10-glacis surface; 11-holocene alluvial; 12-holocene fluvial terraces; 13-tectonic fractures (in discontinuous trace, those inferred from satellite images); 14-hot springs currently active (codes match those of Table 2); 15-recent travertine buildings; 16-seismites; 17-levels of dark lutites; 18-cherts. Codes in red indicate the position of the stratigraphic series sampled (see Fig. 2). * Indicates the position of samples BNA-1, BNA-2, BNA-3, BNA-4, BNA-5, and BN-N at the northeastern of the locality of Benamaurel (Tables 3 and 4). **C** Geographic and geologic context of the Orce-Venta Micena sector in the Baza Basin and lithostratigraphic model of the Orce subbasin with definition of tectono-sedimentary units (TSU) for the Baza Basin:1-dolomites and limestones of the subbetic domain (external zones); 2-alluvial red conglomerates; 3-lacustrine yellow marls; 4-lacustrine limestones; 5-lacustrine marls, sands and gypsum; 6-fluvial and lacustrine red and grey sands, as well as (calci) lutites; 7-lacustrine marls and limestones; 8-alluvial conglomerates; 9-deltaic conglomerates and sands, as well as lacustrine marls; 10-glacis surface; 11-fluvial gravels and sands. Stratigraphic sections: site codes and samples are depicted in Fig. 2. The equivalence between the codes that appear in Fig. 1B, C is the following: 1–1, 4–2 & 8, 5–3 & 4, 6–5, 7–5**,** 8–6 & 7, 9–9**,** 10–10, and 11–11

& Bonadonna, 1989; Martínez-Navarro, 1991; Guerra-Merchán, 1992; Oms et al., 2000a; Gibert & Gibert, 2003; Ros-Montoya, 2010; Maldonado-Garrido et al., 2017) and paleomagnetic data (e.g., Álvarez et al., 2015; Álvarez-Posada et al., 2017; Garcés, 1994; Gibert et al., 2006, 2007; Oms et al., 1994, 1996, 1999, 2000b, 2011; Scott et al., 2007).

The first TSU, which is of Pliocene age, shows a sediment thickness of ~ 150 m. It is characterized by the alternation of marls/calcilutites/lutites and limestones deposited in lacustrine systems, which change towards the edges of the basin to sands and conglomerates of alluvial origin. Forest ecosystems were formed on the margins of the lake as inferred for the Ruscinian (~ 4.5 Ma) Baza-1 paleontological site (Ros-Montoya et al., 2017). Tectonic activity during this stage induced the formation of many soft-sediment deformation structures (i.e., paleo-seismites), which are mainly located at the marginal sites of a paleo-lake (Alfaro et al., 1997) and possibly resulted in deposits with hydrothermal affinities (García-Aguilar et al., 2014, 2015). Climate was warm and humid during this stage, which relates to an environment typical of modern subtropical or rainy tropical climates (Foucault & Mélières, 2000; Haywood & Valdés, 2004).

The second TSU has an uppermost Pliocene to Middle Pleistocene age and is the most complex, both lithologically and tectonically. During this stage, a great paleogeographic change took place in the Baza Basin, which involved an ~ E-W expansion linked to an NNW-SSE fracture system. This in turn resulted in intense subsidence

Table 1 Archaeological and paleontological sites in the Baza Basin

Stratigraphic series (key) and references	Paleontological sites	Key of analyzed samples	Age of paleontological sites
Cúllar (**CU**) Ruiz-Bustos, 1976; Peña, 1979; Torrente-Casado, 2010	**CB-1**	CB-1A	Galerian
Baza (**BZ**) Guerra-Merchán, 1992; Ros-Montoya et al., 2017	**BZ-1**	BZ1-A BZ1-B BZ1-Y	Ruscinian
Zújar (**ZU**) Agustí and Oms, 1998 + original data	**ZU-14** **ZU-11** **ZU-10** **ZU-4**	ZU-A3 ZU-B3 ZU-A2 ZU-A1	Middle Villafranchian Early Villafranchian Early Villafranchian Ruscinian
Galera (**GA**) García-Aguilar, 1997 + original data	**NU-3; GA-H** **GA-2; GA-G** **NU-2** **GA-1; GA-C** **CC-1; NU-1**	GA-12 AQ-2 GA-7 GA-6 GA-3B GA-3A GE-1A GE-1B	Middle Villafranchian Middle Villafranchian Ruscinian Ruscinian Ruscinian
Huéscar (**HU**) Mazo et al., 1985 + original data	**HU-1** **CSC-1** **HU-3**	PL-1 CS-1A BQ-3A BQ-3B	Epivillafranchian Ruscinian Ruscinian
Venta Micena (**VM**) Anadón et al., 1987	**VM-2** **VM-1**	VMC1 VMS2 VMC3 VM VMS4 VMC4 VMC	Late Villafranchian
Río Orce (**RO**) Gibert and Gibert, 2003 + original data	**BO-7** **BO-6**	OR-1 OR-1A CCH-1	Late Villafranchian Middle Villafranchian
Barranco León (**BL**) Toro-Moyano et al., 2013	**BL-6** **BL-1** **BL-5** **BL-4** **BL-B** **BL-A** **BL-3; BL-2**	BLYS BLYI BL- BLYM BLE-1	Late Villafranchian
Fuente Nueva-1 (**F1**) Original data	**FN-1**	FN1B FN1A	Middle Villafranchian
Fuente Nueva-2 (**F2**) Original data	**FN-2**	FN2T FN2A FN2B	Late Villafranchian
Fuente Nueva-3 (**F3**) Espigares et al., 2019	**FN-3**	FN3B FN3A FN3M	Late Villafranchian

In blue, those containing macrofaunal remains. In green, those with evidence of human presence. Site codes: CB (Cúllar-Baza); BZ (Baza); ZU (Zújar); GA (Galera); CC (Cañada del Castaño); NU (Nuca); HU (Huéscar); CSC (Canal de San Clemente); VM (Venta Micena); BO (Barranco de Orce); BL (Barranco León); FN-1 (Fuente Nueva-1); FN-2 (Fuente Nueva-2); FN-3 (Fuente Nueva-3). Site codes are positioned in Figs. 1B, C and 2

and the deposition of sediments with a minimum thickness of ~ 280 m in the central sector of the basin. However, geophysical data (Sanz de Galdeano et al., 2007) indicate that sedimentary thickness may be much greater than the one visible. These sediments, contributed by fluvial systems from the adjacent Guadix Basin, filled a large lake of marly-evaporitic sedimentation with an outer rim of detrital inputs (García-Aguilar & Martín, 2000; García-Aguilar

& Palmqvist, 2011; Vera, 1970). Tectonic activity during this stage resulted in synsedimentary normal faults, tilting, local unconformities, and seismites (Alfaro et al., 1997, 2000; Vera et al., 1984). The lower section of this unit shows selenitic and microcrystalline gypsum levels of centimeter thickness, which alternate with layers of light-colored marls towards the basin center or with sandstones towards the edges (García-Aguilar et al., 2013). Climate at this stage was semi-arid, with cyclic oscillations within the Bond frequency timing band (Bond et al., 1997; García-Aguilar et al., 2013; Hagelberg et al., 1994), which generated alternating periods of inundation and desiccation of the lake linked to the deposition of marls or sandstones and gypsum, respectively.

The upper section of this TSU outcrops mainly in the Orce area, a sub-basin in the NE sector of the Baza Basin, which has an extent of ~ 170 km^2 (Fig. 1B, C) and shows ~ 35 m thick extensive outcrops that correspond to the Lower to Middle Pleistocene. The Orce sub-basin preserves a unique fossil record of terrestrial vertebrates, including two archaeological sites dated to ~ 1.4 Ma (see review in Palmqvist et al., 2016) that mark the earliest presence of hominins in Western Europe: Barranco León (BL) and Fuente Nueva-3 (FN3). BL and FN3 preserve huge assemblages of skeletal remains of large mammals and Oldowan tools, which are linked through the presence of anthropogenic cut and percussion marks, as well as a human deciduous tooth in the case of BL, which is at this moment the oldest hominin fossil found in Western Europe (Espigares et al., 2013, 2019; Martínez-Navarro et al., 1997, 2014; Oms et al., 2000a, 2000b; Palmqvist et al., 2023; Titton et al., 2021; Toro-Moyano et al., 2013; Yravedra et al., 2021, 2022). Moreover, the Venta Micena site (VM, 1.6–1.5 Ma), which is slightly older than BL/FN3 and has been interpreted as a denning area of the giant hyena *Pachycrocuta brevirostris* (Arribas & Palmqvist, 1998; Palmqvist & Arribas, 2001; Palmqvist et al., 2022b), provides an excellent record of the large mammal community that preceded the hominin dispersal in the basin (Martínez-Navarro, 1991; Mendoza et al., 2005; Rodríguez-Gómez et al., 2017). The varied lithological composition of the Orce area, with alternations of fluvial red detrital facies and lacustrine carbonate-marly facies that locally show gypsum deposits (restricted to the center of the lacustrine system in this area) and cherts, points to a paleogeographic model of fluvio-lacustrine sedimentation highly variable in time and space. This resulted in open plains with forest patches in the emerged areas surrounding the fluvio-lacustrine system (García-Aguilar & Palmqvist, 2011; Mendoza et al., 2005; Palmqvist et al., 2022a; Scott et al., 2007).

The third TSU of the Baza Basin has a Middle Pleistocene to Upper Pleistocene age, showing a maximum thickness of 70 m. During this stage, the activity of major faults (Baza and Galera) resulted in some tectonic blocks that developed an effective subsidence, which allowed a continuous sedimentation. This TSU is composed of conglomerates and sands towards the basin edges, which change to lutites, marls and marly limestones deposited in shallow lacustrine environments towards the basin center. In the upper part of this unit and at the basin edges, alluvial facies (mainly red conglomerates and sands) prograde over lacustrine facies. This TSU is represented in several sectors of the basin perimeter (Fig. 1B, C) and the most significant paleontological sites are Huéscar-1 and Cúllar-Baza-1 (Ruiz-Bustos, 1976; Peña et al., 1977; Mazo et al., 1985; Alberdi & Bonadonna, 1989; Agustí et al., 2000; Torrente Casado, 2010; Ros-Montoya et al., 2018).

Finally, during the late Middle Pleistocene (~ 400 ka: García-Tortosa et al., 2008a, 2008b) or in Late Pleistocene times (100–17 ka: Viseras & Fernández, 1992; Calvache & Viseras, 1997; 42 ka: Azañón et al., 2006), the hydrographic network of the sedimentary depression was captured by the Guadiana Menor River, a tributary of the Guadalquivir River. This resulted in the transit from an endorheic regime to an exorheic one, leading to a stage in which erosion dominated over sedimentation. As a result, a badlands landscape predominates now in the region, linked to a mean annual precipitation (MAP) of ~ 300 mm in the innermost part of the sedimentary depression (https://es.climate-data.org). However, climate was more humid during the late Early Pleistocene, with an estimated MAP of ~ 700 mm in BL/FN3 and ~ 850 mm in VM (Palmqvist et al., 2022c).

1.2 Hot springs currently active in the Baza Basin

Tectonic dynamism resulted in hot springs, several of which are currently active in the Baza Basin and other nearby areas (Cruz-Sanjulián et al., 1972; Cruz-Sanjulián & García-Rosell, 1972, 1975; Diputación de Granada-ITGE, 1990; Fig. 1A, B, and Table 2). There are twelve hot springs in the Baza Basin and four in the Guadix Basin, all of them associated with regional faults. In the case of the hot springs of the Baza Basin, their water output temperatures range between 18 °C and 22 °C, except in the case of the 'Baños de Zújar' spring, with 38 °C. The hydrochemistry of the low temperature springs shows a predominance of calcium bicarbonate. In contrast, the high temperature springs mainly show silica, chlorides, and sulphates. This correspondence between high water output temperatures and siliceous-sulphate-chloride hydrochemistry appears also in the > 30 °C hot springs of the Guadix Basin. The current climatic scenario of the Baza Basin shows an average annual temperature of 13.5 °C (13.8 °C in the Baza station and 13.3 °C in the Orce station; https://es.climate-data.org), with strong annual oscillations. Specifically, average temperature ranges between 5 °C and

Table 2 Hot springs currently active in the Guadix-Baza Depression

Hot Springs	Temperature (ºC)	Water flow (l s^{-1})	Conductivity (µS cm^{-1})	Ca^{2+}	Mg^{2+}	Na^{+}	K^{+}	HCO_3^{-}	SO_4^{2-}	Cl^{-}	SiO_2	GeoT (ºC)
1- Los Tubos. Sª Castril-S	22	100	600	3.2	2.7	1.0	0.0	5.3	0.7	0.9	0	
2- Parpacén. Huéscar-S	18	150	750	5.1	3.7	0.6	0.0	4.7	3.0	0.6	0	
3- Fuencaliente Huéscar	19	400	1034	4.8	4.0	3.0	0.1	4.2	2.7	3.1	0	
4- El Marchal. Orce-N	20	10	895	8.3	3.4	0.5	0.0	3.4	8.2	0.6	0	
5- Fuente Almorzara. Orce	19	40	351	3.5	1.6	0.4	0.0	4.5	0.4	0.7	0	
6- Fuencaliente Orce	21	80	1034	6.4	3.6	2.3	0.4	5.4	4.8	2.6	0	
7- Fuente Balsa Alquería Orce-W	19.5	10	844	5.9	2.9	0.6	0.0	4.3	3.9	0.6	0	
8- El Vaho Orce-E	19.5	15	823	5.2	3.2	0.9	0.0	4.2	3.9	1.0	0	
9- Las Calenturas. Jabalcón-SW	18	2	1790	7.7	11.4	2.0	0.4	7.0	12.0	2.4	0	
10- Panadero. Jabalcón-E	18	1	1420	6.8	7.9	0.6	0.1	7.3	7.9	0.7	0	
11- Fuencaliente. Jabalcón-W	21	15	1250	7.7	3.3	0.9	0.1	4.8	6.5	0.7	0	
12- Baños de Zújar. Jabalcón-N	38	180	4700	30.2	12.3	34.2	0.4	2.5	35.2	36.2	42	88 (Na/K)
A- Baños de Alicún	34	240	1525	17.4	7.0	2.8	0.1	4.2	21.9	2.5	16	
B- Fuente Alta. Huélago-W	22	150	610	6.2	2.4	1.7	0.1	3.4	3.6	2.2	11	
C- Baños de Graena	44	10	2650	30.4	8.0	0.9	0.2	2.3	31.4	0.6	54	89 (Na/K)
D- Los Bañuelos. La Peza-NW	30	1	3410	26.8	9.4	4.7	0.4	2.8	31.5	6.1	0	
Range	18-44ºC	Total: 1404 (l s^{-1})	351-4700	3.2-30.4	1.6-12.3	0.4-34.2	0.0-0.4	2.3-7.3	0.4-35.2	0.6-36.2	0-54	

The position of hydrothermal upwellings is shown in Figure 1B. Average composition values (in mg/l), temperatures, water flows and conductivities according to Diputación de Granada-ITGE (1990) and Cruz-Sanjulian et al. (1972). Hot springs A, B, C, and D are located in the Guadix Basin. The other twelve hot springs are placed in the Baza Basin. *GeoT* geothermometers estimated using the Na/K calculation method (Fournier, 1977; Fournier & Truesdell, 1973; Giggenbach et al., 1988)

9 °C from November to March, averaging ~ 25 °C during summer. Likewise, the historical record of annual rainfall averages 335 mm at the Baza station and 366 mm at the Orce station (https://es.climate-data.org). In any case, the average water output temperature of the hot springs in the Baza Basin is 21 °C, which is 7.5 °C higher than the average annual atmospheric temperature in the basin. These data indicate that the water output temperatures of the springs are slightly lower than the average temperatures in summer, but much higher than in autumn and winter. This underlines the thermal character of these hot springs, whose flow rate varies between 1 and 400 l/s.

1.3 Tectonic dynamism

From a tectonic point of view, the Baza Basin lies in the interior of the alpine-type Betic mountain range, showing three main fracture systems, which are NE-SW, NNW-SSE and NNE-SSW oriented (Sanz de Galdeano, 1983, 1990, 2008; Sanz de Galdeano & Vera, 1991, 1992; Sanz de Galdeano et al., 2007, 2012). These fractures played an important role in the tectono-sedimentary evolution of the Betic mountain range and generated a deep step-like geometry, which is indicative of epicortical extension processes (Platt et al., 2013; Sanz de Galdeano & Vera, 1992). Sanz de Galdeano et al. (2007) established two depocenters in the Baza Basin, induced by NNW-SSE and N70ºE faults that resulted in a regional ENE extension, as deduced by gravity maps of regional, residual and Bouguer anomalies: −150 mGal in Benamaurel (central zone of Baza Basin) and −16 mGal at the north of the Orce village (central zone of Orce sub-basin). Considering basement densities of 2.67 g/cm^3 and 2.32 g/cm^3 for the sedimentary infillings of both sectors, respectively (Sanz de Galdeano et al., 2007), these result in basement depths of ~ 1300 m and ~ 500 m, respectively. In this sense, Sanz de Galdeano (2008) highlighted the Cadiz-Alicante N70ºE fault as the boundary of the inferred depocenters in the central Baza and Orce-North sectors. Likewise, Sanz de Galdeano et al., (2012, 2020) described using geological criteria the main active fractures present in the Baza Basin, which have most likely induced the historical earthquakes recorded in this region: the Galera Fault (23 km long and > 5 km deep), the Baza Fault (37 km long and > 10 km deep), the

Botardo-Alfahuara Fault (22 km long and > 5 km deep), the Benamaurel Fault (19 km long and > 10 km deep), and the Cúllar Fault (North and West, ~ 9 km long and 5–10 km deep, deduced in this case only by seismic criteria). Seismic phenomena were frequent during the Plio-Pleistocene, as evidenced by the presence of paleo-seismites (Alfaro et al., 1997; 2000; 2010; Gibert et al., 2005). Therefore, considering a standard value of the upper crustal geothermal gradient of 30º C/km (Gupta & Roy, 2007; Harrison et al., 1990), the depth calculated for these faults and the possible hydrothermal phenomena associated with them, we estimate temperatures of at least 150°–300 °C in their deepest zones.

1.4 Objectives

The main goal of this study is to establish a causal link between the presence of hydrothermal upwelling-related deposits in the continental Plio-Pleistocene infillings of the Baza Basin, their tectono-sedimentary origin, and their paleoecological consequences. For doing so, we have: (i) reviewed and documented the tectono-sedimentary context of the Baza Basin; (ii) performed a detailed field study, sampling selected stratigraphic sections; (iii) studied the sedimentology of these sections, analyzing the geochemical and mineralogical composition of the samples; and (iv) performed both local and high scale (Africa and Eurasia) correlations of the relationship between tectonic activity and thermal springs, on the one hand, and the presence of archeological and paleontological sites, on the other.

2 Materials and Methods

We have reviewed and documented the tectono-sedimentary context of the main archaeological and paleontological sites of the Baza Basin, as well as the sedimentary and compositional models of many modern and ancient thermal springs worldwide distributed together with the paleoanthropological sites linked to these springs. Field work in the Baza Basin consisted of geological mapping and observations at a mesoscopic scale of lithologies and their sedimentary structures, as well as of the main faults affecting the sedimentary infillings of the basin. Detailed stratigraphic profiles were obtained and the different sedimentary facies present in them were sampled (Fig. 2). Extensive sediment sampling was carried out along the stratigraphic record surveyed (Fig. 1B, C, Fig. 2) to perform mineral and chemical analyses for identifying those facies potentially associated with a hydrothermal origin.

In this study, we have analyzed 56 samples located throughout the Baza Basin, which correspond to eight types of lithologies: calcilutites, lutites, dark lutites, marls, travertines, cherts, gypsum, and native sulfur. All samples were obtained in clean field sections. For each sample, ~200 g of sediments were stored in an airtight bag, which was marked with the corresponding acronym (abbreviations of samples collected from sections/sites are indicated in Fig. 2). These samples were subjected in the laboratory to grinding and mixing in an agate mortar. Then, ~20 g were randomly selected from each sample for performing the analyses. The samples were analyzed geochemically by means of X-ray fluorescence (XRF). In addition, 14 of these samples were selected for analyzing their mineralogy by means of X-ray diffraction (XRD). All measurements were carried out at the Central Services of Support to Research ('Servicios Centrales de Apoyo a la Investigación', SCAI) of the University of Málaga (UMA).

2.1 Elemental analysis

Chemical analyses of the abundance of major and some trace elements were carried out using a Thermo Fisher ADVANT'XP wavelength dispersive atomic fluorescence spectrometer (XRF). This equipment consists of an autosampler with capacity for a total of 161 samples, a Rh tube and a goniometer with three collimators and four crystals that allow measuring from F to U. The measurements were obtained in a He atmosphere with the sample in bead. The results were analyzed with Thermofisher's UniQuant software, which allows the semi-quantification of unknown materials without the need of standards or reference materials. Measurement errors ranged between 0.3% and 1.5% for major elements, raising to 5% in the case of minor elements. The detection limit of these analyses was of 0.01%, which was quoted in the corresponding tables as "bld" (i.e., below the detection limit).

In order to evaluate the influence of hydrothermal activity, the ratios (Fe + Mn)/Ti and Al/(Al + Fe + Mn) were calculated (Boström et al., 1973; Madondo et al., 2021; Murray, 1994; Zhang et al., 2023). Moreover, an Al–Fe–Mn ternary diagram was also used to differentiate between hydrothermal, detrital or biogenic origins (Adachi et al., 1986).

2.2 Mineralogical analysis

Fourteen samples, selected a priori as potentially indicative of being generated in a hydrothermal context, were analyzed by X-ray Diffraction (XRD) based on the XRF data. The measurements were obtained with an X'Pert PRO MPD diffractometer from PANalytical and measured in high resolution conditions. The X-ray tube has a Cu anode and the diffractometer in the incident beam consists of a Johansson-type primary monochromator with a Ge (111) crystal, which provides a strictly monochromatic Cu

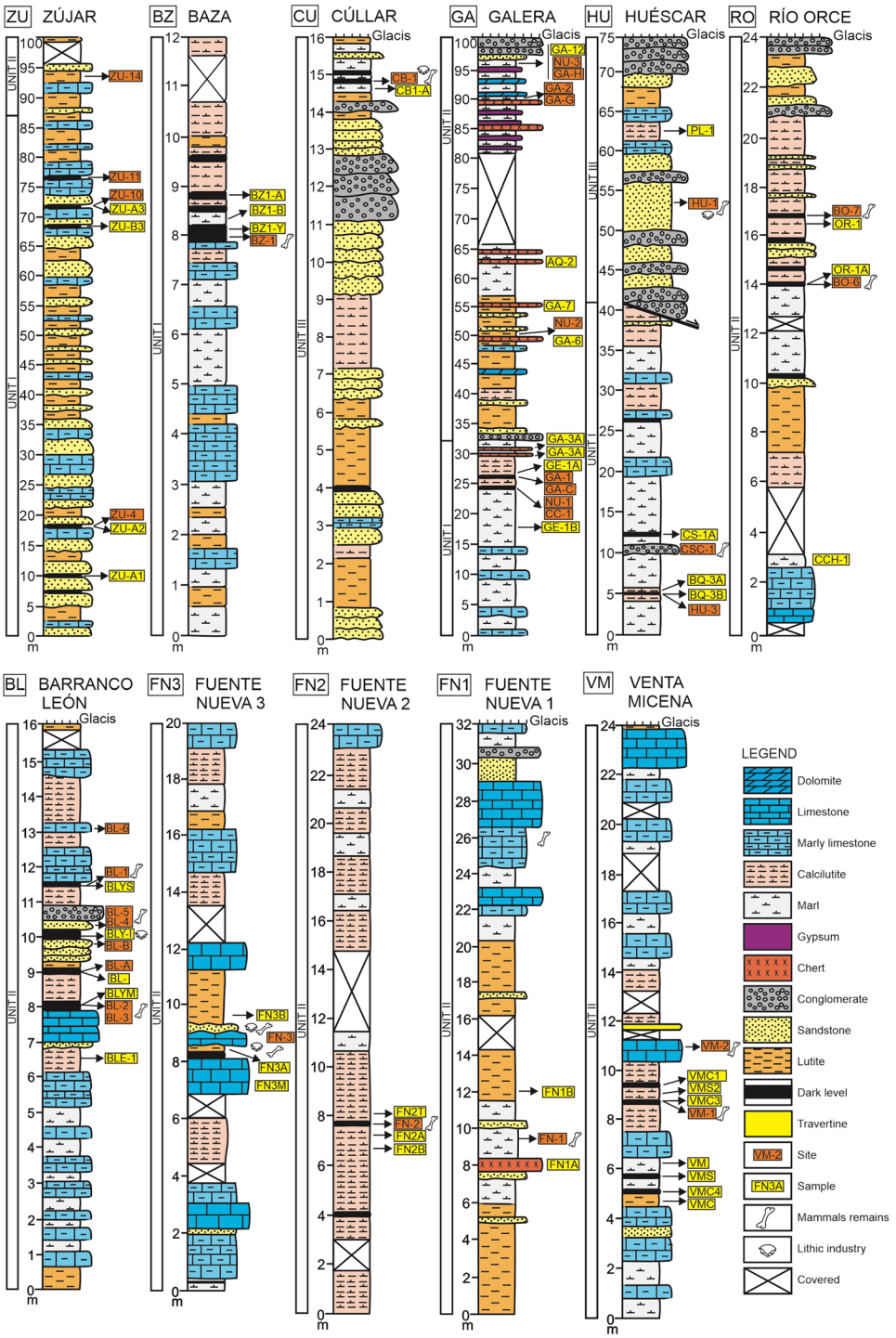

Fig. 2 Stratigraphic profiles of the Baza Basin. The codes with the position of these series are shown in Fig. 1B, C

$K_{\alpha 1}$ radiation. Random powder X-ray diffraction (XRD) of bulk-rocks was used for the identification of mineral phases, measuring the diffraction angles and the intensities of the diffracted beams. This allows to compare the resulting diffraction pattern with a reference database. The comparison was carried out with PDF-4 + 2021 (Gates-Rector & Blanton, 2019). When the acquired data were of sufficient quality (i.e., measured with a wide range of angles, good resolution and high intensity/noise ratio), they were used not only to identify mineral phases but also to measure them in a semi-quantitative fashion. To determine the proportion of phyllosilicate in the global samples, the phyllosilicates (4.46 Å)/quartz (3.343 Å) peak-area ratio was estimated from XRD patterns of randomly oriented powder. D-spacing and the full width at half-high maximum (FWHM) were determined on the (101) reflection

peak of the opal specimen in order to establish the type of opal polymorphs (Elzea et al., 1994). For mineral abundance, the results of the analyses were expressed semi-quantitatively; the error of the estimates ranged from 5 to 10%. For each sample, a relative range of abundance was indicated for each mineral.

3 Results

Almost one hundred archeological and paleontological sites with vertebrate remains dated between the Early Pliocene (Ruscinian) and the late Early Pleistocene (Galerian) have been described in the Baza Basin (e.g., Cuevas et al., 1984; Agustí, 1985; Mazo et al., 1985; Moyà-Solà et al., 1987; Alberdi & Bonadonna, 1989; Martínez-Navarro, 1991; Sesé, 1994; Soria & Ruiz-Bustos, 1992; Guerra-Merchán, 1992; Ros-Montoya, 2010; Maldonado-Garrido et al., 2017; Ros-Montoya et al., 2017, 2018; Martínez-Navarro et al., 2018). Thirty-three of these sites were selected by their archaeological or paleontological relevance, as well as by their clear geographic, stratigraphic and chronological definition (Table 1). Of these sites, 82% (27 out of 33) lie in the Orce sub-basin. Thirteen sites (39%) yielded macrovertebrate remains, with evidence of hominin presence in four of them. These sites were also positioned in a stratigraphic series (Fig. 2). In terms of age, 27% of sites are from the Ruscinian, 6% from the Lower Villafranchian, 18% from the Middle Villafranchian, 43% from the Upper Villafranchian, 3% from the Epivillafranchian, and the remaining 3% from the Galerian.

The field study showed the presence of 17 levels of cherts, all located in the Orce sub-basin, mainly to the south of the town of Galera (Fig. 1C). Some paleontological sites (e.g., FN-1, GA-2 and NU-2) are situated just a few decimeters above these siliceous deposits (Fig. 2). Chert beds typically occur in irregular shaped strata, with a lateral extent ranging from 7 m to > 200 m, and a thickness of 8–80 cm (Fig. 3A, C). The cartographic relationship between the appearance of cherts and the presence of tectonic fractures is remarkable (Fig. 1C; Fig. 3G, I, J). Lithologically, these cherts appear as white, dark gray or light brown massive facies. At an outcrop scale, they show abundant diaclases, micropores, changes of coloration, and the presence of conchoidal fractures. In some cases, the cherts appear with decimeter to centimeter-scale gypsum mineralizations within them (Fig. 3H). Another remarkable aspect is that these cherts appear in different sedimentary contexts, in stratigraphic contact with other six types of facies: limestones, marls, gypsum, (calci)lutites, and sandstones (Fig. 2).

3.1 Elemental analysis

Quantitative analyses of chemical elements were performed (Tables 3 and 4). The results were plotted in the Al–Fe-Mn diagram and the two following ratios were calculated: (Fe + Mn)/Ti and Al/(Al + Fe + Mn) (Fig. 5 and Table 5). A common feature of hydrothermal deposits is an Al/(Al + Fe + Mn) ratio of < 0.4, along with a (Fe + Mn)/Ti ratio of > 15 (Boström et al., 1973; Murray, 1994; Zhang et al., 2023). Forty-two out of the fifty-six samples analyzed did not show mineral and/or geochemical indicators that could a priori be linked to hydrothermal contexts, while 14 provided preliminary results that are compatible with a hydrothermal origin according to the Al–Fe-Mn diagram and the (Fe + Mn)/Ti − Al/(Al + Fe + Mn) ratios (Boström et al., 1973; Adachi et al., 1986; Yamamoto, 1987; Murray, 1994; Yamamoto et al., 2013, Fig. 5 and Table 5). Eight of these samples (AQ-2, GA-3A, GA-3B, GA-6, GA-7, SX-A, FN1A and CN-1) correspond to cherts, three to travertines (CCH-B, TCV and TE100), two to calcilutites (PL-1 and OR-1) and one to dark lutites (BZ1-A). Except for the dark lutites of the Pliocene site of Baza-1 (Figs. 1B and 2), all the others come from materials in the Orce sub-basin of Upper Pliocene to Upper Pleistocene age. The (Fe + Mn)/Ti and Al/(Al + Fe + Mn) ratios of these samples agree with conditions of hydrothermalism for the samples of travertines and calcilutites, but not for sample the dark lutites. The last sample provided results of 13.24 and 0.42, respectively. Although these values are very close to the limit of hydrothermal conditions (> 15 and < 0.4, respectively), they are placed outside the area of hydrothermalism. These geochemical ratios could not be applied to chert samples, because neither Al nor Ti were measured in them.

Chert samples showed SiO_2 concentrations in excess of 90%, with the exception of two samples, FN1A and GA-6, which exhibited higher concentrations of other compounds (e.g., 14.23% of CaO in FN1A and 5.72% in GA-6). Their variance in composition may be attributed to the presence of calcite in the case of FN1A and gypsum in the case of GA-6, in which a concentration of 6.6% of SO_3 was measured (Table 3). Other trace elements are present in proportions < 1% by weight. The geochemical composition of the cherts exhibits an uneven distribution of trace elements (Table 4). Al was absent in all cases, and this was also the case for Mn except for samples CN1 and FN1A, in which this element was recorded with abundances of < 0.03%. Fe, Ca, and Cl were consistently detected in all samples. Moreover, Mg, S, K, and Cu were present in every sample except CN1, but the proportions of these elements were lower than in the other samples analyzed in this study.

The five additional samples linked a priori to a hydrothermal origin include travertines, dark lutites and calcilutites.

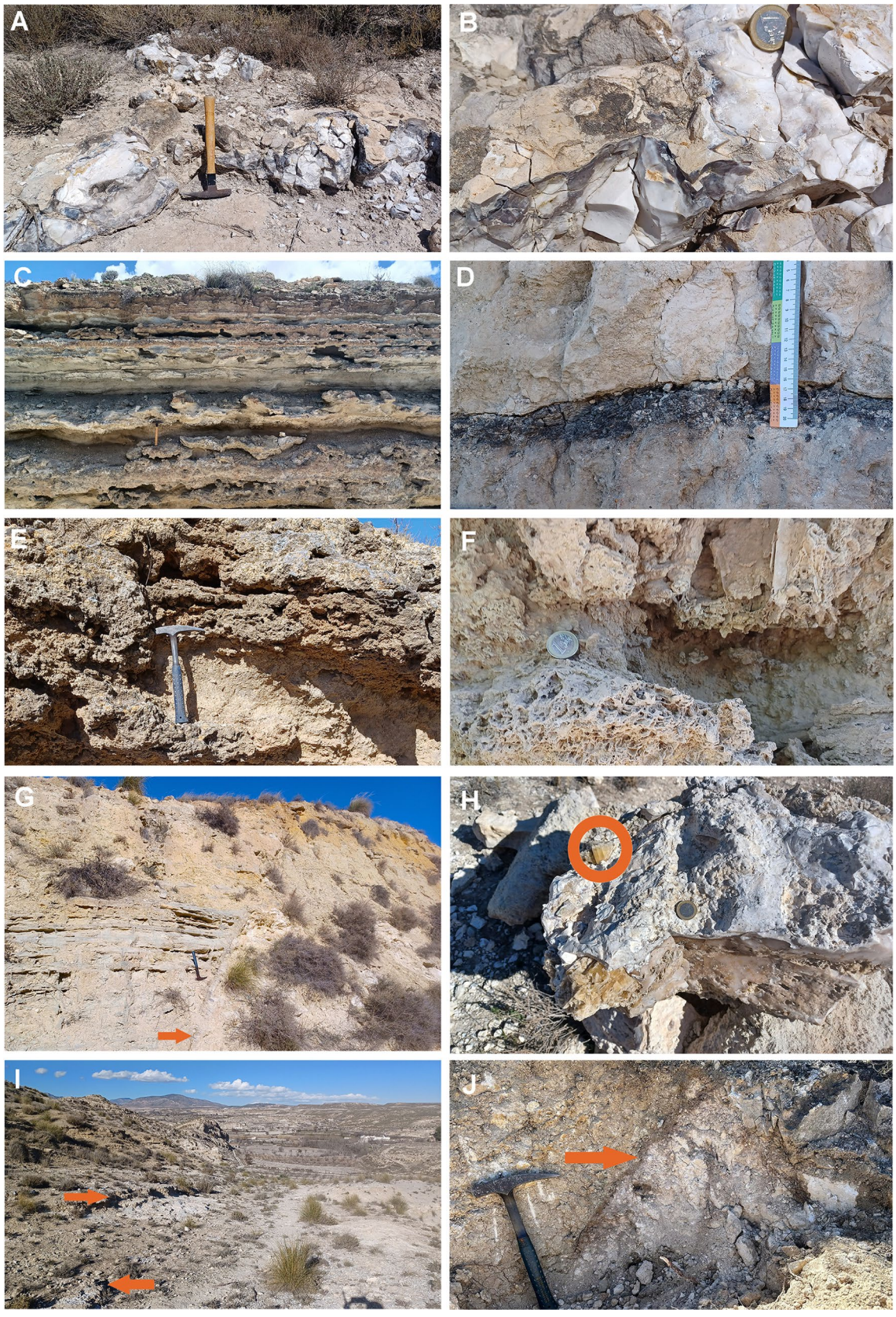
A
B
C
D
E
F
G
H
I
J

◂**Fig. 3** Field images of cherts and other facies linked to hydrothermal scenarios and associated to tectonic fractures. **A** Deposits of light colored cherts, which are located 3 km to the NW of the Orce town (sample SX-A, Fig. 1C); **B** detail of white cherts located close to the FN1 paleontological site (sample FN1A, Fig. 2); **C** thin level of grey to blue cherts (just at the top of the hammer), located at south of the Galera town (sample GA-6, Fig. 2); note the presence of deformed layers at the bottom of this image. **D** dark level located at the BZ-1 Pliocene site (sample BZ-1A, Fig. 2). **E** travertines (sample TE100, Fig. 1C) located west of Orce. **F** detail of these travertine facies. **G** NE-SW oriented tectonic fault present at the south of Galera (marked with an orange arrow), which affects the chert levels; the fault plane appears to be filled with gypsum ore. **H** mineral association between gypsum crystals (marked with an orange circle) and cherts, near the locality of Galera. **I** ~ 3 m wide chert dyke (the limits of the dyke are marked with orange arrows) with a NE-SW orientation, which coincides with a tectonic fracture near Galera (Fig. 1C). **J** detail of the N105°E tectonic contact between a chert layer and a deposit of calciarenites (marked with an orange arrow), which appears close to the paleontological site of FN1 (Fig. 1C)

The travertine levels (samples CCH-B, TCV and TE100, Fig. 1C) are located to the west of the town of Orce. They consist of brown stratiform layers (Fig. 3E) in sedimentary unconformity with the materials deposited below them, which form patchy structures with a lateral development limited to a few meters or, in the case of samples TCV and TE100, to ~25 m. Internal annular carbonate growths developed over previous vegetal structures are visible in these travertines (Fig. 3F). Pisolitic gravels of chaotic aspect and centimeter-scale speleothems are also common. The other travertines present in the Baza Basin show stratiform levels of decimetric thickness in the Venta Micena sector (Fig. 2), where they are stratigraphically close to the paleontological sites of this area, and there are also travertine buildings of metric thickness in the vicinity of currently active hydrothermal springs in the Zújar sector (Fig. 1B). According to the dating of similar travertine deposits in the Alicún de las Torres current hot spring, which is located in the Guadix Basin (Crespo et al., 2014; Hernández et al., 2000), the age of these travertines is Middle to Late Pleistocene.

The dark lutites that show a geochemical profile compatible with a hydrothermal origin consist of a ~ 5 cm thick level that is located at 45 cm from the top of the Baza-1 paleontological site (Figs. 2 and 3D). From a lithological point of view, these lutites show dark gray tones and contain sub-millimeter-scale parallel laminations, root remains, small fragments of gastropod shells, oxidations, and micas randomly distributed in the sediment. The presence of dark lutites in the Baza Basin is commonly recorded in thin layers present in most of the stratigraphic series of Plio-Pleistocene age (Fig. 2). Mesoscopic scale sedimentary structures of traction origin and linked to detrital deposits (e.g., sandy microlevels, coarsening/finning upward sequences, imbrications, or scour-marks) are absent. Analyses of sample BZ1-A (Tables 3 and 4) showed a main chemical composition of Si > Fe > Al > Ca > K > Mg. Compared to other dark lutites studied, BZ1-A stands out for its notably higher concentration of Fe_2O_3, which reaches 11.19%. This iron content exceeds those of other samples of dark lutites. Additionally, this sample exhibits elevated levels of K, Mn, S, Cl, Ba, Cu, Rb, Pb, Sn, and Cs compared to the average contents of the samples of dark lutites.

Calcilutites are present in all stratigraphic profiles except Zújar (Fig. 2) and use to appear as light-colored levels of decimetric to metric thickness. From a lithological point of view, they typically exhibit massive facies or scarce internal arrangement, although sometimes there are internal shallowing-upward sequences with edaphogenic-type facies of reddish tones situated at their top. The PL-1 calcilutite sample shows a main geochemical composition of Ca > Si > Fe > Al > Mg (Tables 3 and 4). The rest of the elements detected appeared with concentrations < 0.6%. In comparison with other calcilutites of the basin, this sample has the highest CaO values and the lowest of SiO_2, Al_2O_3, K_2O, TiO_2, Na_2O, and SO_3. Finally, the OR-1 calcilutite sample shows a main geochemical composition of Si > Ca > Mn > Al > Fe > Mg. The rest of the elements detected appear with concentrations < 0.7%. This sample exhibits the highest MnO value (~ 10 times more) compared to the average of the calcilutite samples. Additionally, geochemical analyses revealed the presence of some trace elements in the samples (Table 4). Of these, Ba stands out, being exclusively detected in four samples a priori linked to hydrothermal environments: BZ1-A (dark lutites), OR-1 (calcilutites), TCV (travertines), and TE100 (travertines).

3.2 Mineralogical analysis

The XRD data of cherts show that opal is the principal phase (Table 6, Fig. 4). The $d_{(101)}$ (> 4.07 Å) and the full width at half-high maximum (FWHM) reflection peak intensity of opal (101) indicate that CT is the polymorph of the opal (Elzea et al., 1994). Most of the samples taken in Galera showed the presence of gypsum in the XRD data, as evidenced by geochemistry (high CaO and SO_3 contents, Table 3) and field observations (Fig. 3H). The presence of silicates and carbonates in some samples (e.g., CN-1, GA-3B and SX-A) may come from the remains of the sedimentary materials above and/or below the levels where these samples were obtained, due to the irregular morphology of the chert strata. Travertine samples mainly consist of calcite (Table 6) and, to a lesser extent, pyrolusite. In addition, other mineral species such as gypsum and halite were found. The XRD data from these samples agree with the expectations from geochemical (Tables 3 and 4) and lithological data. The analyses carried out on the calcilutites of samples PL-1 and OR-1 (Table 6) showed a mineral composition of calcite, quartz and phyllosilicates (muscovite and paragonite). In

Table 3 Quantitative elemental analysis for major elements using XRF and means and standard deviations for each lithology

Sample	Location / Site	Age	SiO_2	Al_2O_3	Fe_2O_3	MnO	MgO	CaO	Na_2O	K_2O	TiO_2	P_2O_5	ZrO_2	SO_3	LOI
SX-A	Northwest Orce	Middle Villafr.	87.61	bld	0.14	bld	0.13	4.42	bld	0.05	bld	0.02	bld	0.07	7.53
FN1A	Fuente Nueva-1	Middle Villafr.	68.28	bld	1.36	0.02	0.41	14.23	0.09	bld	bld	0.02	bld	1.17	14.08
CN1	Cañada del Negro	Middle Villafr.	94.98	bld	0.22	0.01	bld	0.61	bld	bld	bld	0.01	bld	bld	4.05
AQ-2	Galera	Early Villafr.?	93.50	bld	0.09	bld	0.71	0.24	0.16	0.02	bld	bld	bld	0.09	5.09
GA-7	Galera	Ruscinian	93.87	bld	0.06	bld	0.50	0.60	0.11	0.03	bld	bld	bld	0.48	4.26
GA-6	Galera	Ruscinian	79.82	bld	0.17	bld	0.47	5.72	0.21	0.05	bld	bld	bld	6.60	6.87
GA-3B	Galera	Ruscinian	95.52	bld	0.04	bld	0.18	0.33	bld	0.02	bld	bld	bld	1.02	2.84
GA-3A	Galera	Ruscinian	95.04	bld	0.05	bld	0.24	0.59	bld	0.01	bld	bld	bld	0.36	3.65
TCV	West Orce	Galerian	4.04	0.58	2.59	6.10	1.72	42.05	0.76	1.19	0.09	0.04	0.02	3.9	34.92
TE100	West Orce	Galerian	0.91	0.08	3.30	3.28	1.84	43.12	1.23	1.64	0.01	0.03	bld	1.61	40.83
CCH-B	West Orce	Galerian	0.78	0.57	0.40	0.01	0.84	52.62	0.20	0.30	0.01	0.06	bld	0.81	43.24
SX-B	Northwest Orce	Middle Villafr.	13.91	2.01	0.93	0.02	1.99	44.31	bld	0.57	0.13	0.06	bld	0.18	35.82
BNA-1	Benamaurel	Middle Villafr.	0.95	0.41	0.15	bld	2.60	8.98	bld	0.08	0.01	bld	bld	16.28	70.53
BN-N	Benamaurel	Middle Villafr.	0.56	0.31	0.22	bld	1.07	36.97	bld	0.07	0.01	bld	bld	43.74	17.04
BNA-2	Benamaurel	Middle Villafr.	1.46	0.61	0.28	bld	0.52	33.53	bld	0.13	0.02	bld	bld	42.06	21.35
BLYS	Barranco León	Late Villafr.	58.55	15.23	6.97	0.02	2.28	1.50	0.88	1.99	1.06	0.08	0.09	0.25	10.17
BLYI	Barranco León	Late Villafr.	77.32	8.21	3.77	0.04	0.87	1.40	0.92	1.32	2.11	0.07	0.31	0.16	3.24
BL-	Barranco León	Late Villafr.	26.02	4.09	1.97	0.02	1.73	33.99	0.25	0.68	0.58	0.05	0.08	0.24	29.94
BLYM	Barranco León	Late Villafr.	62.17	15.71	5.51	0.04	2.41	1.19	0.89	2.40	1.84	0.10	0.19	0.09	7.01
OR-1A	Río Orce	Late Villafranch.	54.53	17.39	5.03	0.03	3.84	2.80	0.34	3.11	0.94	0.08	0.06	0.05	11.51
VMC1	Venta Micena	Late Villafr.	55.44	16.78	4.55	0.02	4.56	0.85	0.47	2.41	0.82	0.05	0.04	0.13	12.34
VMC3	Venta Micena	Late Villafr.	54.25	16.07	4.66	0.02	5.15	2.71	0.44	2.38	0.82	0.10	0.02	0.21	12.57
VMS4	Venta Micena	Late Villafr.	46.49	9.00	2.93	0.03	2.58	16.37	0.73	1.49	0.85	1.05	0.08	0.73	17.08
VMC4	Venta Micena	Late Villafr.	58.74	10.95	3.28	0.02	2.86	6.47	0.86	1.75	0.89	1.25	0.07	0.14	11.10
ZU-B3	Zújar	Early Villafr.	60.71	17.61	4.85	0.02	2.69	0.56	0.72	3.02	1.06	0.10	0.11	0.07	8.02
ZU-A3	Zújar	Early Villafr.	50.12	19.29	6.62	0.03	5.12	1.29	1.12	3.85	0.84	0.11	0.04	0.02	11.03
GE1A	Galera	Ruscinian	38.30	10.97	3.94	0.02	2.82	19.45	0.22	1.80	0.52	0.11	0.03	0.11	21.26
CS-1A	Huéscar	Ruscinian	55.14	13.54	4.10	0.03	3.99	6.40	0.23	2.29	0.92	0.10	0.08	0.04	12.77
BQ-3B	Huéscar	Ruscinian	40.81	13.77	6.96	0.03	2.55	13.48	0.32	1.81	0.72	0.12	0.03	0.06	18.68
ZU-A2	Zújar	Ruscinian	57.44	10.85	6.69	0.02	8.47	0.48	0.38	1.83	0.63	0.02	0.04	0.03	12.77
BZ1-A	Baza-1	Ruscinian	35.83	10.56	11.19	0.04	1.87	6.79	0.81	3.60	0.99	0.08	0.08	1.11	21.47
BZ1-Y	Baza-1	Ruscinian	43.42	11.96	3.82	0.02	5.50	7.56	0.36	1.86	0.71	0.29	0.05	0.04	23.98
FN3A	Fuente Nueva-3	Late Villafr.	59.30	18.78	5.93	0.03	3.18	0.85	0.45	3.16	1.04	0.12	0.07	0.05	6.76
FN3B	Fuente Nueva-3	Late Villafr.	62.48	13.56	6.90	0.03	2.35	2.15	0.56	2.22	1.15	0.59	0.10	0.11	6.77
VMC	Venta Micena	Late Villafr.	13.37	3.52	1.42	0.02	3.85	39.74	0.22	0.54	0.18	0.03	0.01	0.31	36.40

Table 3 (continued)

BQ-3A	Huéscar	Ruscinian	39.90	13.59	3.64	0.02	3.50	14.15	0.42	2.05	0.64	0.24	0.03	0.10	20.19
PL-1	Huéscar	Epivillafr.	21.83	2.32	2.68	0.03	1.84	37.15	0.13	0.53	0.13	0.08	0.01	0.06	33.04
BLE1	Barranco León	Late Villafr.	32.94	8.10	2.84	0.02	1.69	26.77	1.40	1.40	0.64	0.04	0.07	0.18	23.54
OR-1	Río Orce	Late Villafr.	30.97	4.08	2.88	4.48	1.49	27.38	0.33	0.63	0.50	0.02	0.02	0.17	26.33
FN2T	Fuente Nueva-2	Late Villafr.	33.78	10.23	3.70	0.03	2.93	23.00	0.25	1.28	0.50	0.04	0.03	0.10	23.80
FN2A	Fuente Nueva-2	Late Villafr.	30.74	10.28	3.50	0.03	3.52	23.72	0.41	1.19	0.49	0.08	0.03	0.22	25.55
FN2B	Fuente Nueva-2	Late Villafr.	24.16	7.80	2.57	0.05	3.13	30.58	0.27	1.14	0.36	0.05	0.02	0.23	29.36
VMS2	Venta Micena	Late Villafr.	23.66	5.94	2.21	0.02	2.44	32.89	0.50	1.12	0.31	0.06	0.02	0.18	30.24
TS	Torre del Salar	Middle Villafr.	28.51	5.01	1.95	0.04	12.54	19.45	0.28	1.07	0.33	0.07	0.03	0.19	30.33
FN1B	Fuente Nueva-1	Middle Villafr.	36.15	10.18	4.99	0.05	2.50	21.12	0.35	1.35	0.66	0.05	0.05	0.10	22.26
ZU-A1	Zújar	Ruscinian	39.76	14.25	4.90	0.03	5.12	11.31	0.93	2.83	0.42	0.24	0.02	0.27	19.25
CB-1A	Cúllar Baza 1	Galerian	3.85	1.05	0.56	0.02	2.90	41.80	1.61	0.13	0.06	0.19	0.01	0.53	44.03
FN3M	Fuente Nueva-3	Late Villafr.	7.21	1.77	1.21	0.02	1.31	46.17	0.16	0.30	0.12	0.05	0.02	0.40	40.74
VM	Venta Micena	Late Villafr.	20.20	4.03	1.71	0.03	2.46	37.00	0.19	0.82	0.34	0.06	bld	0.08	32.92
CCH-1	West Orce	Middle Villafr.	17.10	5.99	1.90	0.03	1.99	34.19	0.20	1.02	0.27	0.19	0.01	5.39	31.32
GA-12	Galera	Middle Villafr.	24.78	2.74	1.66	0.05	12.95	23.14	0.31	0.57	0.39	0.03	bld	0.82	32.55
BNA-5	Benamaurel	Middle Villafr.	6.00	1.91	0.87	0.02	15.23	5.78	0.08	0.45	0.07	0.02	bld	32.53	37.00
BNA-3	Benamaurel	Middle Villafr.	10.49	2.90	1.24	bld	5.73	13.30	0.23	0.80	0.14	0.03	bld	30.20	34.92
BNA-4	Benamaurel	Middle Villafr.	8.39	2.74	1.22	0.03	16.79	20.38	0.28	0.64	0.11	0.06	bld	14.36	34.96
GE1B	Galera	Ruscinian	15.40	4.57	1.72	0.03	1.86	39.79	0.13	0.76	0.21	0.11	0.01	0.33	34.72
BZ1-B	Baza-1	Ruscinian	9.30	2.27	1.05	0.02	2.61	43.62	0.15	0.39	0.16	0.15	0.02	0.21	39.46

Means ± Standard deviations	SiO_2	Al_2O_3	Fe_2O_3	MnO	MgO	CaO	Na_2O	K_2O	TiO_2	P_2O_5	ZrO_2	SO_3	LOI
Cherts	88.58 ±9.80		0.27 ±0.45	0.02 ±0.01	0.38 ±0.20	3.34 ±4.88	0.14 ±0.06	0.03 ±0.01		0.02 ±0.01		1.40 ±2.33	6.05 ±3.62
Travertines	4.91 ±6.19	0.81 ±0.83	1.81 ±1.36	2.35 ±2.93	1.60 ±0.52	45.53 ±4.82	0.73 ±0.52	0.93 ±0.60	0.06 ±0.06	0.05 ±0.02	0.02	1.62 ±1.63	38.70 ±3.99
Sulphur	0.95	0.41	0.15		2.60	8.98		0.08	0.01			16.28	70.53
Gypsum	1.01 ±0.64	0.46 ±0.21	0.25 ±0.04		0.80 ±0.39	35.25 ±2.43		0.10 ±0.05	0.01 ±0.01			42.90 ±1.19	19.19 ±3.05
Dark lutites	51.49 ±12.05	13.06 ±3.99	5.11 ±2.14	0.03 ±0.01	3.49 ±1.84	7.25 ±9.01	0.58 ±0.29	2.21 ±0.82	0.96 ±0.42	0.22 ±0.36	0.08 ±0.07	0.20 ±0.29	14.41 ±6.79
Lutites	43.76 ±22.59	12.36 ±6.39	4.47 ±2.45	0.03 ±0.01	3.22 ±0.64	14.22 ±18.03	0.41 ±0.14	1.99 ±1.08	0.75 ±0.44	0.25 ±0.25	0.05 ±0.04	0.14 ±0.11	17.53 ±14.08
Calciluti tes	30.25 ±5.77	7.82 ±3.57	3.22 ±1.05	0.48 ±1.41	3.72 ±3.27	25.34 ±7.36	0.49 ±0.39	1.25 ±0.62	0.43 ±0.16	0.07 ±0.06	0.03 ±0.02	0.17 ±0.07	26.37 ±4.31
Marls	12.27 ±6.79	3.00 ±1.48	1.31 ±0.43	0.03 ±0.01	6.38 ±6.12	30.52 ±13.95	0.33 ±0.45	0.59 ±0.27	0.19 ±0.11	0.09 ±0.07	0.01 ±0.01	8.48 ±12.85	36.26 ±4.03

The results are expressed as oxides weight %. LOI column indicates Loss of Ignition of each sample (%) relative with volatile components. Facies key: cherts (white); travertines (orange); sulphur (yellow); gypsum (light yellow); dark lutites (grey); lutites (blue); calcilutites (pink); marls (violet). Red colored cells indicate the maximum amounts for this element. Green colored cells indicate the minimum amount for this element, above limit detection. *bld* below limit detection (<0.01%)

Table 4 Quantitative elemental analysis for minor elements using XRF and means and standard deviations for each lithology

Sample	Cl	F	SrO	Cr_2O_3	V_2O_5	As_2O_3	NiO	ZnO	CuO	BaO	MoO_3	WO_3	Co_3O_4	PbO	CeO_2	Rb_2O	RuO_4	PdO	SnO_2	Cs_2O
SX-A	bld	bld	bld	bld	0.01	bld	bld	bld	0.02	bld	bld	bld	bld	bld	bld	bld	bld	bld	bld	bld
FN1A	0.01	bld	0.13	bld	bld	0.1	0.02	bld	bld	bld	0.04	0.02	bld	bld	bld	bld	bld	bld	bld	bld
CN1	0.04	bld	bld	bld	bld	bld	0.02	bld	bld	bld	bld	0.02	bld	bld	bld	bld	0.02	bld	bld	bld
AQ-2	0.10	bld	bld	bld	bld	bld	bld	bld	0.01	bld	bld	bld	bld	bld	bld	bld	bld	bld	bld	bld
GA-7	0.08	bld	bld	bld	bld	bld	bld	bld	0.02	bld	bld	bld	bld	bld	bld	bld	bld	bld	bld	bld
GA-6	0.09	bld	bld	bld	bld	bld	bld	bld	0.01	bld	bld	bld	bld	bld	bld	bld	bld	bld	bld	bld
GA-3B	0.05	bld	bld	bld	bld	bld	bld	bld	bld	bld	bld	bld	0.01	bld	bld	bld	bld	bld	bld	bld
GA-3A	0.04	bld	bld	bld	bld	bld	bld	bld	0.02	bld	bld	bld	bld	bld	bld	bld	bld	bld	bld	bld
TCV	0.91	bld	0.77	0.00	0.01	bld	0.03	bld	bld	0.20	0.04	bld	0.01	bld	bld	bld	bld	bld	bld	bld
TE100	1.62	bld	0.14	0.01	0.04	bld	0.06	bld	bld	0.10	bld	bld	0.03	bld	bld	bld	bld	bld	bld	bld
CCH-B	0.15	bld	bld	bld	bld	bld	bld	bld	0.01	bld	bld	bld	bld	bld	bld	bld	bld	bld	bld	bld
SX-B	0.05	bld	bld	bld	bld	bld	bld	bld	0.01	bld	bld	bld	bld	bld	bld	bld	bld	bld	bld	bld
BNA-1	0.01	bld	bld	bld	bld	bld	bld	bld	bld	bld	bld	bld	bld	bld	bld	bld	bld	bld	bld	bld
BN-N	0.02	bld	bld	bld	bld	bld	bld	bld	0.01	bld	bld	bld	bld	bld	bld	bld	bld	bld	bld	bld
BNA-2	0.02	bld	bld	bld	bld	bld	bld	bld	0.02	bld	bld	bld	bld	bld	bld	bld	bld	bld	bld	bld
BLYS	0.13	bld	0.04	0.06	0.27	0.08	0.03	0.01	bld	bld	bld	bld	0.01	bld	bld	bld	bld	bld	bld	bld
BLYI	0.02	bld	0.02	0.02	0.07	bld	0.02	bld	bld	bld	0.01	bld	bld	bld	bld	bld	bld	0.01	bld	bld
BL-	0.01	bld	0.21	0.01	0.03	bld	0.02	bld	bld	bld	0.01	0.01	bld	bld	bld	bld	bld	0.01	bld	bld
BLYM	0.15	bld	0.04	0.03	0.08	bld	0.03	bld	bld	bld	bld	bld	bld	bld	bld	0.01	bld	bld	bld	bld
OR-1A	0.05	bld	0.04	0.03	0.04	bld	0.03	0.02	bld	bld	bld	bld	bld	bld	bld	0.01	bld	bld	bld	bld
VMC1	0.14	1.06	0.04	0.03	0.04	0.09	0.03	0.01	0.01	bld	bld	bld	bld	bld	bld	0.01	bld	0.01	bld	bld
VMC3	0.36	bld	0.03	0.03	0.03	0.08	0.00	0.03	0.01	bld	bld	bld	bld	bld	bld	bld	bld	bld	bld	bld
VMS4	0.2	bld	0.17	0.02	0.06	bld	0.03	0.01	bld	bld	bld	0.01	bld	bld	bld	bld	bld	0.01	bld	bld
VMC4	0.22	1.06	0.09	0.02	0.06	0.07	0.02	bld	bld	bld	bld	bld	bld	bld	bld	bld	bld	bld	bld	bld
ZU-B3	0.12	bld	0.03	0.05	0.04	bld	0.03	0.06	0.01	bld	bld	bld	bld	0.02	0.02	0.02	bld	bld	bld	bld
ZU-A3	0.23	bld	0.04	0.02	0.03	bld	0.03	0.03	0.01	bld	bld	bld	0.01	bld	bld	0.02	0.04	bld	bld	bld
GE1A	0.02	bld	0.13	0.01	0.06	0.11	0.03	bld	bld	bld	bld	bld	bld	bld	bld	bld	bld	bld	bld	bld
CS-1A	0.01	bld	0.11	0.04	0.03	0.06	0.03	0.02	0.01	bld	bld	bld	bld	bld	bld	bld	bld	bld	bld	bld
BQ-3B	0.11	bld	0.10	0.05	0.10	bld	0.04	0.03	bld	bld	bld	bld	0.01	bld	0.02	bld	0.03	0.03	bld	bld
ZU-A2	0.03	bld	0.03	0.03	0.02	bld	0.03	0.13	bld	bld	0.01	bld	0.01	bld	bld	bld	bld	bld	bld	bld
BZ1-A	4.25	bld	0.24	0.04	0.06	bld	0.02	0.04	0.04	0.37	0.05	bld	0.01	0.04	0.02	0.06	bld	bld	0.13	0.12
BZ1-Y	0.05	bld	0.06	0.03	0.04	0.10	0.03	0.02	bld	bld	0.03	bld	bld	bld	bld	bld	bld	bld	bld	bld
FN3A	0.03	bld	0.04	0.03	0.04	bld	0.03	0.02	bld	bld	bld	bld	bld	bld	bld	0.02	bld	bld	bld	bld
FN3B	0.05	bld	0.06	0.06	0.37	bld	0.03	0.03	bld	bld	bld	bld	0.01	bld	0.02	bld	bld	bld	bld	bld
VMC	0.29	bld	0.08	0.00	0.01	bld	bld	bld	bld	bld	bld	bld	bld	bld	bld	bld	bld	bld	bld	bld
BQ-3A	0.18	1.10	0.07	0.04	0.03	bld	0.03	0.03	0.01	bld	bld	bld	bld	bld	bld	bld	bld	0.01	bld	bld
PL-1	0.04	bld	0.06	0.01	bld	bld	0.02	bld	bld	bld	bld	bld	bld	bld	bld	bld	0.01	0.01	bld	bld
BLE1	0.09	bld	0.07	0.02	0.02	0.11	0.02	bld	bld	bld	bld	bld	bld	bld	bld	bld	bld	bld	bld	bld
OR-1	0.10	bld	0.14	0.01	0.02	bld	0.04	bld	bld	0.27	0.01	bld	0.03	bld	bld	bld	0.01	bld	bld	bld
FN2T	0.01	bld	0.10	0.02	0.02	0.11	0.02	bld	bld	bld	bld	bld	bld	bld	bld	bld	bld	0.01	bld	bld
FN2A	0.03	bld	0.10	0.01	0.02	bld	0.03	bld	bld	bld	bld	bld	bld	bld	bld	bld	bld	bld	bld	bld
FN2B	0.03	bld	0.14	0.01	0.02	bld	0.03	bld	bld	bld	bld	bld	bld	bld	bld	bld	bld	0.01	bld	bld
VMS2	0.13	bld	0.10	bld	0.02	0.10	0.02	bld	bld	bld	bld	bld	bld	bld	bld	bld	bld	bld	bld	bld
TS	0.04	bld	0.04	0.01	0.02	bld	0.03	bld	bld	bld	bld	bld	bld	bld	bld	bld	0.01	0.01	bld	bld
FN1B	0.01	bld	0.09	0.01	0.02	bld	0.02	bld	bld	bld	bld	bld	bld	bld	bld	bld	bld	bld	bld	bld
ZU-A1	0.28	bld	0.20	0.02	0.03	bld	0.03	0.03	bld	bld	bld	bld	0.01	bld	bld	bld	bld	0.01	bld	bld

Table 4 (continued)

CB-1A	2.68	bld	0.44	0.01	0.01	0.06	0.01	bld	bld	bld	bld	bld	bld	bld	bld	bld	0.02	0.02	bld	bld
FN3M	0.04	bld	0.35	bld	0.01	0.09	bld	bld	bld	bld	bld	bld	bld	bld	bld	bld	bld	bld	bld	bld
VM	0.01	bld	bld	bld	0.01	0.11	0.02	bld	bld	bld	bld	bld	bld	bld	bld	bld	bld	bld	bld	bld
CCH-1	0.04	bld	0.28	0.01	0.01	bld	0.02	bld	bld	bld	bld	bld	bld	bld	bld	bld	0.01	bld	bld	bld
GA-12	0.01	bld	bld	bld	bld	bld	bld	bld	0.02	bld	bld	bld	bld	bld	bld	bld	bld	bld	bld	bld
BNA-5	0.01	bld	bld	bld	bld	bld	bld	bld	0.01	bld	bld	bld	bld	bld	bld	bld	bld	bld	bld	bld
BNA-3	0.02	bld	bld	bld	bld	bld	bld	bld	bld	bld	bld	bld	bld	bld	bld	bld	bld	bld	bld	bld
BNA-4	0.03	bld	bld	bld	bld	bld	bld	bld	0.01	bld	bld	bld	bld	bld	bld	bld	bld	bld	bld	bld
GE1B	0.02	bld	0.23	0.01	0.02	bld	0.02	bld	bld	bld	bld	0.02	bld	bld	bld	bld	bld	bld	bld	bld
BZ1-B	0.01	bld	0.39	bld	0.02	0.10	0.02	bld	bld	bld	bld	bld	bld	bld	bld	bld	0.01	bld	bld	bld

Means ± Standard deviations	Cl	F	SrO	Cr_2O_3	V_2O_5	As_2O_3	NiO	ZnO	CuO	BaO	MoO_3	WO_3	Co_3O_4	PbO	CeO_2	Rb_2O	RuO_4	PdO	SnO_2	Cs_2O
Cherts	0.06 ±0.03		0.13		0.01	0.1	0.02 ±0.01		0.02 ±0.01		0.04	0.02 ±0.00	0.01				0.02			
Travertines	0.68 ±0.74		0.46 ±0.45	0.01 ±0.01	0.03 ±0.02		0.05 ±0.02		0.01 ±0.01	0.16 ±0.05	0.04		0.02 ±0.01							
Sulphur	0.01																			
Gypsum	0.02 ±0.01								0.02 ±0.01											
Dark lutites	0.36 ±1.01	1.06 ±0.00	0.08 ±0.07	0.03 ±0.01	0.06 ±0.06	0.08 ±0.02	0.03 ±0.01	0.03 ±0.03	0.02 ±0.01	0.37	0.02 ±0.02	0.01 ±0.00	0.01 ±0.01	0.03 ±0.01	0.02 ±0.01	0.02 ±0.02	0.04 ±0.01	0.01 ±0.01	0.13	0.12
Lutites	0.14 ±0.12	1.1	0.06 ±0.02	0.03 ±0.02	0.11 ±0.17		0.03 ±0.01	0.03 ±0.01	0.01				0.01		0.02	0.02		0.01		
Calcilutites	0.08 ±0.08		0.10 ±0.05	0.01 ±0.01	0.02 ±0.01	0.11 ±0.01	0.03 ±0.01	0.03		0.27	0.01		0.02 ±0.01				0.01 ±0.01	0.01 ±0.01		
Marls	0.29 ±0.84		0.34 ±0.08	0.01 ±0.01	0.01 ±0.01	0.09 ±0.02	0.02 ±0.01		0.01 ±0.01			0.02					0.01 ±0.01	0.02		

The results are expressed as oxides weight %. Facies key: cherts (white); travertines (orange); sulphur (yellow); gypsum (light yellow); dark lutites (grey); lutites (blue); calcilutites (pink); marls (violet). Red colored cells indicate the maximum amounts for this element. Green colored cells indicate the minimum amount for this element, above limit detection. *bld* below limit detection (< 0.01%)

addition, dolomite and plagioclase were both present as trace amounts. Finally, the geochemistry of the sample of dark lutites with hydrothermal markers (BZ1-A) consisted mainly of phyllosilicates (> 50%: muscovite, paragonite, kaolinite, and chlorite) and quartz (Table 6). Accessory minerals included feldspars, calcite, dolomite, lepidocrocite, halite, and gypsum. The high FeO_3, CaO, SO_3, and Cl (Tables 3 and 4) contents justified the presence of lepidocrocite, gypsum and halite.

4 Discussion

On a cartographic scale, 14 samples linked to hydrothermal environments were found in the vicinity of traces of the main tectonic fractures present in the basin (García-Tortosa et al., 2011; Sanz de Galdeano et al., 2007, 2012; Fig. 1B, C): samples AQ-2, GA-3A, GA-3B, GA-6, GA-7, and PL-1 are close to the NE-SW Galera Fault; sample CN1 is close to the NW–SE Alfahuara-Botardo Fault; sample BZ-1A is close to the NNW-SSE Baza Fault; and samples SX-A, FN1A, OR-1, CCH-B, TCV, and TE100 are all in the vicinity of WNW-ESE oriented fractures. This suggests the connection between materials with evidence of hydrothermal activity and their position close to tectonic fractures, as evidenced by the fact that the current thermal springs in the basin are found on or in the vicinity of traces of tectonic fractures (Fig. 1B). At an outcrop scale, the relationship between chert deposits and tectonic fractures is evident (Fig. 3G, I, J).

4.1 Origin of cherts and other facies potentially generated in hydrothermal contexts

Chert layers appear in the NE sector of the Baza Basin (Orce sub-basin) and are cartographically associated with fracture traces. In fact, a chert dyke (Fig. 3I) was recognized to the SE of the town of Galera, coincident with the trace of a NE-SW fault that shows synsedimentary features (Sánchez-Roa et al., 2016). In the case of Fuente Nueva-1 and Galera, the chert deposits are found near levels rich in paleontological remains (Fig. 2).

Hydrothermal deposits often show high concentrations of iron and manganese, while aluminum and titanium are reliable indicators of sedimentary input (Adachi et al., 1986; Boström et al., 1973; Murray, 1994; Zhang et al., 2023). This is why many research studies use the ratios (Fe + Mn)/Ti and Al/(Al + Fe + Mn) to identify hydrothermal influence (Table 5). The application of the Al–Fe–Mn diagram (Adachi et al., 1986; Yamamoto, 1987; Yamamoto et al., 2013) to the chert samples (Fig. 4) showed a geochemical

Table 5 Geochemical ratios of (Fe + Mn)/Ti and Al/(Al + Fe + Mn) of analyzed samples

Sample	Location / Site	Age	Al	Fe	Mn	Ti	(Fe+Mn)/Ti	Al/(Al+Fe+Mn)
SX-A	NW Orce	Middle Villafr.	bld	0.10	bld	bld		
FN1A	Fuente Nueva-1	Middle Villafr.	bld	0.95	0.02	bld		
CN1	Cañada del Negro	Middle Villafr.	bld	0.15	0.01	bld		
AQ-2	Galera	Early Villafr.?	bld	0.06	bld	bld		
GA-7	Galera	Ruscinian	bld	0.04	bld	bld		
GA-6	Galera	Ruscinian	bld	0.12	bld	bld		
GA-3B	Galera	Ruscinian	bld	0.03	bld	bld		
GA-3A	Galera	Ruscinian	bld	0.04	bld	bld		
TCV	W Orce	Galerian-Aurelian	0.31	1.81	4.72	0.05	121.14	0.05
TE100	W Orce	Galerian-Aurelian	0.04	2.31	2.54	0.01	808.77	0.01
CCH-B	W Orce	Galerian-Aurelian	0.30	0.28	0.01	0.01	40.17	0.51
SX-B	NW Orce	Middle Villafr.	1.06	0.65	0.02	0.08	8.67	0.61
BNA-1	Benamaurel	Middle Villafr.	0.22	0.11	bld	0.01		
BN-N	Benamaurel	Middle Villafr.	0.16	0.15	bld	0.01		
BNA-2	Benamaurel	Middle Villafr.	0.32	0.19	bld	0.01		
BLYS	Barranco León	Late Villafr.	8.06	4.88	0.02	0.64	7.70	0.62
BLYI	Barranco León	Late Villafr.	4.35	2.64	0.03	1.27	2.11	0.62
BL-	Barranco León	Late Villafr.	2.17	1.38	0.02	0.35	4.01	0.61
BLYM	Barranco León	Late Villafr.	8.31	3.85	0.03	1.10	3.52	0.68
OR-1A	Río Orce	Late Villafr.	9.20	3.52	0.02	0.56	6.29	0.72
VMC1	Venta Micena	Late Villafr.	8.88	3.18	0.02	0.49	6.51	0.74
VMC3	Venta Micena	Late Villafr.	8.51	3.26	0.02	0.49	6.66	0.72
VMS4	Venta Micena	Late Villafr.	4.76	2.05	0.02	0.51	4.07	0.70
VMC4	Venta Micena	Late Villafr.	5.80	2.29	0.02	0.53	4.33	0.72
ZU-B3	Zújar	Early Villafr.	9.32	3.39	0.02	0.64	5.36	0.73
ZU-A3	Zújar	Early Villafr.	10.21	4.63	0.02	0.50	9.24	0.69
GE1A	Galera	Ruscinian	5.81	2.76	0.02	0.31	8.89	0.68
CS-1A	Huéscar	Ruscinian	7.17	2.87	0.02	0.55	5.24	0.71
BQ-3B	Huéscar	Ruscinian	7.29	4.87	0.02	0.43	11.33	0.60
ZU-A2	Zújar	Ruscinian	5.74	4.68	0.02	0.38	12.43	0.55
BZ1-A	Baza-1	Ruscinian	5.59	7.83	0.03	0.59	13.24	0.42

Table 5 (continued)

BZ1-Y	Baza-1	Ruscinian	6.33	2.67	0.02	0.43	6.31	0.70
FN3A	Fuente Nueva-3	Late Villafr.	9.94	4.15	0.02	0.62	6.69	0.70
FN3B	Fuente Nueva-3	Late Villafr.	7.18	4.83	0.02	0.69	7.03	0.60
VMC	Venta Micena	Late Villafr.	1.86	0.99	0.02	0.11	9.35	0.65
BQ-3A	Huéscar	Ruscinian	7.19	2.55	0.02	0.38	6.68	0.74
PL-1	Huéscar	Epivillafr.	1.23	1.88	0.02	0.08	24.35	0.39
BLE1	Barranco León	Late Villafr.	4.29	1.99	0.02	0.38	5.22	0.68
OR-1	Río Orce	Late Villafr.	2.16	2.01	3.47	0.30	18.30	0.28
FN2T	Fuente Nueva-2	Late Villafr.	5.41	2.59	0.02	0.30	8.71	0.68
FN2A	Fuente Nueva-2	Late Villafr.	5.44	2.45	0.02	0.29	8.41	0.69
FN2B	Fuente Nueva-2	Late Villafr.	4.13	1.80	0.04	0.22	8.51	0.69
VMS2	Venta Micena	Late Villafr.	3.14	1.55	0.02	0.19	8.40	0.67
TS	Torre del Salar	Middle Villafr.	2.65	1.36	0.03	0.20	7.05	0.66
FN1B	Fuente Nueva-1	Middle Villafr.	5.39	3.49	0.04	0.40	8.92	0.60
ZU-A1	Zújar	Ruscinian	7.54	3.43	0.02	0.25	13.70	0.69
CB-1A	Cúllar Baza-1	Galerian	0.56	0.39	0.02	0.04	11.32	0.58
FN3M	Fuente Nueva-3	Late Villafr.	0.94	0.85	0.02	0.07	11.98	0.52
VM	Venta Micena	Late Villafr.	2.13	1.20	0.02	0.20	5.98	0.64
CCH-1	W Orce	Middle Villafr.	3.17	1.33	0.02	0.16	8.35	0.70
GA-12	Galera	Middle Villafr.	1.45	1.16	0.04	0.23	5.11	0.55
BNA-5	Benamaurel	Middle Villafr.	1.01	0.61	0.02	0.04	14.31	0.62
BNA-3	Benamaurel	Middle Villafr.	1.54	0.87	bld	0.08		
BNA-4	Benamaurel	Middle Villafr.	1.45	0.85	0.03	0.07	13.58	0.62
GE1B	Galera	Ruscinian	2.42	1.20	0.02	0.13	9.74	0.66
BZ1-B	Baza-1	Ruscinian	1.20	0.73	0.02	0.10	7.82	0.62

Means ± Standard deviations	Al	Fe	Mn	Ti	(Fe+Mn)/Ti	Al/(Al+Fe+Mn)
Cherts		0.19 ±0.31	0.01 ±0.01			
Travertines	0.43 ±0.44	1.26 ±0.95	1.82 ±2.27	0.04 ±0.04	244.69 ±379.03	0.29 ±0.31
Sulphur	0.22	0.11		0.01		
Gypsum	0.24 ±0.11	0.17 ±0.03		0.01 ±0.01		
Dark lutites	6.91 ±2.11	3.57 ±1.50	0.02 ±0.01	0.58 ±0.25	6.90 ±3.20	0.66 ±0.08

Samples with hydrothermal values are highlighted in red. All values are expressed in % of total weight. Facies key: cherts (white); travertines (orange); sulphur (yellow); gypsum (light yellow); dark lutites (grey); lutites (blue); calcilutites (pink); marls (violet). *bld* below limit detection (< 0.01%)

Table 6 X-ray mineralogical data of the samples taken in the stratigraphic profiles of the Baza Basin with a marked hydrothermal context (see Fig. 4): xxx and dark blue cells: dominant (> 50%); xx and blue cells: significant (25-50%); x and light blue cells: subordinate (5-25%); tr and yellow cells: traces (< 5%). Question marks (?): questionable

Sample	Lithology	Age	Qz	Opl	Kfs	Pl	Cal	Dol	Gp	Hl	Pyl	Lpc	Phyll	$d_{(101)}$ Å	FWHM
SX-A	Cherts	Middle Villafranchian		xxx			x							4.098	0.857
FN1A	Cherts	Middle Villafranchian		xxx			x							4.105	0.759
CN1	Cherts	Middle Villafranchian	x	xxx										4.107	0.734
AQ-2	Cherts	Early Villafranchian?		xxx										4.126	1.114
GA-7	Cherts	Ruscinian		xxx					xx				tr (Ms?)	4.114	0.937
GA-6	Cherts	Ruscinian		xxx				tr	xx					4.114	0.911
GA-3B	Cherts	Ruscinian	xx	xxx										4.097	0.581
GA-3A	Cherts	Ruscinian		xxx				tr	tr					4.114	0.901
TCV	Travertines	Galerian-Aurelian	tr				xxx		x		tr				
TE100	Travertines	Galerian-Aurelian					xxx		tr	tr	tr				
CCH-B	Travertines	Galerian-Aurelian					xxx								
BZ1-A	Dark lutites	Ruscinian	x		tr	tr	tr	tr	tr	tr		tr	xxx (Ms, Pg, Chl, Kln)		
PL-1	Calcilutites	Epivillafranchian	x			tr	xxx	tr					xx (Ms)		
OR-1	Calcilutites	Late Villafranchian	xx			tr	xx	tr					x (Ms, Pg, Chl?)		

Mineral abbreviations according to Warr (2021): Qz (quartz), Opl (opal), Kfs (K-feldspar), Pl (plagioclase), Cal (calcite), Dol (dolomite), Gp (gypsum), Hl (halite), Pyl (pyrolusite), Lpc (lepidocrocite), Phyll (phyllosilicates), Ms (muscovite), Pg (paragonite), Chl (chlorite). $d_{(101)}$: position of the (101) reflection peak of the opal polymorph. *FWHM* full width at half-high maximum peak intensity of (101) reflection peak. Codes for samples location are similar to those shown in Figs. 1 and 2

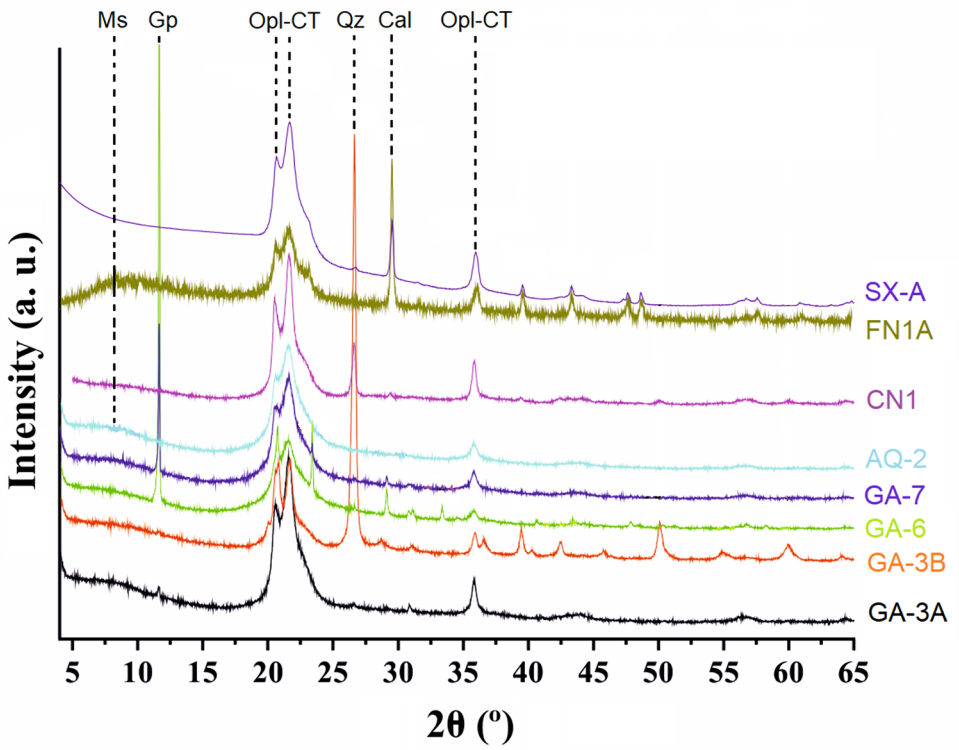

Fig. 4 X-ray diffraction diagrams of the eight studied samples of cherts. Abbreviations for minerals follow Warr (2021): Ms (muscovite), Gp (gypsum), Opl-CT (opal-CT), Qz (quartz), Cal (calcite). Vertical dashed striped lines indicate the position of the mean peaks for each mineral. For more information, see Table 6

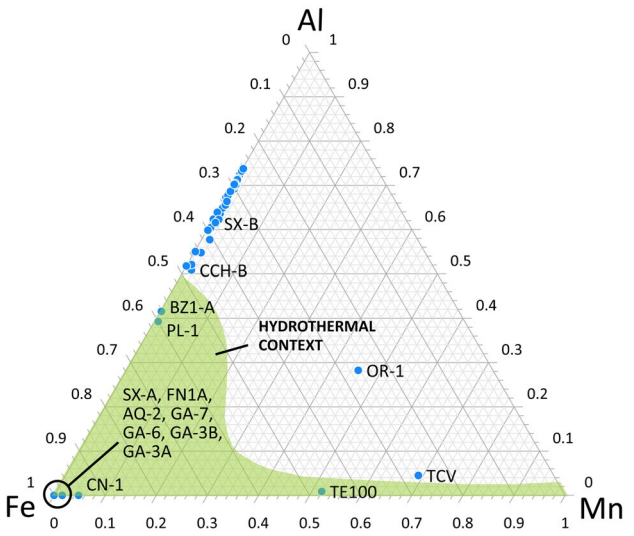

Fig. 5 Al–Fe-Mn diagram applied to all samples analyzed in this study. The points represented correspond to the values in Table 5. The green area indicates a hydrothermal origin (Adachi et al., 1986; Yamamoto, 1987). The samples labeled outside the green area are those that show other geochemical evidence of hydrothermalism (see Table 5)

composition in agreement with a hydrothermal origin. Although Al–Fe–Mn diagrams have been applied to deposits of marine origin (Adachi et al., 1986; Yamamoto, 1987; Boncheva et al., 2023; El-Moghazy et al., 2023; Jurkowska & Swierczewska-Gladysz, 2024; among others), they have also been applied to continental environments (Madondo et al., 2021; Zhou et al., 2022). The results obtained in the analysis of the chert samples from the Baza Basin are compatible with a hydrothermal origin for them if we consider other evidence (see below) and also according to the Al–Fe–Mn contents and main trace elements present in the siliceous rocks of the North Pacific (Adachi et al., 1986). On the opposite, the (Fe + Mn)/Ti and Al/(Al + Fe + Mn) ratios have been used in sediments to determine their hydrothermal origin (Boström et al., 1973; Murray, 1994; Zhang et al., 2023). Therefore, the data obtained from the chert samples are expected to be more reliable than those derived from samples without chert contents. In any case, the use of both methods is complementary and the comparison of their results in these continental environments allows their evaluation as proxies in this sedimentary context. The main mineral composition of opal-CT in the chert samples indicates a silica mineral phase linked to hydrothermal conditions (Flörke et al., 1990; Fröhlich, 2020; Kano & Taguchi, 1982; Lynne et al., 2005).

Silica-rich deposits linked to > 250ºC hydrothermal fluids have been associated with tectonic fractures in Permian cherts based on their geochemical analyses and Al–Fe–Mn diagrams (for review and references, see Zhou et al., 2022). According to the Na/K calculation method (Fournier, 1977; Fournier & Truesdell, 1973; Giggenbach et al., 1988), the estimates obtained with geothermometers for the high-temperature hot springs that are currently active in the Guadix-Baza Depression are 88–89 °C. A similar situation occurs in Alhama de Granada, SE Spain (López-Chicano et al., 2001). Moreover, the hot springs of the Guadix-Baza Depression (Diputación de Granada-ITGE, 1990; Table 2) show a direct relationship between their output water temperature and silica contents (García-Aguilar et al., 2014), which can reach up to 54 mg/l at 44 °C in the Graena spring. According to the standard values of the upper crustal geothermal gradient, tectonic and geophysical gravimetry data, Sanz de Galdeano et al. (2007) suggested a temperature range in the deep traces of the main faults of the Baza Basin of 150–300 °C, which agrees with a hydrothermal scenario. These temperatures are compatible with those inferred for the formation of Permian chert nodules in the Junggar Basin (Zhou et al., 2022).

The trace-element contents of the cherts of the Baza Basin are very variable depending on the sample considered, because each of them shows a particular geochemical profile. The case of sample FN1A, which is located a few decimeters below the Fuente Nueva-1 site, stands out for its variety of trace elements, many of them not recorded in other deposits (e.g., Sr, As, Mo, and W; Table 4). In this sense, the presence of As has been associated with hydrothermal fluids near tectonic fractures west of the Orce sub-basin (Sánchez-Roa et al., 2016) and the presence of Sr has also been linked to hydrothermal contexts in the Plio-Pleistocene lacustrine environments of the Guadix-Baza Depression (García-Aguilar et al., 2014). On the other hand, the variety of geochemical profiles found in the chert samples is compatible with the variety of hydrochemical profiles (both qualitatively and quantitatively) and output temperatures present in the hot springs that are currently active in the basin (Table 2). These hydrochemical profiles must be linked to the geometry of the tectonic fractures associated with each hot spring and to the different lithological substrates that the hydrothermal fluids passed through on their way to the surface. This cause-effect relationship could be extrapolated to the ancient Plio-Pleistocene hydrothermal upwellings in the Baza Basin, whose salt contents, output temperatures and water flow would have varied depending on the tectonic, lithological, and structural features present in each case.

The hydrochemical composition of the hot springs that are currently active in the basin with output temperatures of > 35 °C (Cruz-Sanjulián et al., 1972; Cruz-Sanjulián & García-Rosell, 1972, 1975; Diputación de Granada-ITGE, 1990; Table 2) shows silica contents of > 40 mg/l, high sulfate values and the presence of chlorides. Similar conditions are widely documented in hydrothermally active regions, such as the Dead Sea-Jordan River Basin in Israel (Levitte & Eckstein, 1978), Yellowstone in USA (Nordstrom et al.,

2005), Mount Tafta in Iran (Shakeri et al., 2008) or Denizli in Turkey (Özler, 2000), among others. On the other hand, White et al. (1956) and Fournier and Rowe (1966) established the hydrochemical conditions linked to the solubility and subsequent precipitation of silica in thermal waters. They defined a solubility of 315 mg/l for silica at 90 °C and 110 mg/l at 25 °C, demonstrating a correspondence between the output temperature of the hot springs and their silica contents. The rapid rise of hot waters to the surface results in silica oversaturation due to cooling and degasification. Dissolution by high-temperature waters of deep rocks and their subsequent ascent through tectonic fractures is common. In the case of cherts, however, these hot springs should have shown much higher output temperatures (> 35 °C) than in the atmosphere. Considering the climatic conditions inferred for the Early Pleistocene in the Baza Basin, these thermal pools would have originated small areas with a stable and warm microclimate throughout the year, suitable for the ecological development of a diverse mammalian community, especially during the cold periods of the Pleistocene (Lisiecki & Raymo, 2007; Paillard, 2017).

Under these conditions, cherts originated from the dissolution at depth conditions of rocks with elevated siliceous contents (e.g., quartzites and mica-schists of the Internal Zones of the Betic mountain range; Baena Pérez et al., 1979; Martín García et al., 1980; Villalobos et al., 2006) in high-temperature fluids. According to the most plausible calculated Na/K geothermometers (88–89 °C) and considering the standard geothermal gradient in the upper crust (25–30 °C/km, Harrison et al., 1990; Gupta & Roy, 2007), the estimated depth in the Baza Basin for the dissolution of silica agrees with the basement depth calculated from seismic profiles, 2150 m (Alfaro et al., 2008). This depth is similar to the estimation for present-day hot springs in Algeria (Belhai et al., 2017) and indicates the presence of a deep fracture network affecting the basin substrate in the Guadix-Baza Depression, where the hot springs would dissolve components of the rocks bound to them. These depth values linked to the origin of thermal upwellings in the basin are lower than the depth range of the tectonic fractures in the basin (5–10 km), which has been estimated using geological and geophysical criteria (Sanz de Galdeano et al., 2012, 2020).

Travertine levels of decimetric thickness and associated with a hydrothermal context have been detected in the southern bank of the Orce River, west to the town of Orce. The application of the Al–Fe-Mn diagram and the (Fe + Mn)/Ti and Al/(Al + Fe + Mn) ratios to these samples showed a composition compatible with a hydrothermal origin (Fig. 5, Table 5).

Furthermore, the Al–Fe-Mn diagram suggests that sample BZ1-A of dark lutites may have had some hydrothermal influence. Moreover, the mineralogy of this sample (Table 6) indicates a primarily detrital deposit (quartz, paragonite and chlorite) with halite precipitation due to evaporation processes. It is noteworthy that the presence of Sr and Mo was detected in this sample (Table 4), as these elements have been found under a hydrothermal context in the Galera deposits (Sánchez-Roa et al., 2016). Despite having very high iron contents, the hydrothermal ratios (Fe + Mn)/Ti and Al/(Al + Fe + Mn)) suggest that this level has not a hydrothermal origin. Given the discrepancy between the Al–Fe–Mn diagram and these ratios, it is important to note that the diagram was designed for analyzing siliceous materials (Adachi et al., 1986) while the ratios are typically used for sediments (You et al., 2020; Zhang et al., 2023). As a result, it is plausible that the ratios provide a more accurate indication of hydrothermalism in these dark lutites. However, although the values in these ratios are close to those expected in hydrothermal environments, they are not within the hydrothermal zone. This casts doubts on whether BZ1-A was influenced by hydrothermalism. In any case, it is remarkable that BZ1-A is the only sample among the 17 samples of dark lutites analyzed that fits the diagram of hydrothermalism.

The calcilutite samples that provided geochemical indicators of hydrothermal activity correspond to two metric scale levels located near the localities of Huéscar (sample PL-1) and Orce (sample OR-1, Fig. 2). In both cases, they are placed in the vicinity of paleontological sites with macrofauna. The application of the (Fe + Mn)/Ti and Al/(Al + Fe + Mn) ratios to these samples (Table 5) shows values that are compatible with a hydrothermal origin for them. In the case of sample PL-1, the Al–Fe–Mn diagram (Fig. 4) shows further evidence of its hydrothermal origin. From the mineralogical point of view, the composition of these samples shows quartz, calcite, dolomite, muscovite, paragonite, and plagioclase (Table 6). This association of minerals can be considered detrital-inherited by sedimentary processes, as evidenced by the lithological characteristics observed in the outcrops where the samples were taken. In addition to the previous arguments, the presence of significant amounts of Ba in samples BZ1-A (dark lutites), OR-1 (calcilutites), TCV (travertines), and TE100 (travertines) adds further evidence on the hydrothermal context associated with their deposition (Jankovic, 1982; Canet et al., 2005).

The hydrothermal markers in samples Pl-1, OR-1 and BZ1-A, whose lithologies contain inherited detrital elements, could be interpreted as due to minerals originating from source areas with metamorphic substrates. However, these hydrothermal markers do not appear in other deposits that are lithologically and sedimentologically similar to these three samples, which indicates that the high Fe and Mn contents should have a hydrothermal origin. Concerning the sedimentary context of the cherts and other deposits linked to hydrothermal conditions and their association with archaeological and paleontological sites, it is worth noting

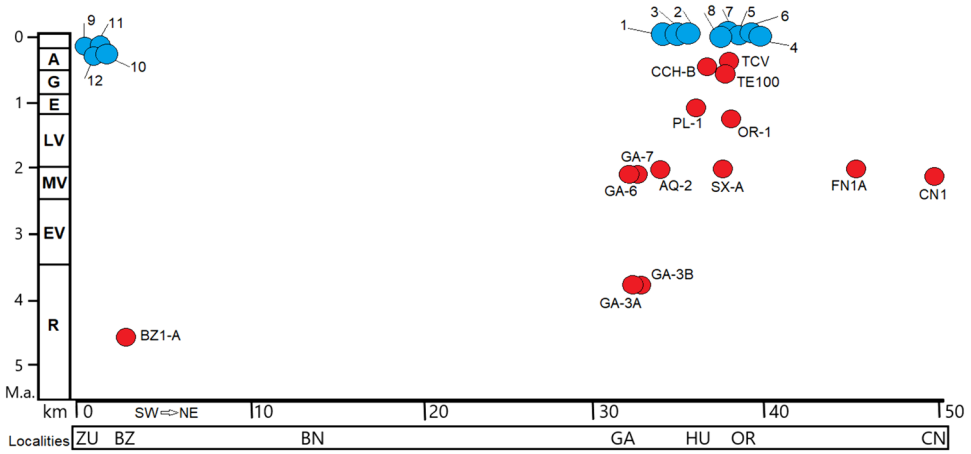

Fig. 6 Spatio-temporal position of the samples with a hydrothermal origin and of those hot springs currently active in the Baza Basin. The X-axis indicates a SW-NE line along the Baza Basin, between the localities of Zújar and Cañada del Negro (NE of Orce), with a length of ~ 50 km. Key for localities: ZU-Zújar, BZ-Baza, BN-Benamaurel, GA-Galera, HU-Huéscar, OR-Orce, CN-Cañada del Negro. Key of chronological periods (Y-axis): R-Ruscinian, EV-Early Villafranchian, MV-Middle Villafranchian, LV-Late Villafranchian, E-Epivillafranchian, G-Galerian, A-Aurelian. Red points show the position of the samples linked to a hydrothermal context. Blue points show the position of the hot springs currently active in the Baza Basin (code numbers are similar to those of Table 2)

that these levels frequently appear on the top and/or bottom of the sites as well as in lateral connection with facies linked to a diversity of sedimentary scenarios.

4.2 Paleogeographical reconstruction of hydrothermal activity in the basin

The spatio-temporal correlation between the coordinates of the 14 samples with evidence of past hydrothermal activity and the position of the hot springs that are currently active in the Baza Basin allows us to propose a general model of paleogeographic evolution of the basin in relation to its hydrothermal activity (Fig. 6). This model makes it possible to specify the cause-effect relationships between the tectonic dynamism of the basin and the occurrence of hydrothermal phenomena linked to tectonic fractures (Fig. 1B, C) at specific places and times that generated in each case different geochemical and mineral markers in the sedimentary environments. These environments can be very diverse, since they do not show a direct genetic relationship with the position of the hydrothermal upwellings. In this way, the cherts, travertines, calcilutites, and dark lutites (i.e., the facies in which hydrothermal markers have been detected) correspond to different sedimentary environments, which include lacustrine zones with some depth (calcilutites), marshy environments (dark lutites), occasional upwellings in favor of tectonic fractures (cherts) and waterfalls or pools of thermal waters (travertines), according with the most plausible sedimentary models (Prothero & Schwab, 2004; Reading, 1978). Among these sedimentary environments, those linked to the cherts could be considered the only ones with a direct causal relationship between these facies and the presence of hydrothermal activity.

As shown in Fig. 6, hydrothermal phenomena appear discontinuously in the Baza Basin from the late Pliocene (Ruscinian) to the present. In this sense, there seems to be a gap between the upper Ruscinian and the middle Villafranchian, together with a gap in the lower upper Villafranchian. However, the presence of hydrothermal activity during these periods cannot be ruled out. Its demonstration would depend on a wide sampling of the different sedimentary facies linked to these periods, preferably located near tectonic fractures. Regarding the geographical distribution, it is evident that hydrothermal activity concentrates in the Galera-Orce-Cañada del Negro sector (Orce sub-basin). This points to an intense tectonic activity in this sub-basin during the Plio-Pleistocene, particularly in four intervals: late Ruscinian, middle Villafranchian, lattermost Villafranchian and Galerian to present, with the presence of hydrothermal phenomena that induced mineral and/or geochemical markers in the sedimentary environments associated to these places and times. Likewise, the Baza area seems to show a similar pattern to the Orce sub-basin for the Ruscinian, associated with an important tectonic fracture, the Baza Fault. It is also evident that each node of hydrothermal activity seems to demonstrate a particular physico-chemical characteristic, as shown by the compositional variety of the deposits linked to this activity. In this regard, factors such as the hydrochemical composition and physical parameters of the hydrothermal fluids, the sedimentary environments where they acted and (micro)biological factors would give rise to a wide range of situations. This pattern could have played an important role in the development of local ecosystems in the vicinity

of the nodes of hydrothermal activity. Finally, it is evident how these hydrothermal phenomena coincide quite closely in their spatio-temporal coordinates with the position of important paleontological sites, as happens in the case of BZ-1, FN1, HU-1, and BO-7 (Fig. 2). If we further extend these spatio-temporal coordinates to a wider range, we see other important sites (e.g., BL, FN-3 and VM) that appear in a geographic and/or chronostratigraphic position close to the nodes of hydrothermal activity. This allows us to establish a possible paleoecological relationship between the presence of hydrothermal phenomena and the occurrence of paleontological sites in the Baza Basin.

4.3 Paleoecological implications of hydrothermal activity in the basin

A contribution of thermal waters would play a role in maintaining during the dry season a minimum level in the water table of the lacustrine environments of the Baza Basin. This would in turn allow the development of a luxurious vegetational cover in the surroundings of the hot springs, which would sustain a large vertebrate community. The hot springs of the Baza Basin led to the appearance of thermal pools of variable extent and length, with waters that differed from the main lacustrine systems in their composition and

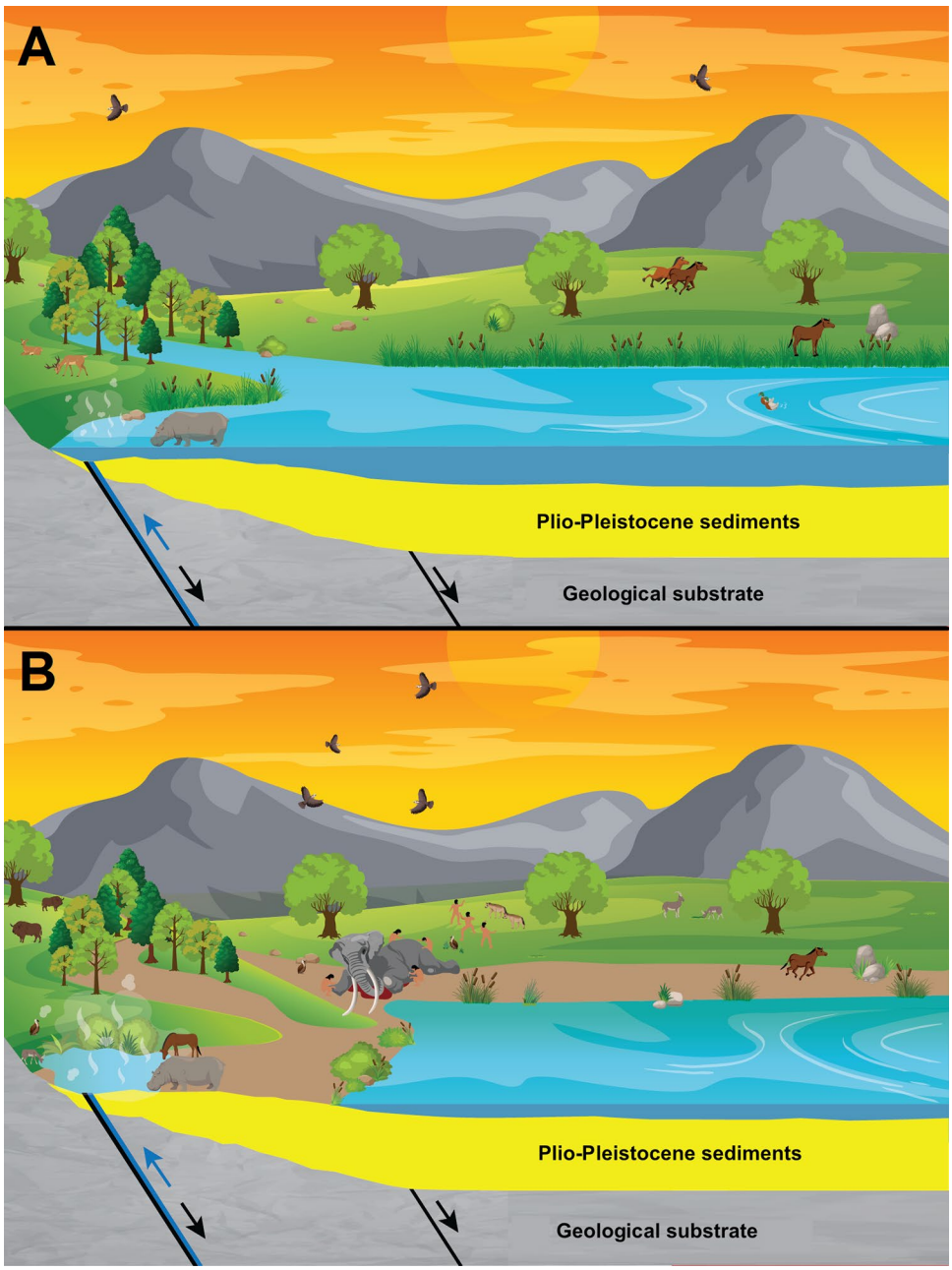

Fig. 7 Paleoecological reconstruction of the landscape in the vicinity of a lacustrine system of the Baza Basin linked to a thermal upwelling. **A** High-stand level in the lacustrine system. **B** Lowstand level in the lacustrine system. The trace of the fault positioned to the left indicates the position of a local hot spring. Drawing by Sandra Ramírez Cherbuy—InkScience

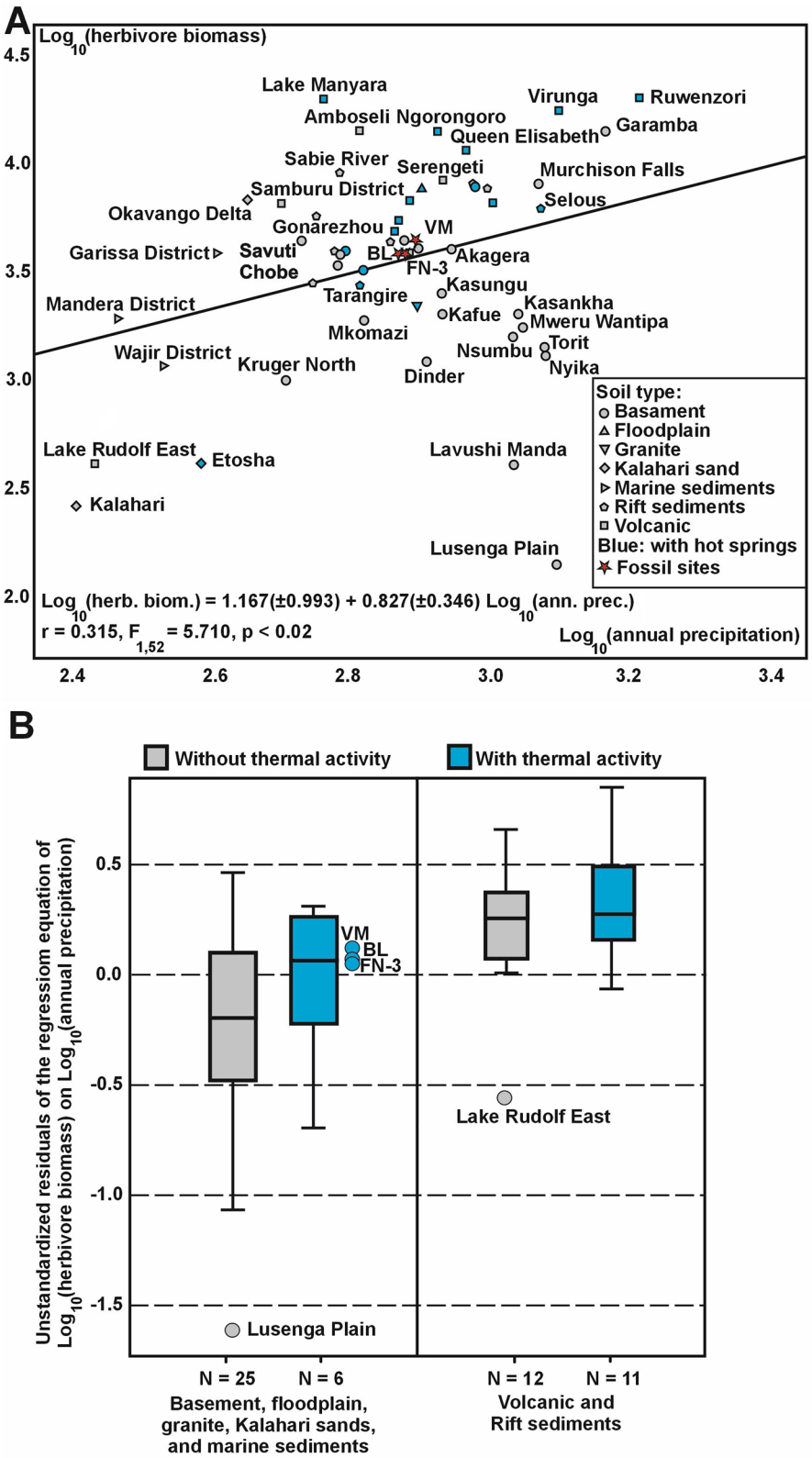

Fig. 8 **A** Least-squares relationship between the logarithms of annual precipitation (mm) and herbivore prey biomass (kg/km^2) in 54 National Parks and Game Reserves of Africa [data on mean annual rainfall from Fick and Hijmans (2017); data on prey biomass from Bell (1981) and Hatton et al. (2015)]. The values estimated for the paleontological site of Venta Micena (VM) and the archaeological sites of Barranco León (BL) and Fuente Nueva-3 (FN-3) in the Baza Basin, not used for deriving the equation, are also shown [rainfall estimates based on Blain et al. (2016) for BL and FN3, and Palmqvist et al. (2022c) for VM; prey biomass estimates taken from Rodríguez-Gómez et al. (2022)]. **B** Whiskler box-plots for the unstandardized residuals of the regression equation of A, differentiating between sediment types and between localities with or without thermal activity

physical properties. These hot springs would support in part the ecological pyramid of the Baza Basin in a specific network of spatio-temporal nodes, concentrating the plants and animals in their surroundings, which would in turn result in a concentration of ungulate carcasses in the vicinity of the hot springs (Fig. 7). This is reflected in some of the most

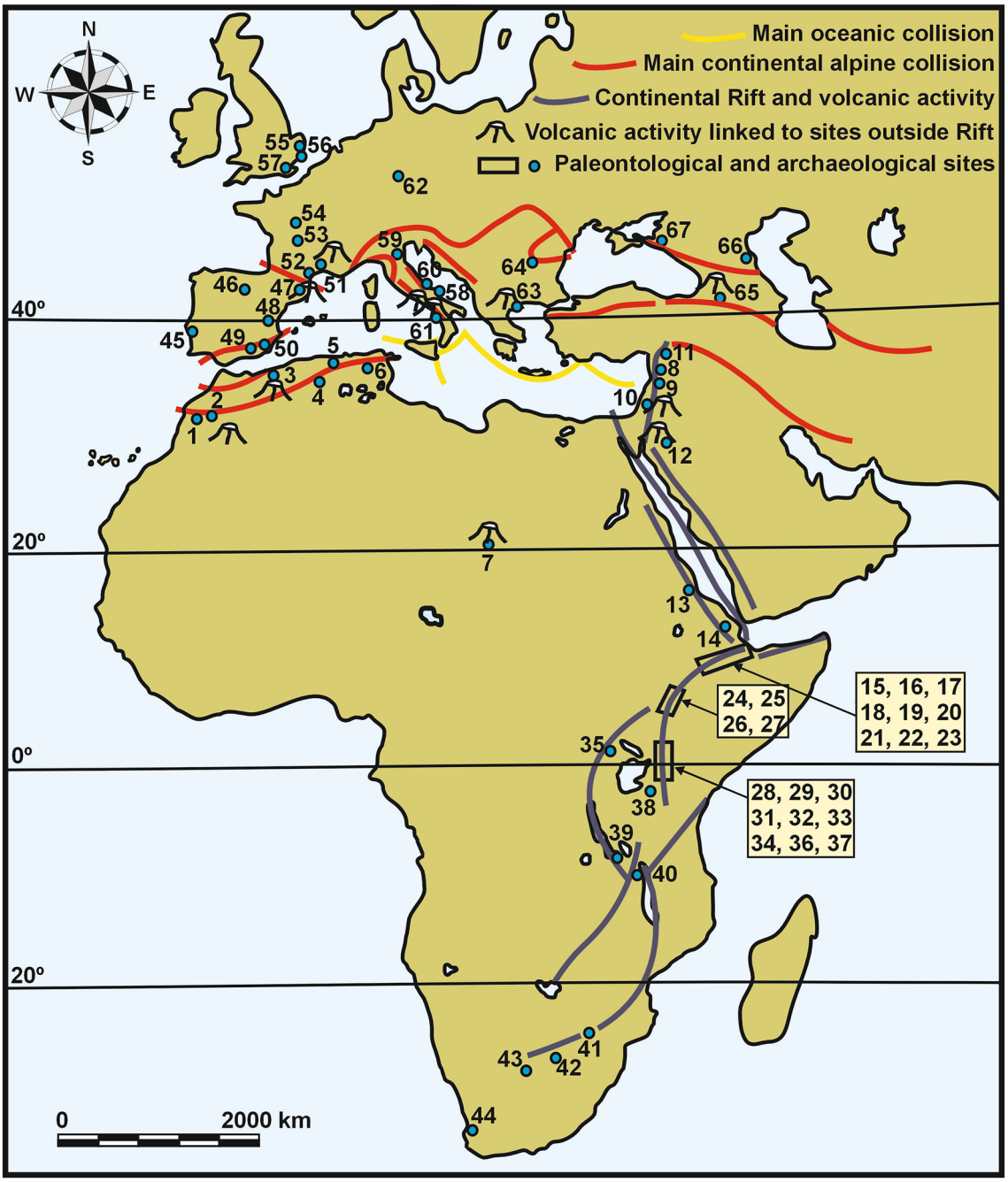

important deposits of the basin, such as the Pliocene sites of Baza-1 and Fuente Nueva-1, which are both linked to a level of dark lutites and to a level of cherts, respectively. From a sedimentary point of view, this provides evidence on the role of hydrothermal events as hot spots for the concentration of terrestrial fauna.

The relationship between some ecological factors linked to contexts with thermal waters is shown in Fig. 8A, which depicts a direct, statistically significant relationship between prey biomass (kg/km^2) and annual rainfall (mm) values in a set of African Natural Parks and Game Reserves (data compiled from Bell (1981) and Hatton et al. (2015); see also Coe et al. (1976) for a similar relationship). However, there is considerable scatter around the least-squares regression line, which primarily depends on soil type and, secondarily, on the presence of thermal springs (Fig. 8B), which increase the net primary productivity thanks to their saline contents (García-Aguilar et al., 2014, 2015; Palmqvist et al., 2022a). Figure 8 also includes the mean estimates of carrying capacity for the Orce sites (3827.8 kg/km^2 for VM and 3307.6 kg/km^2 for BL/FN-3), obtained using an approach based on the

◂**Fig. 9** Map of Africa and Western Eurasia showing the position of selected archaeological and paleontological sites, as well as the geologically active areas. Site codes and references: 1: Ain Maarouf (Geraads et al., 1992); 2: Djebel Irhoud (Hublin et al., 2017); 3: Tighenif (Sahnouni & Van der Made, 2009); 4: N'Gaous and Ket Sefiane (Sala et al., 2016); 5: Ain Hanech, El Kherba and Ain Boucherit (Sahnouni et al., 2018); 6: Oued Sarrat (Martínez-Navarro et al., 2014); 7: Toros Menalla (Brunet et al., 2002); 8: Qesem Cave (Barkai et al., 2003); 9: Gesher B. Ya'akov and Ma'ayan Barukh (Goren-Inbar et al., 2000; Ronen et al., 1980); 10: Ubeidiya, Evron Quarry, Revadim Quarry, and Bizat Ruhama (Tchernov, 1987; Tchernov et al., 1994; Martínez-Navarro et al., 2012; Yeshurun et al., 2011; Marder et al., 2007); 11: Latamne (Guérin et al., 1993); 12: Ti´s Al Gahdah (Stimpson et al., 2016); 13: Buia and Engel Ela-Ramud (Abbate et al., 1998; Martínez-Navarro et al., 2016); 14: Hadar and Dikkita-Dikia (Alemseged et al., 2006; Johanson et al., 1978); 15: Gona I and II (Semaw et al., 1997); 16: Middle-Awash, Aramis I and II, Maka, and Bouri (Asfaw et al., 2002; White et al., 1993, 1994, 2003); 17: Fejej (Barsky et al., 2011); 18: Gadeb (Williams et al., 1979); 19: Melka-Kunture (Morgan et al., 2012); 20: Asbole and Bodo (Conroy et al., 1978; Geraads et al., 2004); 21: Konso-Gardula (Asfaw et al., 1992); 22: Shungura (Boaz & Howell, 1977; Howell et al., 1987); 23: Woranso Mille (Haile-Selassie et al., 2010); 24: Koobi-Fora (Bunn, 1981; Lepre & Kent, 2015; Lepre et al., 2007); 25: Lokalalei and Lomekwi (Harmand et al., 2015); 26: Ileret (Jungers et al., 2015); 27: Chesowanja (Gowlett et al., 1981); 28: Kilombe and Kapturin (Gowlett, 2005); 29: Kanjera (Plummer & Bishop, 2016); 30: Kariandusi (Shipton, 2011); 31: Kanapoi and Lothagam (Kissel & Hawks, 2015; Leakey et al., 1995); 32: Lukeino-Tugen Hills (Sawada et al., 2002); 33: Kantis (Mbua et al., 2016); 34: Olorgesailie (Potts, 1994); 35: Nyabusosi (Texier, 1995); 36: Peninj (De la Torre et al., 2003); 37: Olduvai (Leakey & Leakey, 1964); 38: Laetoli (Magori & Day, 1983); 39: Kalombo Falls (Duller et al., 2015); 40: Uraha Hill and Chiwondo (Bromage et al., 1995); 41: Sterkfontein, Swartkrans, Drimden, Makapansgat, Malapa, Haasgat Cave, Kromdraai Cave, Cooper's Cave, and Gladysvale Cave (Herries, 2011; Herries & Shaw, 2011; Herries & Adams, 2013; Herries et al., 2014; Herries et al., 2018; Latham & Herries, 2004; Dirks et al., 2010; Kuman & Clarke, 2000; Kuman, 2007; De Ruiter et al., 2009); 42: Taung (McKee, 1993); 43: Wonderwerk Cave (Chazan et al., 2008); 44: Elandsfontein (Braun et al., 2013); 45: Aroeira (Daura et al., 2017); 46: Atapuerca (Bermúdez de Castro et al., 1997; Carbonell et al., 2008; Parés & Pérez-González, 1999); 47: Valparadis (Martínez et al., 2013); 48: Alto de las Picarazas (Gabarda et al., 2016); 49: Orce, Cúllar and Solana del Zamborino (Álvarez-Posada et al., 2017; Espigares et al., 2013; Martínez-Navarro et al., 1997; Oms et al., 2000a, 2000b; Toro-Moyano et al., 2013; Torrente Casado, 2010); 50: Cueva Victoria (Gibert et al., 2016); 51: Bois-de-Riquet and Vallonet Cave (Bourguignon et al., 2016; Michel et al., 2017); 52: Tautavel-Arago (Barsky & de Lumley, 2010; Byrne, 2004); 53: Pont-de-Lavaud (Bahain et al., 2007; Lombera-Hermida et al., 2016); 54: Lunery-Rosières (Despriée et al., 2009); 55: Happisburgh (Parfitt et al., 2010); 56: Pakefield (Parfitt et al., 2005); 57: Swanscombe (Lister, 1986); 58: Pirro Nord (López-García et al., 2015); 59: Ca'Belvedere di Monte Poggiolo (Bahain et al., 2007); 60: Isernia la Pineta (Bahain et al., 2007; Coltorti et al., 2005); 61: Ciampate di Diavolo (Mietto et al., 2003); 62: Untermassfeld (Baales, 2014); 63: Petralona Cave (Poulianos, 1984); 64: Kozarnika Cave I and II (Sirakov et al., 2010); 65: Dmanisi and Akhalkalaki (Lordkipanidze et al., 2007; Vekua, 1986); 66: Muhkai II (Amirkhanov et al., 2016; Michel et al., 2017); 67: Kermek, Rodniki, Bogatyri-Sinyaya, Balka, and Tsymbal (Michel et al., 2017; Shchelinsky et al., 2010)

Weibull model (see Rodríguez-Gómez et al., 2022, 2024), and the estimates of annual rainfall, based on the composition of the herpetological assemblages in the case of BL/FN-3 (700 mm for BL and 738 mm for FN-3; Blain et al., 2016) and on the abundance of nitrogen isotopes in the bone collagen retrieved from the fossils of large mammals from VM (800 mm; Palmqvist et al., 2022c, 2023). As deduced for the Baza Basin, the presence of thermal waters provided a variety of salts and trace elements. These mineral nutrients allowed the development of a diverse plant community and the translation of this biodiversity to the local trophic pyramid, thus configuring a sort of ecological "Eden" on a limited spatio-temporal scale. Given that some species of mammals, for example the hippopotamuses, used these thermal pools and watered them, their salinity (at least where the fossil remains are found) must have been of < 5 g/l (Palmqvist et al., 2022a). In this environmental context, the ancient hominin settlers of the Baza Basin sought such places as preferential sources of water and a variety of trophic resources.

Figure 8B shows that although the productivity of the African National Parks and Game Reserves mainly depends on annual precipitation, as noted above, it also relates to soil type and to the presence of thermal waters, which contribute to increase the productivity of the terrestrial ecosystems and their herbivore biomass. Specifically, the areas with volcanic and Rift sediments have more positive residuals in the regression equation of Fig. 8A than those with other types of sediments (i.e., basement, floodplain, granite, Kalahari sands, and marine sediments; see also Bell, 1981). Similarly, the areas with active hot springs show greater values of prey biomass than those in which thermal activity is absent (Fig. 8B).

4.4 Correlation of the proposed model for the Baza Basin with other World sites

A large-scale geographical position of 103 African, West Asian and European sites, which range in age from 7.5 to 0.35 Ma, shows a close relationship with those areas that show high tectonic and geothermal activity (Fig. 9). Most of these sites appear in areas that evidence intense geological activity related to seismotectonic, volcanic and hydrothermal phenomena during the Plio-Pleistocene, and even up to present days. These sites usually show tuffaceous levels, volcanic ashes, seismites, or lacustrine deposits potentially fed by thermal waters. This is also the case of the archaeological deposits of Java (Indonesia), where volcanism and seismicity are common and particularly intense (Delinom, 2009).

These sites range in age from the appearance of the first hominins in Africa to the arrival of *Homo sapiens* in Morocco, as detected in the Jebel Irhoud site (Hublin et al., 2017). Figure 9 shows that 88% of the sites are found in

areas where volcanic, seismic, tectonic, and hydrothermal phenomena have been common since Late Miocene times (and in many cases up to present days). Of all these sites, 71% appear in sedimentary facies of lacustrine or fluvio-lacustrine origin, as happens throughout the East African Rift, while the other sites are found in karst cavities (21%) and in sedimentary formations of fluvial or marine-littoral origin (8%). Most paleoanthropological sites placed in geologically stable areas are found in karst cavities and fluvial paleo-terraces. If we consider the sedimentary origin and the tectonic environment of these sites, 67% of them are found in lacustrine or fluvio-lacustrine facies located in tectonically active areas with hot springs.

The network of spatio-temporal nodes of hydrothermal phenomena in the Baza Basin seems to be related with the presence of hominin settlements, as evidenced by four archaeological localities: the late Early Pleistocene sites of Barranco León and Fuente Nueva-3, the Early-Middle Pleistocene site of Huéscar-1, and the early Middle Pleistocene site of Cúllar-Baza-1. This possible association led us to the proposal of a new idea on the distribution of paleoanthropological sites on a global scale during the Plio-Pleistocene.

A number of African and Eurasian sites can be compared with those that characterized the Plio-Pleistocene environments of the Baza Basin. Throughout the East African Rift Valley, from Mozambique-Malawi to Ethiopia and Eritrea, following the Red Sea and the Levantine Corridor to Anatolia and Georgia, the main archaeological deposits are found in volcanic contexts and scenarios characterized by intense tectonic activity, which resulted in geothermal anomalies during the Neogene-Quaternary (Adamia, 2013; Glerum et al., 2020; Morley et al., 1992; Schlüter, 1997). More specifically, a relationship between hydrothermal activity and paleoanthropological deposits of 1.7 Ma has been evidenced by microbial markers in Olduvai Gorge by Sistiaga et al. (2020), who used a similar model to the one proposed here for the Baza Basin. Such correspondence also occurs in several European sites linked to recent hydrothermal and seismo-tectonic activity, for example the Acheulean site of Rodafnidia, Lesvos Island (Galanidou et al., 2013, 2016). This shows the common relationship between areas with intense geothermal activity and the presence of archaeological sites with hominin remains and fossils of large mammals.

Tectonic activity is a source of geomorphological variability (i.e., landscape roughness) and ecological diversity (Coppens, 1994; Foley, 1987; Gamble, 1993) and has been linked to the first hominins that evolved in the African Rift, because it allowed them to obtain stable resources: the tectonic and volcanic movements that generated the East African Rift System resulted in a broken, hilly rough country of complex topography where the early hominins could hunt and hide (Bailey et al., 2000, 2011). Moreover, environmental roughness probably characterized the whole route of early hominin dispersal (King & Bailey, 2006). We suggest here that tectonic and hydrothermal activity are significantly linked to the evolution of the human lineage due to the consumption strategies of hominins and their risk of exposure to confrontation with carnivores. In fact, carnivores could have predated the own hominins (Treves & Palmqvist, 2007) and were also competitors in the access to meat, although they were also providers of carrion (Espigares et al., 2013; Palmqvist et al., 2022a, 2023). According to the evidence unearthed from the fossil sites of Orce, the hominins developed a scavenging behavior as a successful strategy to obtain animal resources in the Baza Basin (Espigares et al., 2019; Palmqvist et al., 2023). Analyses on resource partitioning among the members of the carnivore guild suggest that scavenging was the optimal strategy for these hominin populations (Rodríguez-Gómez et al., 2016). Anatomical evidence from late Early Pleistocene sites younger than those of Orce, such as level TD6 from Gran Dolina in Sierra de Atapuerca, suggests that these humans had lesser throwing skills than modern humans, which would hinder a hunting activity based on throwing cobbles against prey, although it would not have limited other hunting strategies (Bermúdez de Castro et al., 2020; however, for an opposite interpretation see García-Martínez et al., 2021).

A heterogeneous environment would be useful for exploiting different ecological niches in the case of an opportunistic species like *Homo* sp., relatively weak for a direct confrontation with the large carnivores. Moreover, these mosaic habitats would also provide protection from cursor predators in the open environments and from ambushing carnivores in the closed ones, as the hominins could inhabit the boundary zones between different environments, both for protecting themselves from predators and for exploiting the resources of these environments (see Treves & Palmqvist, 2007). In ecology, the transition zones between different ecosystems are called ecotones. We propose that rather than a generalist species, the early members of *Homo* would be specialized in exploiting the ecotones, thus showing adaptations to consume resources from different environments. According to an analysis of avifauna in Lower, Middle and Upper Paleolithic sites (Finlayson et al., 2011), there is a significant association between hominin presence and mosaic habitats (i.e., habitats with many ecotones).

On the other hand, hominin absence of Sierra de Atapuerca during the early Middle Pleistocene has been linked to a greater environmental homogeneity than during previous periods (Rodríguez et al., 2011; Rodríguez-Gómez et al., 2014). Today, the areas with highest ecosystem diversity are two regions with active tectonics, the African Rift and the Himalayan range, in accordance with the ecoregions defined by Olson et al. (2001). The richness of ecoregions per unit area observed in the African Rift is probably lower nowadays than during the Plio-Pleistocene, because tectonic

activity was higher at that time (Bailey et al., 2000; King & Bailey, 2006). This diversity of ecoregions seems to relate to the diversity in the values of abiotic and biotic variables that can be observed in the region. For these reasons, the African Rift would provide a high diversity of habitats in which a generalist or ecotone-specialist species, such as early *Homo,* could have efficiently exploited these environments for resources and shelter. This model can be proposed for the ancient hominin populations found in the archaeological sites of the Baza Basin (for a review on the paleodemography of these populations, see Palmqvist et al., 2022a).

From a paleoecological point of view, the Ngorongoro Crater in the African Rift Valley is a model that can be correlated with the sites of the Baza Basin and other deposits found in geologically active areas. In Ngorongoro, the hydrothermal influence of the crater lakes has a seasonal pattern. As a result, the populations of large mammals are dispersed in the wet season, while during the dry season they concentrate near the pastures that surround the hot springs. These waters lose their ecological influence at ~ 700 m from their point of emergence, changing to alkaline (pH ~ 8) waters with high saline contents (DeoCampo, 2002). The list of species that live in the crater within a radius of ~ 100 m around the thermal springs includes buffaloes, gazelles, hippopotamuses, rhinoceroses, zebras, elephants, antelopes, wild boars, hyenas, foxes, cheetahs, jackals, and lions. This fauna is strikingly similar to the one that inhabited the Baza Basin during the Plio-Pleistocene in terms of their distribution among modes of locomotion, feeding types and body size classes (Mendoza et al., 2005).

5 Conclusions

Hot springs have been important for faunal and hominin survival during the Plio-Pleistocene, favoring the dispersal of mammalian species as documented in the Baza Basin, which preserves one of the continental sequences with greater stratigraphic completeness of Europe, including the earliest archaeological evidence of hominin presence in the northern Mediterranean latitudes during the late Early Pleistocene. In this basin, hot springs form a network of spatio-temporal nodes, which are particularly concentrated in the Orce sub-basin, showing permanent siliceous waters with temperatures > 35 °C. These hot springs played an important ecological role during the summer, when seasonal rain-fed springs became dry, and also helped to maintain locally warm temperatures in winter, thus aiding the survival of water dependent vertebrates adapted to warm and moist climates, including the members of early *Homo.*

Nearly one hundred Plio-Pleistocene archaeological and paleontological localities are recorded in the perimeter of the Baza Basin. Most of these sites were generated in connection with tectono-sedimentary processes, as evidenced by the presence of paleo-seismites, ancient hot springs and faulting. The lithological, mineralogical and geochemical composition of the chert levels present in the Orce sub-basin suggests a high-temperature hydrothermal origin for these deposits. Other types of sedimentary facies present in the basin, such as travertines, dark lutites or calcilutites, were influenced by this network of spatio-temporal nodes of hot springs, showing diverse geochemical and mineralogical indicators associated with this hydrothermal origin. The mineral nutrients provided by the hot springs prompted the development of a luxurious vegetation, which in turn allowed the development of a diverse community of large mammals, including the first hominins that dispersed in Western Europe.

Acknowledgements We gratefully acknowledge the in-depth revision of this manuscript by editor Prof. M. Reolid and two anonymous reviewers, who provided many insightful comments and suggestions that helped us to improve its contents. We dedicate this paper to our colleague and friend Prof. F. Olóriz, who has been a permanent source of inspiration for all of us.

Funding Funding for open access publishing: Universidad Málaga/CBUA. This work was supported by Consejería de Economía, Innovación, Ciencia y Empleo,Junta de Andalucía, EXP: BC.03.174/19 10153, M. Patrocinio Espigares, Research Groups RNM-146, Paul Palmqvist, RNM-199, Paul Palmqvist,UMA18-FEDERJA-188, M. Patrocinio Espigares, PAIDI 2020 postdoctoral grant, Isidoro Campaña, Generalitat de Catalunya, 2021SGR 01238 (AGAUR), Bienvenido Martínez-Navarro, Comunidad de Madrid, Programa de Atracción de Talento, Guillermo Rodríguez-Gómez, Ministerio de Ciencia e Innovación, CEX2019-000945-M, Bienvenido Martínez-Navarro.

Data availability The data that support the findings of this study are available on request from the corresponding authors.

Declarations

Conflict of interest On behalf of all authors, the corresponding author states that there is no conflict of interest.

Research involving human participants and/or animals This research involved no human participants and/or animals.

Informed consent All authors participated in this research, contributed to elaborating the manuscript contents and agreed in submitting it for publication in Journal of Iberian Geology.

References

Abbate, E., Albianelli, A., Azzaroli, A., Benvenuti, M., Tesfamariam, B., Bruni, P., Cipriani, N., Clarke, R. J., Ficcarelli, G., Macchiarelli, R., Napoleone, G., Papini, M., Rook, L., Sagri, M., Tecle, T. M., Torre, D., & Villa, I. (1998). A one-million-year-old *Homo* cranium from the danakil (afar) depression of eritrea. *Nature, 393*, 458–460. https://doi.org/10.1038/30954

Adachi, M., Yamamoto, K., & Sugisaki, R. (1986). Hydrothermal chert and associated siliceous rocks from the northern pacific their geological significance as indication on ocean ridge activity. *Sedimentary Geology, 47*, 125–148. https://doi.org/10.1016/0037-0738(86)90075-8

Adamia, S. A. (2013) Geology of Georgia–Eastern black sea: a review. 125th Anniversary Annual Meeting & Expo, Denver, Colorado USA. Geological Society of America Abstracts with Programs, 45, 672.

Agustí, J. (1985). Bioestratigrafía de los depósitos plio-pleistocenos de la depresión de Guadix-Baza (prov. De Granada). *Paleontología i Evolució, 18*, 13–18.

Agustí, J., Oms, O., Parés, J. M., Martínez-Navarro, B., & Turq, A. (2000). Dating and correlation of early human occupation in the Baza formation (Guadix-Baza Basin, SE Spain). *Early Humans at the Gates of Europe, 92*, 113–122.

Alberdi, M. T., & Bonadonna, F. P., Eds. (1989). Geología y Paleontología de la Cuenca de Guadix-Baza. Trabajos sobre el Neógeno-Cuaternario 11. Museo Nacional de Ciencias Naturales, CSIC, Madrid, 1–173.

Alemseged, Z., Spoor, F., Kimbel, W. H., Bobe, R., Geraads, D., Reed, D., & Wynn, J. G. (2006). A juvenile early hominin skeleton from Dikika, Ethiopia. *Nature, 443*, 296–301. https://doi.org/10.1038/nature05047

Alfaro, P., Delgado, J., Sanz de Galdeano, C., Galindo-Zaldívar, J., García-Tortosa, F. J., López-Garrido, A. C., López-Casado, C., Marín-Lechado, C., Gil, A., & Borque, M. J. (2008). The Baza fault: a major active extensional fault in the central Betic Cordillera (south Spain). *International Journal of Earth Sciences, 97*, 1353–1365. https://doi.org/10.1007/s00531-007-0213-

Alfaro, P., Estévez, A., Moretti, M., & Soria, J. M. (2000). Estructuras sedimentarias de deformación en el Mioceno superior-Cuaternario de la Cordillera Bética. *Revista Sociedad Geologica De España, 13*, 79–89.

Alfaro, P., Gibert, L., Moretti, M., García-Tortosa, F. J., Sanz de Galdeano, C., Galindo- Zaldívar, J., & López-Garrido, A. C. (2010). The significance of giant seismites in the Plio-Pleistocene Baza palaeo-lake (S Spain). *Terra Nova, 22*, 172–179. https://doi.org/10.1111/j.1365-3121.2010.00930.x

Alfaro, P., Moretti, M., & Soria, J. M. (1997). Soft-sediment deformation structures induced by earthquakes (seismites) in Pliocene lacustrine deposits (Guadix-Baza Basin, central Betic Cordillera). *Eclogae Geologicae Helvetiae, 90*, 531–540.

Álvarez, C., Parés, J. M., Granger, D., Duval, M., Sala, R., & Toro, I. (2015). New magnetostratigraphic and numerical age of the Fuente Nueva-3 site (Guadix-Baza Basin, Spain). *Quaternary International, 389*, 224–234. https://doi.org/10.1016/j.quaint.2015.04.044

Álvarez-Posada, C., Parés, J. M., Sala, R., Viseras, C., & Pla-Pueyo, S. (2017). New magnetostratigraphic evidence for the age of Acheulean tools at the archaeo-palaeontological site "Solana del Zamborino" (Guadix–Baza Basin, S Spain). *Scientific Reports, 7*, 1–9. https://doi.org/10.1038/s41598-017-14024-5

Amirkhanov, H. A., Ozherelyev, D. V., Sablin, M. V., & Agadzhanyan, A. K. (2016). Faunal remains from the oldowan site of Muhkai II in the north caucasus: potential for dating and palaeolandscape reconstruction. *Quaternary International, 395*, 233–241. https://doi.org/10.1016/j.quaint.2014.12.061

Arribas, A., & Palmqvist, P. (1998). Taphonomy and palaeoecology of an assemblage of large mammals: hyaenid activity in the lower Pleistocene site at Venta Micena (Orce, Guadix-Baza Basin, Granada, Spain). *Geobios, 31*, 3–47. https://doi.org/10.1016/S0016-6995(98)80056-9

Asfaw, B., Beyene, Y., Suwa, G., Walter, R. C., White, T. D., Wolde Gabriel, G., & Yemane, T. (1992). The earliest Acheulean from Konso-Gardula. *Nature, 30*, 732–735. https://doi.org/10.1038/360732a0

Asfaw, B., Gilbert, W. H., Beyene, Y., Hart, W. K., Renne, P. R., WoldeGabriel, G., Vrba, E. S., & White, T. D. (2002). Remains of *Homo erectus* from Bouri, Middle Awash, Ethiopia. *Nature, 416*, 317–320. https://doi.org/10.1038/416317a

Azañón, J. M., Tuccimei, P., Azor, A., Sánchez-Almazo, I. M., Alonso-Zarza, A. M., Soligo, M., & Pérez-Peña, J. V. (2006). Calcrete features and age estimates from U/Th dating: implications for the analysis of quaternary erosion rates in the northern limb of the Sierra Nevada (Betic Cordillera, Southeast Spain). In A. M. Alonso-Zarza & L. H. Tanner (Eds.), *Paleoenvironmental record and applications of calcretes and palustrine carbonates* (pp. 223–239). https://doi.org/10.1130/2006.2416(14) Special Paper.

Baales, M. (2014). Untermassfeld–Or the struggle for finding the earliest traces of human occupation in Central Europe: a comment on: "Hominin dispersals from the Jaramillo subchron in central and south-western Europe: Untermassfeld (Germany) and Vallparadís (Spain)" by J. Garcia et al., *Quat. Int*. 316 (2013), 73–93. *Quaternary International, 337*, 254–256. https://doi.org/10.1016/j.quaint.2014.05.021

Baena Pérez, J., Guzmán del Pino, J. L., & Voerman, F. (1979). *Memoria explicativa del mapa geológico de España escala 1 :50.000, Hoja 973 (23-39) Chirivel*. Instituto Geologico y Minero de Espana (IGME).

Bahain, J. J., Falguères, C., Voinchet, P., Duval, M., Dolo, J. M., Despriée, J., Garcia, T., & Tissoux, H. (2007). Electron spin resonance (ESR) dating of some European late lower Pleistocene sites. *Quaternaire, 18*, 175–186. https://doi.org/10.4000/quaternaire.1048

Bailey, G. N., Reynolds, S. C., & King, G. C. P. (2011). Landscapes of human evolution: models and methods of tectonic geomorphology and the reconstruction of hominin landscapes. *Journal of Human Evolution, 60*, 257–280. https://doi.org/10.1016/j.jhevol.2010.01.004

Bailey, T., Choi, B. J., Colburn, M., Meissl, M., Shaya, S., Ekerdt, J. G., Sreenivasan, S. V., & Willson, C. G. (2000). Step and flash imprint lithography: template surface treatment and defect analysis. *Journal of Vacuum Science and Technology B, 18*(6), 3572–3577. https://doi.org/10.1116/1.1324618

Barkai, R., Gopher, A., Lauritzen, S. E., & Frumkin, A. (2003). Uranium series dates from Qesem Cave, Israel, and the end of the Lower Palaeolithic. *Nature, 423*, 977–979. https://doi.org/10.1038/nature01718

Barsky, D., Chapon-Sao, C., Bahain, J. J., Beyene, Y., Cauche, D., Celiberti, V., Desclaux, E., de Lumley, H., de Lumley, M.-A., Marchal, F., Moullé, P.-E., & Pleurdeau, D. (2011). The early oldowan stone-tool assemblage from Fejej FJ-1A. *Ethiopia. Journal of African Archaeology, 9*(2), 207–224. https://doi.org/10.3213/2191-5784-10196

Barsky, D., & de Lumley, H. (2010). Early European Mode 2 and the stone industry from the Caune de l'Arago's archeostratigraphical levels "P." *Quaternary International, 223*, 71–86. https://doi.org/10.1016/j.quaint.2009.12.005

Belhai, M., Fujimitsu, Y., Nishijima, J., & Bersi, M. (2017). Hydrochemistry and gas geochemistry of the northeastern Algerian

geothermal waters. *Arabian Journal of Geosciences, 10*, 8. https://doi.org/10.1007/s12517-016-2790-2

Bell, R. H. V. (1981). The effect of soil nutrient availability on community structure in African ecosystems. In B. J. Huntley & B. H. Walker (Eds.), *Ecology of tropical savannas (analysis and synthesis)* (Vol. 42, pp. 193–216). Springer.

Bermúdez de Castro, J. M., Arsuaga, J. L., Carbonell, E., Rosas, A., Martínez, I., & Mosquera, M. (1997). A hominid from the lower pleistocene of Atapuerca, Spain: possible ancestor to neandertals and modern humans. *Science, 276*, 1392–1395. https://doi.org/10.1126/science.276.5317.1392

Bermúdez de Castro, J. M., de Pinillos, M. M., López-Polín, L., Martín-Francés, L., García-Campos, C., Modesto-Mata, M., Rosell, J., & Martinón-Torres, M. (2020). A descriptive and comparative study of two early pleistocene immature scapulae from the TD6. 2 level of the Gran Dolina cave site (Sierra de Atapuerca, Spain). *Journal of Human Evolution, 139*, 102689. https://doi.org/10.1016/j.jhevol.2019.102689

Blain, H. A., Lozano-Fernández, I., Agustí, J., Bailon, S., Granda, L. M., Espigares, M. P., Ros-Montoya, S., Jiménez-Arenas, J. M., Toro-Moyano, I., Martínez-Navarro, B., & Sala, R. (2016). Refining upon the climatic background of the early Pleistocene hominid settlement in Western Europe: Barranco León and Fuente Nueva-3 (Guadix-Baza Basin, SE Spain). *Quaternary Science Reviews, 144*, 132–144. https://doi.org/10.1016/j.quascirev.2016.05.020

Boaz, N. T., & Howell, F. C. (1977). A gracile hominid cranium from upper member G of the Shungura formation, Ethiopia. *American Journal of Physical Anthropology, 46*, 93–108. https://doi.org/10.1002/ajpa.1330460113

Boncheva, I., Andreeva, P., Sachanski, V., Yaneva, M., & Georgiev, S. (2023). Palaeozoic (Silurian–Devonian) cherts from the Balkan Terrane, western Bulgaria: geochemistry, biostratigraphy and depositional settings. *Palaeobiodiversity Palaeoenvironments, 103*, 711–731. https://doi.org/10.1007/s12549-023-00578-y

Bond, G., Showers, W., Cheseby, M., Lotti, R., Almasi, P., de Menocal, P., Priore, P., Cullen, H., Hajdas, I., & Bonani, G. (1997). A pervasive millennial- scale cycle in north Atlantic Holocene and glacial climates. *Science, 278*, 1257–1266. https://doi.org/10.1126/science.278.5341.1257

Boström, M. K., Kraemer, T., & Gartner, S. (1973). Provenance and accumulation rates of opaline silica, Al, Ti, Fe, Mn, Cu, Ni and Co in Pacific pelagic sediments. *Chemical Geology, 11*(2), 123–148. https://doi.org/10.1016/0009-2541(73)90049-1

Bourguignon, L., Crochet, J. Y., Capdevila, R., Ivorra, J., Antoine, P. O., Agustí, J., Barsky, D., Blain, H.-A., Boulbes, N., Bruxelles, L., Claude, J., Cochard, D., Filoux, A., Firmat, C., Lozano-Fernández, I., Magniez, P., Pelletier, M., Ríos Garaizar, J., Testu, A., … De Weyer, L. (2016). Bois-de-Riquet (Lézignan-la-Cèbe, Hérault): a late early pleistocene archeological occurrence in southern France. *Quaternary International, 393*, 24–40. https://doi.org/10.1016/j.quaint.2015.06.037

Braga, J. C., Martín, J. M., & Quesada, C. (2003). Patterns and average rates of late neogene-recent uplift of the Betic Cordillera, SE Spain. *Geomorphology, 50*, 3–26. https://doi.org/10.1016/S0169-555X(02)00205-2

Braun, D. R., Levin, N. E., Stynder, D., Herries, A. I. R., Archer, W., Forrest, F., Roberts, D. L., Bishop, L. C., Matthews, T., Lehmann, S. B., Pickering, R., & Fitzsimmons, K. E. (2013). Mid-pleistocene hominin occupation at elandsfontein, Western Cape, South Africa. *Quaternary Science Reviews, 82*, 145–166. https://doi.org/10.1016/j.quascirev.2013.09.027

Bromage, T. G., Schrenk, F., & Juwayeyi, Y. M. (1995). Paleobiogeography of the Malawi Rift: age and vertebrate paleontology of the Chiwondo Beds, northern Malawi. *Journal of Human Evolution, 28*, 37–57. https://doi.org/10.1006/jhev.1995.1005

Brunet, M., Guy, F., Pilbeam, D., Mackaye, H. T., Likius, A., Ahounta, D., Beauvilain, A., Blondel, C., Bocherens, H., Boisserie, J.-R., De Bonis, L., Coppens, Y., Dejax, J., Denys, C., Duringer, P., Eisenmann, V., Fanone, G., Fronty, P., Geraads, D., … Zollikofer, C. (2002). A new hominid from the Upper Miocene of Chad, Central Africa. *Nature, 418*, 145–151. https://doi.org/10.1038/nature00879

Bunn, H. T. (1981). Archaeological evidence for meat-eating by Plio-Pleistocene hominids from Koobi Fora and Olduvai Gorge. *Nature, 291*, 574. https://doi.org/10.1038/291574a0

Byrne, L. (2004). Lithic tools from Arago cave, Tautavel (Pyrenees-Orientales, France): behavioural continuity or raw material determinism during the Middle Pleistocene. *Journal of Archaeological Science, 31*, 351–364. https://doi.org/10.1016/j.jas.2003.07.008

Calvache, M. L., & Viseras, C. (1997). Long-term control mechanisms of stream piracy processes in southeast Spain. *Earth Surface Processes and Landforms, 22*, 93–105. https://doi.org/10.1002/(SICI)1096-9837(199702)22:2%3c93::AID-ESP673%3e3.0.CO;2-W

Canet, C., Prol-Ledesma, R. M., Proenza, J. A., Rubio-Ramos, M. A., Forrest, M. J., Torres-Vera, M. A., & Rodríguez-Díaz, A. A. (2005). Mn–Ba–Hg mineralization at shallow submarine hydrothermal vents in bahía Concepción, Baja California Sur, Mexico. *Chemical Geology, 224*(1–3), 96–112. https://doi.org/10.1016/j.chemgeo.2005.07.023

Carbonell, E., Bermúdez de Castro, J. M., Parés, J. M., Pérez-González, A., Cuenca-Bescós, G., Ollé, A., Mosquera, M., Huguet, R., van der Made, J., Rosas, A., Sala, R., Valverdú, J., García, N., Granger, D. E., Martinón-Torres, M., Rodríguez, X. P., Stock, G. M., Vergès, J. M., Allué, E., … Arsuaga, J. L. (2008). The first hominin of Europe. *Nature, 452*, 465–470. https://doi.org/10.1038/nature06815

Chazan, M., Ron, H., Matmon, A., Porat, N., Goldberg, P., Yates, R., Avery, M., Sumner, A., & Horwitz, L. K. (2008). Radiometric dating of the earlier stone age sequence in excavation I at wonderwerk cave, South Africa: preliminary results. *Journal of Human Evolution, 55*, 1–11. https://doi.org/10.1016/j.jhevol.2008.01.004

Coe, M. J., Cumming, D. H., & Phillipson, J. (1976). Biomass and production of large African herbivores in relation to rainfall and primary production. *Oecologia, 22*, 341–354. https://doi.org/10.1007/BF00345312

Coltorti, M., Feraud, G., Marzoli, A., Peretto, C., Ton-That, T., Voinchet, P., Bahain, J.-J., Minelli, A., & Hohenstein, U. T. (2005). New 40Ar/39Ar, stratigraphic and palaeoclimatic data on the Isernia La Pineta Lower Palaeolithic site, Molise, Italy. *Quaternary International, 131*, 11–22. https://doi.org/10.1016/j.quaint.2004.07.004

Conroy, G. C., Jolly, C., Cramer, D., & Kalb, J. (1978). Newly discovered fossil hominid skull from the afar depression, Ethiopia. *Nature, 276*, 67–70. https://doi.org/10.1038/276067a0

Coppens, Y. (1994). East side story: the origin of humankind. Scientific American, 270(5), 88–95. https://www.jstor.org/stable/24942699.

Crespo, M. T., Pérez del Villar, L., Delgado, A., Martín, A., & Prado, A. J. (2014). Caracterización mineralógica, geoquímica e isotópica de los travertinos asociados al sistema termal de Alicún de las Torres (provincia de Granada): implicaciones paleoclimáticas y paleoambientales. http://documenta.ciemat.es/handle/123456789/127

Cruz-Sanjulián, J., & García-Rosell, L. (1972). Características hidrogeológicas del sector del Jabalcón (Provincia de Granada). *Boletin Geologico y Minero, LXXXIII–I*, 68–80.

Cruz-Sanjulián, J., & García-Rosell, L. (1975). Termalismo en España meridional. *Boletín Geologico y Minero, 86*, 179–186.

Cruz-Sanjulián, J., García-Rosell, L., & Garrido-Blasco, J. (1972). Aguas termales de la provincia de Granada. *Boletin Geologico y Minero, LXXXIII–III*, 266–275.

Cuevas, F., Martín Penela, A., Rodríguez Fernández, J., Sanz de Galdeano, C., & Vera, J. A. (1984). Première datation du Turolien à la base de la Formation de Guadix (Secteur d'Abla, Almería, Espagne). *Geobios, 17*, 355–361. https://doi.org/10.1016/S0016-6995(84)80100-X

Daura, J., Sanz, M., Arsuaga, J. L., Hoffmann, D. L., Quam, R. M., Ortega, M. C., Santos, E., Gómez, S., Rubio, A., Villaescusa, L., Souto, P., Mauricio, J., Rodrigues, F., Ferreira, A., Godinho, P., Trinkaus, E., & Zilhão, J. (2017). New Middle Pleistocene hominin cranium from Gruta da Aroeira (Portugal). *Proceedings of the National Academy of Sciences, 114*, 3397–3402. https://doi.org/10.1073/pnas.1619040114

De la Torre, I., Mora, R., Dominguez-Rodrigo, M., de Luque, L., & Alcalá, L. (2003). The oldowan industry of peninj and its bearing on the reconstruction of the technological skills of lower pleistocene hominids. *Journal of Human Evolution, 44*, 203–224. https://doi.org/10.1016/S0047-2484(02)00206-3

De Ruiter, D. J., Pickering, R., Steininger, C. M., Kramers, J. D., Hancox, P. J., Churchill, S. E., Berger, L. R., & Backwell, L. (2009). New *Australopithecus robustus* fossils and associated U-Pb dates from Cooper's Cave (Gauteng, South Africa). *Journal of Human Evolution, 56*, 497–513. https://doi.org/10.1016/j.jhevol.2009.01.009

Delinom, R. M. (2009). Structural geology controls on groundwater flow: lembang fault case study, West Java, Indonesia. *Hydrogeology Journal, 17*, 1011–1023. https://doi.org/10.1007/s10040-009-0453-z

DeoCampo, D. M. (2002). Sedimentary structures generated by Hippopotamus amphibius in a Lake-margin Wetland, Ngorongoro Crater, Tanzania. *Palaios, 17*, 212–217. https://doi.org/10.1669/0883-1351(2002)017%3c0212:SSGBHA%3e2.0.CO;2

Despriée, J., Voinchet, P., Gageonnet, R., Dépont, J., Bahain, J. J., Falguères, C., Tissoux, H., Dolo, J.-M., & Courcimault, G. (2009). Les vagues de peuplements humains au Pléistocène inférieur et moyen dans le bassin de la Loire moyenne, région Centre, France. Apports de l'étude des formations fluviatiles. *L'anthropologie, 113*, 125–167. https://doi.org/10.1016/j.anthro.2009.01.007

Diputación de Granada-ITGE. (1990). *Atlas Hidrogeológico de la Provincia de Granada* (p. 107). ITGE.

Dirks, P. H., Kibii, J. M., Kuhn, B. F., Steininger, C., Churchill, S. E., Kramers, J. D., Pickering, R., Farber, D. L., Mériaux, A.-S., Herries, A. I. R., King, G. C. P., & Berger, L. R. (2010). Geological setting and age of *Australopithecus sediba* from southern Africa. *Science, 328*, 205–208. https://doi.org/10.1126/science.1184950

Duller, G. A. T., Tooth, S., Barham, L., & Tsukamoto, S. (2015). New investigations at Kalambo Falls, Zambia: luminescence chronology, site formation, and archaeological significance. *Journal of Human Evolution, 85*, 111–125. https://doi.org/10.1016/j.jhevol.2015.05.003

El-Moghazy, A. F., Deaf, A. S., & Edress, N. A. A. (2023). Integrated organic, inorganic geochemical and palynofacies analyzes to characterize the paleoenvironment of the Tortonian (late miocene) wakar Formation, offshore Nile Delta, Egypt. *Marine and Petroleum Geology, 156*, 106456. https://doi.org/10.1016/j.marpetgeo.2023.106456

Elzea, J. M., Odom, I. E., & Miles, W. J. (1994). Distinguishing well ordered opal-CT and opal-C from high temperature cristobalite by x-ray diffraction. *Analytica Chimica Acta, 286*(1), 107–116. https://doi.org/10.1016/0003-2670(94)80182-7

Espigares, M. P., Martínez-Navarro, B., Palmqvist, P., Ros-Montoya, S., Toro, I., Agustí, J., & Sala, R. (2013). *Homo* vs. *Pachycrocuta*: earliest evidence of competition for an elephant carcass between scavengers at Fuente Nueva-3 (Orce, Spain). *Quaternary International, 295*, 113–125. https://doi.org/10.1016/j.quaint.2012.09.032

Espigares, M. P., Palmqvist, P., Guerra-Merchán, A., Ros-Montoya, S., García-Aguilar, J. M., Rodríguez- Gómez, G., Serrano, F. J., & Martínez-Navarro, B. (2019). The earliest cut marks of Europe: a discussion on hominin subsistence patterns in the Orce sites (Baza Basin, SE Spain). *Scientific Reports, 9*, 1–13. https://doi.org/10.1038/s41598-019-51957-5

Fick, S. E., & Hijmans, R. J. (2017). Worldclim 2: New 1-km spatial resolution climate surfaces for global land areas. *International Journal of Climatology, 37*, 4302–4315. https://doi.org/10.1002/joc.5086

Finlayson, C., Carrión, J., Brown, K., Finlayson, G., Sánchez-Marco, A., Darren, F., Rodríguez-Vidal, J., Fernández, S., Fierro, E., Bernal-Gómez, M., & Giles-Pacheco, F. (2011). The *Homo* habitat niche: using the avian fossil record to depict ecological characteristics of Palaeolithic Eurasian hominins. *Quaternary Science Reviews, 30*(11–12), 1525–1532. https://doi.org/10.1016/j.quascirev.2011.01.010

Flörke, O. W., Graetsch, H., & Jones, J. B. (1990). Hydrothermal deposition of cristobalite. *Neues Jahrbuch für Mineralogie—Monatshefte, 2*, 81–95.

Foley, R. (1987). Hominid species and stone-tool assemblages: how are they related? *Antiquity, 61*(233), 380–392. https://doi.org/10.1017/S0003598X00072938

Foucault, A., & Mélières, F. (2000). Palaeoclimatic cyclicity in central Mediterranean Pliocene sediments: the mineralogical signal. *Palaeogeography, Palaeoclimatology, Palaeoecology, 158*, 311–323. https://doi.org/10.1016/S0031-0182(00)00056-0

Fournier, R. O. (1977). Chemical geothermometers and mixing models for geothermal systems. *Geothermics, 5*, 41–50. https://doi.org/10.1016/0375-6505(77)90007-4

Fournier, R. O., & Rowe, J. J. (1966). Estimation of underground temperatures from the silica content of water from hot springs and wet steam wells. *American Journal of Science, 264*, 685–697. https://doi.org/10.2475/ajs.264.9.685

Fournier, R. O., & Truesdell, A. H. (1973). An empirical Na-K-Ca geothermometer for natural waters. *Geochimica Et Cosmochimica Acta, 37*, 1255–1275. https://doi.org/10.1016/0016-7037(73)90060-4

Fröhlich, F. (2020). The opal-CT nanostructure. *Journal of Non-Crystalline Solids, 533*, 119938. https://doi.org/10.1016/j.jnoncrysol.2020.119938

Gabarda, M. V., Valle, R. M., Calatayud, P. G., Martí, P. G., Pueyo, E., & Casabó, J. (2016). The Lower Palaeolithic site Alto de las Picarazas (Andilla-Chelva, Valencia). *Quaternary International, 393*, 83–94. https://doi.org/10.1016/j.quaint.2015.04.049

Galanidou, N., Cole, J., Iliopoulos, G., & McNabb, J. (2013). East meets West: The middle pleistocene site of rodafnidia on lesvos, Greece. Antiquity, 87 (336). http://antiquity.ac.uk/

Galanidou, N., Athanassas, C., Cole, J., Iliopoulos, G., Katerinopoulos, A., Magganas, A., & McNabb, J. (2016). The Acheulian Site of Rodafnidia, Lisvori, on Lesvos, Greece: 2010–2012. In K. Harvati & M. Roksandic (Eds.), *Paleoanthropology of the balkans and anatolia* (pp. 119–138). Springer.

Gamble, C. (1993). *Timewalkers: The prehistory of global colonization* (p. 320). Penguin Books.

Garcés, M. (1994). Magnetoestratigrafía de los sedimentos lacustres Pliocenos de la sección de Galera (Cuenca de *Guadix-Baza*. Cordilleras Béticas). Acta Geológica Hispánica, 29, 191–194. http://hdl.handle.net/10261/6772

García-Aguilar, J. M. (1997). *La cuenca de Guadix-Baza (Granada) evolución geodinámica y sedimentaria de los depósitos lacustres*

entre el Turoliense superior y el Pleistoceno (p. 544). Universidad de Granada (Spain). Ph.D. Thesis.

García-Aguilar, J. M., Guerra-Merchán, A., Serrano, F., Flores-Moya, A., Delgado-Huertas, A., Espigares, M. P., Ros-Montoya, S., Martínez-Navarro, B., & Palmqvist, P. (2015). A reassessment of the evidence for hydrothermal activity in the neogene-quaternary lacustrine environments of the Baza Basin (Betic Cordillera, SE Spain) and its paleoecological implications. *Quaternary Science Reviews, 112*, 226–235. https://doi.org/10.1016/j.quascirev.2015.02.001

García-Aguilar, J. M., Guerra-Merchán, A., Serrano, F., & Palmqvist, P. (2013). Ciclicidad sedimentaria en depósitos lacustres evaporíticos tipo playa-lake del Pleistoceno inferior en la cuenca de Guadix-Baza (Cordillera Bética, España). *Boletín Geologico y Minero, 124*, 239–251.

García-Aguilar, J. M., Guerra-Merchán, A., Serrano, F., Palmqvist, P., Flores-Moya, A., & Martínez-Navarro, B. (2014). Hydrothermal activity and its paleoecological implications in the latest Miocene to Middle Pleistocene lacustrine environments of the Baza Basin (Betic Cordillera, SE Spain). *Quaternary Science Reviews, 96*, 204–221. https://doi.org/10.1016/j.quascirev.2013.07.009

García-Aguilar, J. M., & Martín, J. M. (2000). Late Neogene to recent continental history and evolution of the Guadix-Baza Basin (SE Spain). *Revista Sociedad Geologica De España, 13*, 65–77.

García-Aguilar, J. M., & Palmqvist, P. (2011). A model of lacustrine sedimentation for the early Pleistocene deposits of Guadix-Baza Basin (southeast Spain). *Quaternary International, 243*, 3–15. https://doi.org/10.1016/j.quaint.2011.02.008

García-Martínez, D., Green, D. J., & Bermúdez de Castro, J. M. (2021). Evolutionary development of the homo antecessor scapulae (Gran Dolina site, Atapuerca) suggests a modern-like development for lower pleistocene. *Scientific Reports, 11*(1), 1–12. https://doi.org/10.1038/s41598-021-83039-w

García-Tortosa, F. J., Alfaro, P., Galindo-Zaldívar, J., Gibert, L., López-Garrido, A. C., Sanz de Galdeano, C., & Ureña, M. (2008b). Geomorphologic evidence of the active Baza fault (Betic Cordillera, south Spain). *Geomorphology, 97*, 374–391. https://doi.org/10.1016/j.geomorph.2007.08.007

García-Tortosa, F. J., Alfaro, P., Galindo-Zaldívar, J., & Sanz de Galdeano, C. (2011). Glacis geometry as a geomorphic marker of recent tectonics: The Guadix-Baza Basin (South Spain). *Geomorphology, 125*, 517–529. https://doi.org/10.1016/j.geomorph.2010.10.021

García-Tortosa, F. J., Sanz de Galdeano, C., Alfaro, P., Jiménez Espinosa, R., Jiménez Millán, J., & Lorite Herrera, M. (2008a). Nueva evidencia sobre la edad del tránsito endorreico-exorreico de la cuenca de Guadix-Baza. *Geogaceta, 44*, 211–214.

Gates-Rector, S. D., & Blanton, T. N. (2019). The powder diffraction file: A quality materials characterization database. *Powder Diffraction, 34*, 352–360. https://doi.org/10.1017/S0885715619000812

Geraads, D., Alemseged, Z., Reed, D., Wynn, J., & Roman, D. C. (2004). The Pleistocene fauna (other than Primates) from Asbole, lower Awash Valley, Ethiopia, and its environmental and biochronological implications. *Geobios, 37*, 697–718. https://doi.org/10.1016/j.geobios.2003.05.011

Geraads, D., Amani, F., & Hublin, J. J. (1992). Le gisement pléistocène moyen de l'Aïn Maarouf près de El Hajeb, Maroc: Présence d'un hominidé. *Comptes Rendus de l'Académie des Sciences, 314*, 319–323.

Gibert, J., & Gibert, L. (2003). Yacimientos de vertebrados asociados al subcrón Olduvai en Europa, Cáucaso y Levante mediterráneo. En torno a fósiles de mamíferos: datación, evolución y paleoambiente. *Coloquios de Paleontología*, *1*, 195–202. https://revistas.ucm.es/index.php/COPA/article/view/COPA0303220195A

Gibert, L., Ortí, F., & Rosell, L. (2007). Plio-Pleistocene lacustrine evaporites of the Baza Basin (Betic Chain, SE Spain). *Sedimentary Geology, 200*, 89–116. https://doi.org/10.1016/j.sedgeo.2007.03.003

Gibert, L., Sanz de Galdeano, C., Alfaro, P., Scott, G., & López Garrido, A. C. (2005). Seismic-induced slump in early pleistocene deltaic deposits of the Baza Basin (SE Spain). *Sedimentary Geology, 179*(3–4), 279–294. https://doi.org/10.1016/j.sedgeo.2005.06.003

Gibert, L., Scott, G. R., & Ferràndez-Canyadell, C. (2006). Evaluation of the Olduvai sub-chron in the Orce Ravine (SE Spain). Implications for Plio-Pleistocene mammal biostratigraphy and the age of Orce archaeological sites. *Quaternary Science Reviews, 25*, 507–525. https://doi.org/10.1016/j.quascirev.2005.03.006

Gibert, L., Scott, G. R., Scholz, D., Budsky, A., Fernàndez, C., Ribot, F., Martin, R. A., & Lería, M. (2016). Chronology for the Cueva Victoria fossil site (SE Spain): Evidence for Early Pleistocene Afro-Iberian dispersals. *Journal of Human Evolution, 90*, 183–197. https://doi.org/10.1016/j.jhevol.2015.08.002

Giggenbach, W. F., Minissale, A. A., & Scandiffio, G. (1988). Isotopic and chemical assessment of geothermal potential of the Coili Albani area, Latium region, Italy. *Applied Geochemistry, 3*, 475–486. https://doi.org/10.1016/0883-2927(88)90020-0

Glerum, A., Brune, S., Stamps, D. S., & Strecker, M. R. (2020). Victoria continental microplate dynamics controlled by the lithospheric strength distribution of the East African Rift. *Nature Communications, 11*, 2881. https://doi.org/10.1038/s41467-020-16176-x

Goren-Inbar, N., Feibel, C. S., Verosub, K. L., Melamed, Y., Kislev, M. E., Tchernov, E., & Saragusti, I. (2000). Pleistocene milestones on the out of Africa corridor at Gesher Benot Yaaqov, Israel. *Science, 289*, 944–947. https://doi.org/10.1126/science.289.5481.944

Gowlett, J. A. J. (2005). *Seeking the palaeolithic individual in east africa and europe during the lower-middle Pleistocene. The hominid individual in context: archaeological investigations of lower and middle palaeolithic landscapes, locales and artifacts* (pp. 50–67). Routledge.

Gowlett, J. A. J., Harris, J. W. K., Walton, D., & Wood, B. A. (1981). Early archaeological sites, hominid remains and traces of fire from Chesowanja, Kenya. *Nature, 294*, 125–129. https://doi.org/10.1038/294125a0

Guérin, C., Eisenmann, V., & Faure, M. (1993). Les grands mammifères du gisement Pléistocène moyen de Latamné (Vallée de l'Oronte, Syrie). Le Paléolithique de la vallée moyenne de l'Oronte (Syrie). Peuplement et environnement. *British Archaeological Reports, 587*, 169–178.

Guerra-Merchán, A. (1992). *Origen y relleno sedimentario de la cuenca neógena del corredor del Almanzora y áreas limítrofes (Cordillera Bética)* (p. 237). Universidad de Granada (Spain). Ph.D. Thesis.

Guerra-Merchán, A., Serrano, F., Hlilab, R., El Kadiri, K., Sanz de Galdeano, C., & Garcés, M. (2014). Tectono-sedimentary evolution of the peripheral Basins of the Alboran Sea in the arc of Gibraltar during the latest Messinian-Pliocene. *Journal of Geodynamics, 77*, 158–170. https://doi.org/10.1016/j.jog.2013.12.003

Gupta, H., & Roy, S. (2007). *Geothermal energy. An alternative resource for the 21st century* (p. 279). Elsevier.

Hagelberg, T. K., Bond, G., & DeMenocal, P. (1994). Milankovitch band forcing of sub-Milankovitch climate variability during the Pleistocene. *Paleoceanography, 9*, 545–558. https://doi.org/10.1029/94PA00443

Haile-Selassie, Y., Saylor, B. Z., Deino, A., Alene, M., & Latimer, B. M. (2010). New hominid fossils from woranso-mille (Central Afar, Ethiopia) and taxonomy of early *Australopithecus*.

American Journal of Physical Anthropology, 141, 406–417. https://doi.org/10.1002/ajpa.21159

Harmand, S., Lewis, J. E., Feibel, C. S., Lepre, C. J., Prat, S., Lenoble, A., Boës, X., Quinn, R. L., Brenet, M., Arroyo, A., Taylor, N., Clément, S., Daver, G., Brugal, J.-P., Leakey, L., Mortlock, R. A., Wright, J. D., Lokorodi, S., Kirwa, C., … Roche, H. (2015). 3.3-million-year-old stone tools from Lomekwi 3, West Turkana, Kenya. *Nature, 521*, 310–315. https://doi.org/10.1038/nature14464

Harrison, R., Mortimer, N. D., & Smarason, O. B. (1990). *Geothermal heating* (p. 556). Pergamon Press.

Hatton, I. A., Mccann, K. S., Fryxell, J. M., Jonathan Davies, T., Smerlak, M., Sinclair, A. R., & Loreau, M. (2015). The predator-prey power law: Biomass scaling across terrestrial and aquatic biomes. *Science, 349*, 6252–6284. https://doi.org/10.1126/science.aac6284

Haywood, A. M., & Valdés, P. J. (2004). Modelling Pliocene warm: Contribution of atmosphere, oceans and cryosphere. *Earth and Planetary Science Letters, 218*, 363–377. https://doi.org/10.1016/S0012-821X(03)00685-X

Hernández, J. D., Martín, M., & Julià, R. (2000). Depósitos travertínicos de Alicún (Depresión de Guadix, Granada: S. España). *Geogaceta, 28*, 35–38.

Herries, A. I. R. (2011). A chronological perspective on the acheulian and its transition to the middle stone age in southern Africa: The question of the Fauresmith. *Int. J. Evol. Biol.* https://doi.org/10.4061/2011/961401

Herries, A. I. R., & Adams, J. (2013). Clarifying the context, dating and age range of the gondolin hominins and *Paranthropus* in South Africa. *Journal of Human Evolution, 65*, 676–681. https://doi.org/10.1016/j.jhevol.2013.06.007

Herries, A. I. R., Kappen, P., Kegley, A., Paterson, D., Howard, D., de Jonge, M., Potze, S., & Adams, J. W. (2014). Palaeomagnetic and synchrotron analysis of >1.95 Ma fossil-bearing palaeokarst at Haasgat, South Africa. *South African Journal of Science, 110*, 3–4. https://doi.org/10.1590/sajs.2014/2013010

Herries, A. I. R., Murszewski, A., Pickering, R., Mallett, T., Joannes-Boyau, R., Armstrong, B., Adams, J. W., Baker, S., Blackwood, A. F., Penzo-Kajewski, P., Kappen, P., Leece, A. B., Martin, J., Rovinsky, D., & Boschian, G. (2018). Geoarchaeological and 3D visualisation approaches for contextualising in-situ fossil bearing palaeokarst in South Africa: A case study from the ~2.61 Ma Drimolen Makondo. *Quaternary International, 483*, 90–110. https://doi.org/10.1016/j.quaint.2018.01.001

Herries, A. I. R., & Shaw, J. (2011). Palaeomagnetic analysis of the Sterkfontein palaeocave deposits: Implications for the age of the hominin fossils and stone tool industries. *Journal of Human Evolution, 60*, 523–539. https://doi.org/10.1016/j.jhevol.2010.09.001

Howell, F. C., Haesaerts, P., & de Heinzelin, J. (1987). Depositional environments, archeological occurrences and hominids from Members E and F of the Shungura Formation (Omo Basin, Ethiopia). *Journal of Human Evolution, 16*, 665–700. https://doi.org/10.1016/0047-2484(87)90019-4

Hublin, J. J., Ben-Ncer, A., Bailey, S. E., Freidline, S. E., Neubauer, S., Skinner, M. M., Bergmann, I., Le Cabec, A., Benazzi, S., Harvati, K., & Gunz, P. (2017). New fossils from Jebel Irhoud, Morocco and the pan-African origin of *Homo sapiens*. *Nature, 546*, 289–292. https://doi.org/10.1038/nature22336

Janković, S. (1982). Sb-As-Tl-Ba mineral assemblage of hydrothermal-sedimentary origin, Gümüsköy Deposit, Kütahya (Turkey). In G. C. Amstutz, G. Frenzel, C. Kluth, G. Moh, A. Wauschkuhn, R. A. Zimmermann, & A. Goresy (Eds.), *Ore genesis: The state of the art* (pp. 143–149). Berlin Heidelberg: Springer.

Johanson, D., White, T. D., & Coppens, Y. (1978). A new species of the genus *Australopithecus* (Primates: Hominidae) from the Pliocene of Eastern Africa. *Kirtlandia, 28*, 1–14.

Jungers, W. L., Grine, F. E., Leakey, M. G., Leakey, L., Brown, F., Yang, D., & Tocheri, M. (2015). New hominin fossils from Ileret (Kolom Odiet), Kenya. *American Journal of Biological Anthropology, 156*, 181–181. https://doi.org/10.1038/s41467-021-22208-x

Jurkowska, A., & Świerczewska-Gładysz, E. (2024). The evolution of the marine Si cycle in the Archean-Palaeozoic—an overlooked Si source? *Earth-Science Reviews, 248*, 104629. https://doi.org/10.1016/j.earscirev.2023.104629

Kano, K., & Taguchi, K. (1982). Experimental study on the ordering of opal-CT. *Geochemical Journal, 16*(1), 33–41. https://doi.org/10.2343/geochemj.16.33

King, G., & Bailey, G. (2006). Tectonics and human evolution. *Antiquity, 80*, 265–286. https://doi.org/10.1017/S0003598X00093613

Kissel, M., & Hawks, J. (2015). What are the Lothagam and Tabarin mandibles? *PaleoAnthropology*. https://doi.org/10.4207/PA.2015.ART94

Kuman, K. (2007). The earlier stone age in South Africa: site context and the influence of cave studies. In T. R. Pickering, K. Schick, & N. Toth (Eds.), *Breathing life into fossils: Taphonomic studies in honour of CK (Bob) Brain* (1st ed., pp. 181–198). Stone Age Institute Press.

Kuman, K., & Clarke, R. J. (2000). Stratigraphy, artifact industries and hominid associations for sterkfontein, member 5. *Journal of Human Evolution, 38*, 827–847. https://doi.org/10.1006/jhev.1999.0392

Latham, A. G., & Herries, A. I. R. (2004). The formation and sedimentary infilling of the cave of hearths and historic cave complex, Makapansgat, South Africa. *Geoarchaeology, 19*, 323–342. https://doi.org/10.1002/gea.10122

Leakey, L. S., & Leakey, M. D. (1964). Recent discoveries of fossil hominids in Tanganyika: at Olduvai and near Lake Natron. *Nature, 202*, 5–7. https://doi.org/10.1038/202005a0

Leakey, M. G., Feibel, C. S., McDougall, I., & Walker, A. (1995). New four-million-year-old hominid species from Kanapoi and Allia Bay, Kenya. *Nature, 376*, 565–571. https://doi.org/10.1038/376565a0

Lepre, C. J., & Kent, D. V. (2015). Chronostratigraphy of KNM-ER 3733 and other area 104 hominins from Koobi Fora. *Journal of Human Evolution, 86*, 99–111. https://doi.org/10.1016/j.jhevol.2015.06.010

Lepre, C. J., Quinn, R. L., Joordens, J. C., Swisher, C. C., III., & Feibel, C. S. (2007). Plio-Pleistocene facies environments from the KBS Member, Koobi Fora Formation: Implications for climate controls on the development of lake-margin hominin habitats in the northeast Turkana Basin (northwest Kenya). *Journal of Human Evolution, 53*, 504–514. https://doi.org/10.1016/j.jhevol.2007.01.015

Levitte, D., & Eckstein, Y. (1978). Correlation between the silica concentration and the orifice temperature in the warm springs along the jordan-dead sea rift valley. *Geothermics, 7*, 1–8. https://doi.org/10.1016/0375-6505(78)90021-4

Lisiecki, L. E., & Raymo, M. E. (2007). Plio-Pleistocene climate evolution: trends and transitions in glacial cycle dynamics. *Quaternary Science Reviews, 26*(1–2), 56–69. https://doi.org/10.1016/j.quascirev.2006.09.005

Lister, A. M. (1986). New results on deer from Swanscombe, and the stratigraphical significance of deer in the middle and upper pleistocene of Europe. *Journal of Archaeological Science, 13*(4), 319–338. https://doi.org/10.1016/0305-4403(86)90052-X

Lombera-Hermida, A., Rodríguez-Álvarez, X. P., Peña, L., Sala-Ramos, R., Despriée, J., Moncel, M. H., Gourcimault, G., Voinchet, P., & Falguères, C. (2016). The lithic assemblage from Pont-de-Lavaud (Indre, France) and the role of the bipolar-on-anvil technique in the lower and early middle pleistocene technology. *Journal of*

Anthropological Archaeology, 41, 159–184. https://doi.org/10.1016/j.jaa.2015.12.002

López-Chicano, M., Cerón, J. C., Vallejos, A., & Pulido-Bosch, A. (2001). Geochemistry of thermal springs, Alhama de Granada (southern Spain). *Applied Geochemistry, 16*(9–10), 1153–1163. https://doi.org/10.1016/S0883-2927(01)00020-8

López-García, J. M., Luzi, E., Berto, C., Peretto, C., & Arzarello, M. (2015). Chronological context of the first hominin occurrence in Southern Europe: The *Allophaiomys ruffoi* (Arvicolinae, Rodentia, Mammalia) from Pirro 13 (Pirro Nord, Apulia, southwestern Italy). *Quaternary Science Reviews, 107*, 260–266. https://doi.org/10.1016/j.quascirev.2014.10.029

Lordkipanidze, D., Jashashvili, T., Vekua, A., de León, M. S. P., Zollikofer, C. P., Rightmire, G. P., Pontzer, H., Ferring, R., Oms, O., Tappen, M., Bukhsianidze, M., Agusti, J., Kahlke, R., Kiladze, G., Martinez-Navarro, B., Mouskhelishvili, A., Nioradze, M., & Rook, L. (2007). Postcranial evidence from early *Homo* from Dmanisi, Georgia. *Nature, 449*, 305–310. https://doi.org/10.1038/nature06134

Lynne, B. Y., Campbell, K. A., Moore, J. N., & Browne, P. R. L. (2005). Diagenesis of 1900-year-old siliceous sinter (opal-A to quartz) at Opal Mound, Roosevelt Hot Springs, Utah, USA. *Sedimentary Geology, 179*(3–4), 249–278. https://doi.org/10.1016/j.sedgeo.2005.05.012

Madondo, J., Canet, C., Nuñez-Useche, F., & González-Partida, E. (2021). Geology and geochemistry of jasperoids from the 'Montaña de Manganeso' district, San Luis Potosí, north-central Mexico. *Revista Mexicana de Ciencias Geológicas, 38*(3), 193–209. https://doi.org/10.22201/cgeo.20072902e.2021.3.1651

Magori, C. C., & Day, M. H. (1983). Laetoli Hominid 18: An early Homo sapiens skull. *Journal of Human Evolution, 12*, 747–753. https://doi.org/10.1016/S0047-2484(83)80130-4

Maldonado-Garrido, E., Piñero, P., & Agustí, J. (2017). A catalogue of the vertebrate fossil record from the Guadix-Baza Basin (SE Spain). *Spanish Journal of Palaeontology, 32*(1), 207–236. https://doi.org/10.7203/sjp.32.1.17040

Marder, O., Milevsk, I., Ackerman, O., Rabinovich, R., Shahack-Gross, R., & Fine, P. (2007). The lower paleolithic site of revadim quarry, Israel. In: Proceedings of the 5th international congress on the archaeology of the ancient near east. Madrid, 481–494.

Martín García, L., Gómez Prieto, J. A., & Delgado Salazar, F. (1980). *Memoria explicativa del mapa geológico de España escala 1:50.000, Hoja 994 Baza* (pp. 22–40). IGME.

Martínez, K., Garcia, J., & Carbonell, E. (2013). Hominin multiple occupations in the early and middle pleistocene sequence of Vallparadís (Barcelona, Spain). *Quaternary International, 316*, 115–122. https://doi.org/10.1016/j.quaint.2013.10.021

Martínez-Navarro, B. (1991). *Revisión sistemática y estudio cuantitativo de la fauna de macromamíferos del yacimiento de Venta Micena (Orce, Granada)* (p. 264). Thesis Universidad Autónoma de Barcelona.

Martínez-Navarro, B., Belmaker, M., & Bar-Yosef, O. (2012). The Bovid assemblage (Bovidae, Mammalia) from the Early Pleistocene site of 'Ubeidiya, Israel: Biochronological and paleoecological implications for the fossil and lithic bearing strata. *Quaternary International, 267*, 78–97. https://doi.org/10.1016/j.quaint.2012.02.041

Martínez-Navarro, B., Carbonell, E., Medin, T., Oms, O., Rodríguez-Álvarez, X. P., Ros-Montoya, S., Araia, D., Tsehaie, L., & Libsekal, Y. (2016). The engel ela-ramud basin: a new plio-pleistocene archeo-paleontological site in Eritrea. *Abstracts book of the 6th annual ESHE meeting* (p. 154). European Society for the study of Human Evolution.

Martínez-Navarro, B., Espigares, M. P., Pastó, I., Ros-Montoya, S., & Palmqvist, P. (2014). Early homo fossil records of Europe. In C. Smith (Ed.), *Encyclopedia of global archaeology* (pp. 2561–2570). Springer. https://doi.org/10.1007/978-3-030-30018-0_646

Martínez-Navarro, B., Ros Montoya, S., Espigares, M. P., Madurell-Malapeira, J., & Palmqvist, P. (2018). Los mamíferos del Plioceno y Pleistoceno de la Península Ibérica. *Boletín del Instituto Andaluz del Patrimonio Histórico, 26*, 206–249. https://doi.org/10.33349/2018.0.4203

Martínez-Navarro, B., Turq, A., Agustí, J., & Oms, O. (1997). Fuente Nueva-3 (Orce, Granada, Spain) and the first human occupation of Europe. *Journal of Human Evolution, 33*, 611–620. https://doi.org/10.1006/jhev.1997.0158

Mazo, A., Sesé, S., Ruiz Bustos, A., & Peña, J. A. (1985). Geología y Paleontología de los yacimientos Plio- Pleistocenos de Huéscar (Depresión de Guadix-Baza, Granada). *Estudios Geológicos, 41*, 467–493. https://doi.org/10.3989/egeol.85415-6726

Mbua, E., Kusaka, S., Kunimatsu, Y., Geraads, D., Sawada, Y., Brown, F. H., Sakai, T., Boisserie, J.-R., Saneyoshi, M., Omuombo, C., Muteti, S., Hirata, T., Hayashida, A., Iwano, H., Danhara, T., Bobe, R., Jicha, B., & Nakatsukasa, M. (2016). Kantis: A new Australopithecus site on the shoulders of the Rift Valley near Nairobi, Kenya. *Journal of Human Evolution, 94*, 28–44. https://doi.org/10.1016/j.jhevol.2016.01.006

McKee, J. K. (1993). Faunal dating of the Taung hominid fossil deposit. *Journal of Human Evolution, 25*, 363–376. https://doi.org/10.1006/jhev.1993.1055

Megías, A. G. (1982). *Introducción al análisis tectosedimentario aplicación al estudio dinámico de cuencas* (pp. 385–402). Actas V Congreso Latinoamericano de Geología.

Mendoza, M., Janis, C. M., & Palmqvist, P. (2005). Ecological patterns in the trophic-size structure of large mammal communities: a 'taxon-free' characterization. *Evolutionary Ecology Research, 7*, 505–530.

Miall, A. D. (1984). *Principles of sedimentary Basin analysis* (p. 490). Springer-Verlag.

Michel, V., Shen, C. C., Woodhead, J., Hu, H. M., Wu, C. C., Moullé, P. É., Khatib, S., Cauche, D., Moncel, M.-H., Valensi, P., Chou, Y.-M., Gallet, S., Echassoux, A., Orange, F., & de Lumley, H. (2017). New dating evidence of the early presence of hominins in Southern Europe. *Science and Reports, 7*, 1–8. https://doi.org/10.1038/s41598-017-10178-4

Mietto, P., Avanzini, M., & Rolandi, G. (2003). Human footprints in Pleistocene volcanic ash. *Nature, 422*, 133. https://doi.org/10.1038/422133a

Morgan, L. E., Renne, P. R., Kieffer, G., Piperno, M., Gallotti, R., & Raynal, J. P. (2012). A chronological framework for a long and persistent archaeological record: Melka Kunture, Ethiopia. *Journal of Human Evolution, 62*, 104–115. https://doi.org/10.1016/j.jhevol.2011.10.007

Morley, C. K., Cunningham, S. M., Harper, R. M., & Wescott, W. A. (1992). Geology and geophysics of the Rukwa rift, East Africa. *Tectonics, 11*(1), 69–81. https://doi.org/10.1029/91TC02102

Moyà-Solá, S., Agustí, J., Gibert, J., & Vera, J. A. (1987). Geología y paleontología del pleistoceno inferior de venta micena. *Paleontología i Evolució, Memoria Especial, 1*, 1–295.

Murray, R. W. (1994). Chemical criteria to identify the depositional environment of chert: General principles and applications. *Sedimentary Geology, 90*(3–4), 213–232. https://doi.org/10.1016/0037-0738(94)90039-6

Nordstrom, D. K., Ball, J. W., & McCleskey, R. B. (2005). Ground water to surface water: Chemistry of thermal outflows in Yellowstone National Park. In W. Inskeep & T. R. McDermott (Eds.), *Geothermal biology and geochemistry in Yellowstone National Park* (pp. 73–94). Montana State University.

Olson, D. M., Dinerstein, E., Wikramanayake, E. D., Burgess, N. D., Powell, G. V., Underwood, E. C., D'Amico, J. A., Itoua, I., Strand, H. E., Morrison, J. C., Loucks, C. J., Allnutt, T. F.,

Ricketts, T. H., Kura, Y., Lamoreux, J. F., Wettengel, W. W., Hedao, P., & Kassem, K. R. (2001). Terrestrial Ecoregions of the World: A New global map of life on Earth provides an innovative tool for conserving biodiversity. *BioScience, 51*(11), 933–938. https://doi.org/10.1641/0006-3568(2001)051[0933:TEOTWA]2.0.CO;2

Oms, O., Agustí, J., Gabàs, M., & Anadón, P. (2000). Lithostratigraphical correlation of micromammal sites and biostratigraphy of the upper pliocene to lower pleistocene in the Northeast Guadix-Baza Basin (southern Spain). *Journal of Quaternary Science, 15*(1), 43–50. https://doi.org/10.1002/(SICI)1099-1417(200001)15:1%3c43::AID-JQS475%3e3.0.CO;2-9

Oms, O., Anadón, P., Agustí, J., & Juliá, R. (2011). Geology and chronology of the continental Pleistocene archeological and paleontological sites of the Orce area (Baza Basin, Spain). *Quaternary International, 243*, 33–43. https://doi.org/10.1016/j.quaint.2011.03.048

Oms, O., Dinarès-Turell, J., Agustí, J., & Parés, J. M. (1999). Refinements of the European mammal biochronology from the magnetic polarity record of the plio-pleistocene zújar section, guadix-baza basin, SE Spain. *Quaternary Research, 51*, 94–103. https://doi.org/10.1006/qres.1998.2018

Oms, O., Dinarés-Turell, J., & Parés, J. M. (1996). Resultados paleomagnéticos preliminares de la sección plio-pleistocena de Fuente Nueva (cuenca de Guadix-Baza, Cordilleras Béticas). *Revista Sociedad Geologica De España, 9*, 89–95.

Oms, O., Garcés, M., Parés, J. M., Agustí, J., Anadón, P., & Juliá, R. (1994). Magnetostratigraphic characterization of a thick lower Pleistocene lacustrine sequence from Baza (Betic chain, Southern Spain). *Physics of the Earth and Planetary Interiors, 85*, 173–180. https://doi.org/10.1016/0031-9201(94)90015-9

Oms, O., Parés, J. M., Martínez-Navarro, B., Agustí, A., Toro, I., Martínez Fernández, G., & Turq, A. (2000b). Early human occupation of Western Europe: Paleomagnetic dates of two paleolithic sites in Spain. *Proceedings of the National Academy of Sciences of the United States of America, 97*(19), 10666–10670. https://doi.org/10.1073/pnas.180319797

Özler, H. M. (2000). Hydrogeology and geochemistry in the Çürüksu (Denizli) hydrothermal field, western Turkey. *Environmental Geology, 39*, 1169–1180. https://doi.org/10.1007/s002540000139

Paillard, D. (2017). The plio-pleistocene climatic evolution as a consequence of orbital forcing on the carbon cycle. *Climate of the past, 13*(9), 1259–1267. https://doi.org/10.5194/cp-13-1259-2017

Palmqvist, P., & Arribas, A. (2001). Taphonomic decoding of the paleobiological information locked in a lower Pleistocene assemblage of large mammals. *Paleobiology, 27*, 512–530. https://doi.org/10.1666/0094-8373(2001)027%3c0512:TDOTPI%3e2.0.CO;2

Palmqvist, P., Duval, M., Diéguez, A., Ros-Montoya, S., & Espigares, M. P. (2016). On the fallacy of using orthogenetic models of rectilinear change in arvicolid teeth for estimating the age of the first human settlements in Western Europe. *Historical Biology, 28*, 734–752. https://doi.org/10.1080/08912963.2015.1025390

Palmqvist, P., Espigares, M. P., Pérez-Claros, J. A., Figueirido, B., Guerra-Merchán, A., Ros-Montoya, S., Rodríguez-Gómez, G., García-Aguilar, J. M., Granados, A., & Martínez-Navarro, B. (2022). Déjà vu: a reappraisal of the taphonomy of quarry VM4 of the early pleistocene site of Venta Micena (Baza Basin, SE Spain). *Scientific Reports, 12*, 705. https://doi.org/10.1038/s41598-021-04725-3

Palmqvist, P., Martínez-Navarro, B., & Arribas, A. (1996). Prey selection by terrestrial carnivores in a lower pleistocene paleocommunity. *Paleobiology, 22*, 514–534. https://doi.org/10.1017/S009483730001650X

Palmqvist, P., Martínez-Navarro, B., Pérez-Claros, J. A., Torregrosa, V., Figueirido, B., Jiménez-Arenas, J. M., Espigares, M. P., Ros-Montoya, S., & De Renzi, M. (2011). The giant hyena *Pachycrocuta brevirostris*: Modelling the bone-cracking behavior of an extinct carnivore. *Quaternary International, 243*, 61–79. https://doi.org/10.1016/j.quaint.2010.12.035

Palmqvist, P., Rodríguez-Gómez, G., Bermúdez de Castro, J. M., García-Aguilar, J. M., Espigares, M. P., Figueirido, B., Ros-Montoya, S., Granados, A., Serrano, F. J., Martínez-Navarro, B., & Guerra-Merchán, A. (2022). Insights on the Early Pleistocene hominin population of the Guadix-Baza Depression (SE Spain) and a review on the ecology of the first peopling of Europe. *Frontiers in Ecology and Evolution, 10*, 881651. https://doi.org/10.3389/fevo.2022.881651

Palmqvist, P., Rodríguez-Gómez, G., & Espigares, M. P. (2022). Climate and environmental conditions in the Guadix-Baza Depression during the first hominin dispersal in Western Europe: Comment on Saarinen et al. (2021). *Quaternary Science Reviews, 297*, 107731. https://doi.org/10.1016/j.quascirev.2022.107731

Palmqvist, P., Rodríguez-Gómez, G., Martínez-Navarro, B., Espigares, M. P., Figueirido, B., Ros-Montoya, S., Guerra-Merchán, A., Granados, A., & García-AguilarPérez-Claros, J. M. J. .A. . (2023). Déjà vu: On the use of meat resources by sabretooth cats, hominins, and hyaenas in the Early Pleistocene site of Fuente Nueva 3 (Guadix-Baza Depression, SE Spain). *Archaeological and Anthropological Sciences, 15*, 17. https://doi.org/10.1007/s12520-022-01712-1

Parés, J. M., & Pérez-González, A. (1999). Magnetochronology and stratigraphy at gran dolina section, Atapuerca (Burgos, Spain). *Journal of Human Evolution, 37*, 325–342. https://doi.org/10.1006/jhev.1999.0331

Parfitt, S. A., Ashton, N. M., Lewis, S. G., Abel, R. L., Coope, G. R., Field, M. H., Gale, R., Hoare, P. G., Larkin, N. R., Lewis, M. D., Karloukovski, V., Maher, B. A., Peglar, S. M., Preece, R. C., Whittaker, J. E., & Stringer, C. B. (2010). Early Pleistocene human occupation at the edge of the boreal zone in northwest Europe. *Nature, 466*, 229–233. https://doi.org/10.1038/nature09117

Parfitt, S. A., Barendregt, R. W., Breda, M., Candy, I., Collins, M., Coope, G. R., Durbidge, P., Field, M. H., Lee, J. R., Lister, A. M., Mutch, R., Penkman, K. E. H., Preece, R. C., Rose, J., Stringer, C. B., Symmons, R., Whittaker, J. E., Wymer, J. J., & Stuart, A. J. (2005). The earliest record of human activity in northern Europe. *Nature, 438*, 1008–1012. https://doi.org/10.1038/nature04227

Peña, J. A., Rodríguez Fernández, J., & Ruiz Bustos, A. (1977). El yacimiento de vertebrados de Cortes de Baza 1 (Depresión de Guadix-Baza). Nota preliminar. *Acta Geológica Hispánica, XII*(1–3), 42–45.

Platt, J. P., Behr, W. M., Johanesen, K., & Williams, J. R. (2013). The Betic-Rif arc and its orogenic hinterland: a review. *Annual Review of Earth and Planetary Sciences, 41*, 313–357. https://doi.org/10.1146/annurev-earth-050212-123951

Playà, E., Ortı, F., & Rosell, L. (2000). Marine to non-marine sedimentation in the upper Miocene evaporites of the Eastern Betics, SE Spain: Sedimentological and geochemical evidence. *Sedimentary Geology, 133*(1–2), 135–166.

Plummer, T., & Bishop, L. (2016). Oldowan hominin behavior and ecology at Kanjera South Kenya. *Journal of Anthropological Sciences, 94*, 29–40. https://doi.org/10.4436/jass.94033

Potts, R. (1994). Variables versus models of early pleistocene hominid land use. *Journal of Human Evolution, 27*, 7–24. https://doi.org/10.1006/jhev.1994.1033

Poulianos, A. N. (1984). Once more on the age and stratigraphy of the petralonian man. *Journal of Human Evolution, 13*, 465–467. https://doi.org/10.1016/S0047-2484(84)80059-7

Prothero, D. R., & Schwab, F. (2004). *Sedimentary geology* (p. 557). Macmillan.

Reading, H. G. (1978). *Sedimentary environment and facies* (p. 569). Blackwell Scientific Publications.

Rodríguez, J., Burjachs, F., Cuenca-Bescós, G., García, N., Van der Made, J., Pérez-González, A., Blain, H.-A., Expósito, I., López-García, J. M., García Antón, M., Allué, E., Cáceres, I., Huguet, R., Mosquera, M., Ollé, A., Rosell, J., Parés, J. M., Rodríguez, X. P., Díez, C., … Carbonell, E. (2011). One million years of cultural evolution in a stable environment at atapuerca (Burgos, Spain). *Quaternary Science Reviews, 30*(11–12), 1396–1412. https://doi.org/10.1016/j.quascirev.2010.02.021

Rodríguez-Gómez, G., Martín-González, J. A., Espigares, M. P., Bermúdez de Castro, J. M., Martínez-Navarro, B., Arsuaga, J. L., & Palmqvist, P. (2024). From meat availability to hominin and carnivore biomass: A paleosynecological approach to reconstructing predator-prey biomass ratios in the Pleistocene. *Quaternary Science Reviews, 328*, 108474. https://doi.org/10.1016/j.quascirev.2023.108474

Rodríguez-Gómez, G., Mateos, A., Martín-González, J. A., Blasco, R., Rosell, J., & Rodríguez, J. (2014). Discontinuity of human presence at atapuerca during the early middle pleistocene: A matter of ecological competition? *PLoS One, 9*(7), e101938. https://doi.org/10.1371/journal.pone.0101938

Rodríguez-Gómez, G., Palmqvist, P., Martínez-Navarro, B., Martín-González, J. A., & Bermúdez de Castro, J. M. (2022). Mean body size estimation in large mammals and the computation of biomass in past ecosystems: An application to the Pleistocene sites of Orce and Sierra de Atapuerca (Spain). *Comptes Rendus Palevol, 21*(10), 207–233. https://doi.org/10.5852/cr-palevol2022v21a10

Rodríguez-Gómez, G., Palmqvist, P., Rodríguez, J., Mateos, A., Martín-González, J. A., Espigares, M. P., Ros-Montoya, S., & Martínez-Navarro, B. (2016). On the ecological context of the earliest human settlements in Europe: resource availability and competition intensity in the carnivore guild of Barranco León-D and Fuente Nueva-3 (Orce, Baza Basin, SE Spain). *Quaternary Science Reviews, 143*, 69–83. https://doi.org/10.1016/j.quascirev.2016.05.018

Rodríguez-Gómez, G., Palmqvist, P., Ros-Montoya, S., Espigares, M. P., & Martínez-Navarro, B. (2017). Resource availability and competition intensity in the carnivore guild of the Early Pleistocene site of Venta Micena (Orce, Baza Basin, SE Spain). *Quaternary Science Reviews, 164*, 154–167. https://doi.org/10.1016/j.quascirev.2017.04.006

Ronen, A., Ohel, M. Y., Lamdan, M., & Assaf, A. (1980). Acheulean artifacts from two trenches at Ma'ayan Barukh. *Israel Exploration Journal, 30*, 17–33.

Ros-Montoya, S. (2010). *Los Proboscídeos del Plio-Pleistoceno de las Cuencas de Guadix-Baza y Granada* (p. 403). Thesis Universidad de Granada (Spain). Ph.D. Thesis.

Ros-Montoya, S., Martínez-Navarro, B., Espigares, M. P., Guerra-Merchán, A., García-Aguilar, J. M., Piñero, P., Rodríguez-Rueda, A., Agustí, J., Oms, O., & Palmqvist, P. (2017). A new Ruscinian site in Europe: Baza-1 (Baza Basin, Andalusia, Spain). *Comptes Rendus Palevol, 16*(7), 746–761. https://doi.org/10.1016/j.crpv.2017.05.005

Ros-Montoya, S., Palombo, M. R., Espigares, M. P., Palmqvist, P., & Martínez-Navarro, B. (2018). The mammoth from the archaeopaleontological site of Huéscar-1: A tile in the puzzling question of the replacement of Mammuthus meridionalis by Mammuthus trogontherii in the late Early Pleistocene of Europe. *Quaternary Science Reviews, 197*, 336–351. https://doi.org/10.1016/j.quascirev.2018.08.017

Ruiz-Bustos, A. (1976). *Estudio sistemático y ecológico sobre la fauna del Pleistoceno medio en las depresiones granadinas*. El yacimiento de Cúllar de Baza I. Ph. D. Thesis University of Grenade (Spain), 293 p.

Sahnouni, M., Parés, J. M., Duval, M., Cáceres, I., Harichane, Z., van der Made, J., Pérez-González, A., Abdessadok, S., Kandi, N., Derradji, A., Medig, M., Boulaghraif, K., & Semaw, S. (2018). 1.9-million- and 2.4-million-year-old artifacts and stone tool–cutmarked bones from Ain Boucherit, Algeria. *Science, 362*, 1297–1301. https://doi.org/10.1126/science.aau0008

Sahnouni, M., & van der Made, J. (2009). The oldowan in North Africa within a biochronological framework. The cutting edge: new approaches to the archaeology of human origins stone age. *Institute Press, 3*, 179–210.

Sala, R., Benito-Calvo, A., Harichane, Z., Chacón Navarro, M. G., & Amara, A. (2016). A Middle Pleistocene human occupation of an ancient humid Basin close to the Chotts Region (N'Gaous, Algeria). CENIEH: http://hdl.handle.net/20.500.12136/986

Sánchez-Roa, C., Jiménez-Millán, J., Abad, I., Faulkner, D. R., Nieto, F., & García-Tortosa, F. J. (2016). Fibrous clay mineral authigenesis induced by fluid-rock interaction in the Galera fault zone (Betic Cordillera, SE Spain) and its influence on fault gouge frictional properties. *Applied Clay Science, 134*, 275–288. https://doi.org/10.1016/j.clay.2016.06.023

Sanz de Galdeano, C., & Vera, J. A. (1991). Una propuesta de clasificación de las cuencas neógenas béticas. Acta Geológica Hispánica, 26, 205–227. http://hdl.handle.net/10261/6802

Sanz de Galdeano, C. (1983). Los accidentes y fracturas principales de las Cordilleras Béticas. *Estudios Geológicos, 39*, 157–165.

Sanz de Galdeano, C. (1990). Geologic evolution of the Betic Cordilleras in the Western Mediterranean, Miocene to the present. *Tectonophysics, 172*, 107–119. https://doi.org/10.1016/0040-1951(90)90062-D

Sanz de Galdeano, C. (2008). The Cádiz-Alicante Fault: An important discontinuity in the Betic Cordillera. *Revista Sociedad Geologica De España, 21*, 49–58.

Sanz de Galdeano, C., Azañón, J. M., Cabral, J., Ruano, P., Alfaro, P., Canora, C., Ferrater, M., García-Tortosa, F. J., García-Mayordomo, J., Gràcia, E., Insua-Arévalo, J. M., Jiménez-Bonilla, A., Lacan, P. G., Marín-Lechado, C., Martín-Banda, R., Martín González, F., Martínez-Díaz, J. J., Martín-Rojas, I., Masana, E., … Simón, J. L. (2020). Active faults in Iberia. In C. Quesada & J. Oliveira (Eds.), *The geology of Iberia: A geodynamic approach. Regional geology reviews* (pp. 33–75). Springer Nature.

Sanz de Galdeano, C., Delgado, J., Galindo-Zaldívar, J., Marín, C., Alfaro, P., & García-Tortosa, F. J. (2007). Principales rasgos geológicos deducidos a partir de los mapas gravimétricos de la Cuenca de Guadix-Baza. In C. Sanz de Galdeano & J. A. Peláez (Eds.), *La cuenca de Guadix-Baza Estructura, tectónica activa, sismicidad, geomorfología y dataciones existentes* (pp. 101–110). Granada.

Sanz de Galdeano, C., García-Tortosa, F. J., Peláez, J. A., Alfaro, P., Azañón, J. M., Galindo-Zaldívar, J., López Casado, C., López Garrido, A. C., Rodríguez-Fernández, J., & Ruano, P. (2012). Main active faults in the Granada and Guadix-Baza Basins (Betic Cordillera). *Journal of Iberian Geology, 38*, 209–223. https://doi.org/10.5209/rev_JIGE.2012.v38.n1.39215

Sanz de Galdeano, C., & Vera, J. A. (1992). Stratigraphic record and palaeogeographical context of the Neogene Basins in the Betic Cordillera, Spain. *Basin Research, 4*, 21–36. https://doi.org/10.1111/j.1365-2117.1992.tb00040.x

Sawada, Y., Ickford, M., Senut, B., Masayuki, T., Tamaki Miura, H., Kashine, C. C., Tadahiro, C., & Hirokazu, F. (2002). The age of *Orrorin tugenensis*, an early hominid from the Tugen Hills, Kenya. *Comptes Rendus Palevol, 1*(5), 293–303. https://doi.org/10.1016/S1631-0683(02)00036-2

Schlüter, T. (1997). *Geology of East Africa* (p. 484). Gebrüder Borntraeger.

Scott, G. R., Gibert, L., & Gibert, J. (2007). Magnetostratigraphy of the Orce region (Baza Basin), SE Spain: New chronologies for Early Pleistocene faunas and hominid occupation sites. *Quaternary Science Reviews, 26*, 415–435. https://doi.org/10.1016/j.quascirev.2006.09.007

Sebastián Pardo, E. (1979). *Mineralogía de los materiales plioceno-pleistocenos de la depresión de guadix-baza* (p. 311). Universidad de Granada.

Semaw, S., Renne, P., Harris, J. W., Feibel, C. S., Bernor, R. L., Fesseha, N., & Mowbray, K. (1997). 2.5-million-year-old stone tools from Gona, Ethiopia. *Nature, 385*, 333–336. https://doi.org/10.1038/385333a0

Sesé, C. (1994). Paleoclimatological interpretation of the Quaternary small mammals of Spain. *Geobios, 27*, 753–767. https://doi.org/10.1016/S0016-6995(94)80060-X

Shakeri, A., Moore, F., & Kompani-Zare, M. (2008). Geochemistry of the thermal springs of Mount Taftan, southeastern Iran. *Journal of Volcanology Geothermal Basics, 178*, 829–836. https://doi.org/10.1016/j.jvolgeores.2008.05.001

Shchelinsky, V. E., Dodonov, A., Bigushe, V. S., Kulakov, S. A., Simakovab, A. N., Tesakov, A. S., & Titov, V. V. (2010). Early Palaeolithic sites on the Taman Peninsula (Southern Azov Sea region, Russia): Bogatyri/Sinyaya Balka and Rodniki. *Quaternary International, 223*, 28–35. https://doi.org/10.1016/j.quaint.2009.08.017

Shipton, C. (2011). Taphonomy and behaviour at the acheulean site of Kariandusi, Kenya. *African Archaeological Review, 28*, 141. https://doi.org/10.1007/s10437-011-9089-1

Sirakov, N., Guadelli, J. L., Ivanova, S., Sirakova, S., Boudadi-Maligne, M., Dimitrova, I., Fernandez, P., Ferrier, C., Guadelli, A., Iordanova, D., Iordanova, N., Kovatcheva, M., Krumov, I., Leblanc, J.-C., Miteva, V., Popov, V. V., Spassov, R., Taneva, S., & Tsanova, T. (2010). An ancient continuous human presence in the balkans and the beginnings of human settlement in western Eurasia: A lower pleistocene example of the lower palaeolithic levels in kozarnika cave (North-western Bulgaria). *Quaternary International, 223*, 94–106. https://doi.org/10.1016/j.quaint.2010.02.023

Sistiaga, A., Husaina, F., Uribelarreac, D., Martín-Perea, D. M., Troy Ferland, T., Freeman, K. H., Diez-Martín, F., Baquedano, E., Mabulla, A., Domínguez-Rodrigo, M., & Summons, R. E. (2020). Microbial biomarkers reveal a hydrothermally active landscape at Olduvai Gorge at the dawn of the Acheulean, 1.7 Ma. *Proceedings of the National Academy of Sciences of the United States of America, 117*(40), 24720–24728. https://doi.org/10.1073/pnas.2004532117

Soria, J. M. (1993). *La sedimentación neógena entre sierra arana y el río guadiana menor. Evolución desde un margen continental hasta una cuenca intramontañosa* (p. 292). Universidad de Granada. Ph.D. Thesis.

Soria, J. M., & Ruiz-Bustos, A. (1992). Nuevos datos sobre el inicio de la sedimentación continental en la cuenca de Guadix, Cordillera Bética. *Geogaceta, 11*, 92–94.

Stimpson, C. M., Lister, A., Partona, A., Clark-Balzana, L., Breezec, P. S., Drake, N. A., Groucutt, Huw, S., Jennings, R. P., Scerri, E., White, T. S., Zahir, M., Duval, M., Grün, R., Al-Omari, A., Al-Murayyi, K. S. M., Zalmout, I. S., Almufarreh, Y., & Memesh, A. M. (2016). Middle Pleistocene vertebrate fossils from the Nefud Desert, Saudi Arabia: implications for biogeography and palaeoecology. *Quaternary Science Reviews, 143*, 13–36. https://doi.org/10.1016/j.quascirev.2016.05.016

Tchernov, E. (1987). The age of the 'Ubeidiya formation, an early hominid site in the Jordan Valley, Israel. *Journal of Earth Sciences, 36*, 3–36.

Tchernov, E., Horwitz, L. K., Ronen, A., & Lister, A. (1994). The faunal remains from evron quarry in relation to other lower paleolithic sites in the southern Levant. *Quaternary Research, 42*, 328–339. https://doi.org/10.1006/qres.1994.1083

Texier, P. J. (1995). The oldowan assemblage NY18 site at Nyabusosi (Toro-Uganda). *Comptes Rendus Palevol, 320*, 647–653.

Titton, T., Oms, O., Barsky, D., Bargalló, A., Serrano-Ramos, A., García-Solano, J., Sánchez-Bandera, C., Yravedra, J., Blain, H.-A., Toro-Moyano, I., Jiménez Arenas, J. M., & Sala-Ramos, R. (2021). Oldowan stone knapping and percussive activities on a raw material reservoir deposit 1.4 million years ago at Barranco León (Orce, Spain). *Archaeological and Anthropological Sciences, 13*, 108. https://doi.org/10.1007/s12520-021-01353-w

Toro-Moyano, I., Martínez-Navarro, B., Agustí, J., Souday, C., Bermúdez de Castro, J. M., Martinón-Torres, M., Fajardo, B., Duval, M., Falguères, C., Oms, O., Parés, J. M., Anadón, P., Julià, R., García-Aguilar, J. M., Moigne, A.-M., Espígares, M. P., Ros-Montoya, S., & Palmqvist, P. (2013). The oldest human fossil in Europe, from Orce (Spain). *Journal of Human Evolution, 65*, 1–9. https://doi.org/10.1016/j.jhevol.2013.01.012

Torrente Casado, R. (2010). Aportes al estudio de las primeras ocupaciones humanas en el sur de la Península Ibérica. El caso de Cúllar-Baza 1. *Arqueología y Territorio, 7*, 1–19.

Treves, A., & Palmqvist, P. (2007). Reconstructing hominin interactions with mammalian carnivores (6.0–1.8 Ma). In S. L. Gursky & K. A. I. Nekaris (Eds.), *Primate anti-predator strategies developments in primatology series: progress and prospects* (pp. 355–381). Springer.

Vekua, A. K. (1986). Lower pleistocene mammalian fauna of akhalkalaki (Southern Georgia, 1708 USSR). *Palaeontographia Italica, 74*, 63–96.

Vera, J. A. (1970). Estudio estratigráfico de la depresión de guadix-baza. *Boletin Geológico y Minero, 81*, 429–462.

Vera, J. A., Fernández, J., López-Garrido, A. C., & Rodríguez-Fernández, J. (1984). Geología y estratigrafía de los materiales plioceno-pleistocenos del sector Orce-Venta Micena (Prov. Granada). *Paleontología i Evolució, 18*, 3–11.

Villalobos, M., Roldán, F. J., & Lupiani, E. (2006). *Memoria explicativa del mapa geológico de España escala 1:50.000, Hoja 972 (22–39) Cúllar-Baza*. Instituto Geológico y Minero de España.

Viseras, C., & Fernández, J. (1992). Sedimentary basin destruction inferred from the evolution of drainage systems in the Betic Cordillera, southern Spain. *Journal of the Geological Society of London, 149*, 1021–1029. https://doi.org/10.1144/gsjgs.149.6.1021

Warr, L. N. (2021). IMA–CNMNC approved mineral symbols. *Mineralogical Magazine, 85*(3), 291–320. https://doi.org/10.1180/mgm.2021.43

White, D. E., Brannock, W. W., & Murata, K. J. (1956). Silica in hot-spring waters. *Geochimica et Cosmochimica Acta, 10*, 27–59. https://doi.org/10.1016/0016-7037(56)90010-2

White, T. D., Asfaw, B., De Gusta, D., Gilbert, H., Richards, G. D., Suwa, G., & Howell, F. C. (2003). Pleistocene *Homo sapiens* from Middle Awash, Ethiopia. *Nature, 423*, 742–747. https://doi.org/10.1038/nature01669

White, T. D., Hart, W. K., Walter, R. C., Wolde, G., de Heinzelin, J., Clark, J. D., Asfaw, B., & Vrba, E. (1993). New discoveries of *Australopithecus* at Maka in Ethiopia. *Nature, 366*, 261–265. https://doi.org/10.1038/366261a0

White, T. D., Suwa, G., & Asfaw, B. (1994). *Australopithecus ramidus*, a new species of early hominid from Aramis, Ethiopia. *Nature, 371*, 306–312. https://doi.org/10.1038/371306a0

Williams, M. A. J., Williams, F. M., Gasse, F., Curtis, G. H., & Adamson, D. A. (1979). Plio-Pleistocene environments at Gadeb prehistoric site, Ethiopia. *Nature, 282*, 29–33. https://doi.org/10.1038/282029a0

Yamamoto, K. (1987). Geochemical characteristics and depositional environments of cherts and associated rocks in the franciscan

and shimanto terranes. *Sedimentary Geology, 52*(1–2), 65–108. https://doi.org/10.1016/0037-0738(87)90017-0

Yamamoto, M., Nakamura, R., Oguri, K., Kawagucci, S., Suzuki, K., Hashimoto, K., & Takai, K. (2013). Generation of electricity and illumination by an environmental fuel cell in deep-sea hydrothermal vents. *Angewandte Chemie International Edition, 52*(41), 10758–10761. https://doi.org/10.1002/anie.201302704

Yeshurun, R., Zaidner, Y., Eisenmann, V., Martínez-Navarro, B., & Bar-Oz, G. (2011). Lower Paleolithic hominin ecology at the fringe of the desert: Faunal remains from Bizat Ruhama and Nahal Hesi, Northern Negev. *Israel Journal of Ecology and Evolution, 60*, 492–507. https://doi.org/10.1016/j.jhevol.2010.01.008

You, J., Liu, Y., Zhou, D., Zheng, Q., Vasichenko, K., & Chen, Z. (2020). Activity of hydrothermal fluid at the bottom of a lake and its influence on the development of high-quality source rocks: Triassic Yanchang Formation, southern Ordos Basin, China. *Australian Journal of Earth Sciences, 67*(1), 115–128. https://doi.org/10.1080/08120099.2019.1612783

Yravedra, J., Solano, J. A., Courtenay, L. A., Saarinen, J., Linares-Matás, G., Luzón, C., Serrano-Ramos, A., Herranz-Rodrigo, D., Cámara, J. M., Ruiz, A., Titton, S., Rodríguez-Alba, J. J., Mielgo, C., Blain, H.-A., Agustí, J., Sánchez-Bandera, C., Montilla, E., Toro-Moyano, I., Fortelius, M., … Jiménez-Arenas, J. M. (2021). Use of meat resources in the early pleistocene assemblages from fuente nueva 3 (Orce, Granada, Spain). *Archaeological and Anthropological Sciences, 13*, 213. https://doi.org/10.1007/s12520-021-01461-7

Yravedra, J., Solano, J. A., Herranz-Rodrigo, D., Linares-Matás, G. J., Saarinen, J., Rodríguez-Alba, J. J., Titton, S., Serrano-Ramos, A., Courtenay, L. A., Mielgo, C., Luzón, C., Cámara, J., Sánchez-Bandera, C., Montilla, E., Toro-Moyano, I., Barsky, D., Fortelius, M., Agusti, J., Blain, H.-A., … Jiménez-Arenas, J. M. (2022). Unravelling hominin activities in the zooarchaeological assemblage of Barranco León (Orce, Granada, Spain). *Journal of Paleolithic Archaeology, 5*, 6. https://doi.org/10.1007/s41982-022-00111-1

Zhang, K., Liu, R., Bai, E., Zhao, Z., Peyrotty, G., Fathy, D., Chang, Q., Liu, Z., Yang, K., Xu, C., & Liu, Z. (2023). Biome responses to a hydroclimatic crisis in an early cretaceous (Barremian–Aptian) subtropical inland lake ecosystem, Northwest China. *Palaeogeography, Palaeoclimatology, Palaeoecology, 622*, 111596. https://doi.org/10.1016/j.palaeo.2023.111596

Zhou, J., Yang, H., Liu, H., & Jiao, Y. (2022). The Depositional mechanism of hydrothermal chert nodules in a lacustrine environment: A case study in the middle permian lucaogou formation, junggar basin, Northwest China. *Minerals, 12*(10), 1333. https://doi.org/10.3390/min12101333